DISSERTAÇÃO DE MESTRADO

Análise de SNIR e BER para Redes Acústicas Subaquáticas

Rubén Ortega Blanco

Brasília, Agosto de 2015

UNIVERSIDADE DE BRASÍLIA

FACULDADE DE TECNOLOGIA

MASTER DEGREE THESIS

**SNIR and BER Analysis for
Underwater Acoustic Networks**

Rubén Ortega Blanco

Brasília, Agosto de 2015

UNIVERSIDADE DE BRASÍLIA

FACULDADE DE TECNOLOGIA

UNIVERSIDADE DE BRASILIA
Faculdade de Tecnologia

DISSERTAÇÃO DE MESTRADO

Análise de SNIR e BER para Redes Acústicas Subaquáticas

Rubén Ortega Blanco

Relatório submetido ao Departamento de Engenharia

Elétrica como requisito parcial para obtenção

do grau de Mestre em Engenharia de Sistemas Eletrónicos e de Automaçõa

Banca Examinadora

Prof. Renato M. de Moraes, CIN/UFPE   _____
Orientador

Prof. Marcelo M. Carvalho, ENE/UnB   _____
Examinador interno

Prof. Andre C. Drummond, CIC/UnB   _____
Examinador externo

UNIVERSIDADE DE BRASÍLIA
FACULDADE DE TECNOLOGIA
DEPARTAMENTO DE ENGENHARIA ELÉTRICA

ANÁLISE DE SNIR E BER PARA REDES ACÚSTICAS
SUBAQUÁTICAS

RUBÉN ORTEGA BLANCO

DISSERTAÇÃO DE MESTRADO SUBMETIDA AO DEPARTAMENTO DE ENGENHARIA ELÉTRICA DA FACULDADE DE TECNOLOGIA DA UNIVERSIDADE DE BRASÍLIA, COMO PARTE DOS REQUISITOS NECESSÁRIOS PARA A OBTENÇÃO DO GRAU DE MESTRE.

APROVADA POR:

_____
RENATO MARIZ DE MORAES, Dr., ENE/UNB
(ORIENTADOR)
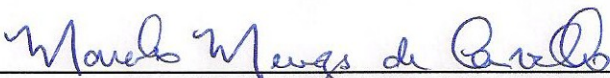
_____
MARCELO MENEZES DE CARVALHO, Dr., ENE/UNB
(EXAMINADOR EXTERNO)

_____
ANDRÉ COSTA DRUMMOND, Dr., CIC/UNB
(EXAMINADOR EXTERNO)

Brasília, 11 de agosto de 2015.

FICHA CATALOGRÁFICA

REFERÊNCIA BIBLIOGRÁFICA

CESSÃO DE DIREITOS

Agradecimentos

Quisiera agradecer primeramente a mis padres por su apoyo incondicional, a mis abuelos por estar siempre para mi y a mis otros abuelos, Ia, Arci, Api y Aya. Agradecer a mis amigos Noel, Chicho, Raul, Julio, Yarisley y a todos los demas. Gracias a Leti por su apoyo y su ayuda. Los quiero a todos.

Gracias tambien a mi profesor Renato M. de Moraes por confiar en mi para este trabajo, por darme esta maravillosa oportunidad. Obrigado professor!! Agradecer a la Universidade de Brasilia por abrirme sus puertas y finalmente a Brasil por dejarme estudiar aca.

Rubén Ortega Blanco

RESUMO

O objetivo do seguinte trabalho é determinar um modelo matemático que permita-nos obter a Relação Sinal Ruído mais Interferência (SNIR do Inglês Signal-to-Noise plus Interference Ratio), a Taxa de Erro de Bits (BER do Inglês Bit Error Rate) de um salto e a Taxa de Erro de Bits fim-a-fim numa rede acústica submarina.

Com esse propósito foi desenvolvido um modelo matemático que permite o cálculo destes parâmetros considerando a interferência para o protocolo de acesso ao meio (MAC do Inglês Medium Access Control) ALOHA puro. Também foi necessário desenvolver antes diferentes parâmetros da rede, tais como, distância média do salto, distância média até o nó central, distância média entre os nós, número médio de saltos na rota e desvio médio.

Com o uso deste modelo também é possível obter o valor da frequência ótima utilizando uma função de otimização. Comparações entre a Taxa de Erro de Bits de um salto e fim-a-fim também forem feitas, para diferentes valores de máximo ângulo de desvio na topologia de rede usada. Estas comparações demonstran quando pode ser mais convenente o uso de um salto ou múltiple-salto.

Simulações Monte-Carlo e modelo forem comparados com o propósito de validar os resultados obtidos. Estas comparações demostram a grande similitude entre nosso modelo e as simulações de Monte-Carlo. Além disso foi possível o estudo do comportamento da SNIR e do BER variando importante parâmetros da rede tais como frequência de transmissão, número de nós, raio da esfera e máximo ângulo de desvio. Os resultados obtidos provarem que a SNIR para um salto diminui com o aumento do número de nós e o raio da esfera, mas aumenta com o incremento da potência de transmissão. O comportamento de BER é contrário ao comportamento de SNIR. Também foi possível observar a existência da frequência ótima, onde os melhores valores de SNIR e o BER são obtidos.

ABSTRACT

The objective of this work is to find a mathematical model that allow us to obtain the Signal-to-Noise plus Interference Ratio (SNIR), the One-Hop Bit Error Rate (BER) and the End-to-End Bit Error Rate for an Underwater Acoustic Network (UAN).

Considering this, it was developed a model that includes the interference as an important impairment and for ALOHA MAC (Medium Access Control) protocol. In addition, it was necessary to obtain before several parameters from the network, such as, average distance of the hop, average distance between nodes, average distance to the central node, average number of hops and average deviation.

With this model, it is also possible to find the optimal value of frequency using an optimization function. It was made comparisons between the One-Hop BER and the End-to-End BER for various values of maximal deviation angle. This comparison shows when it is more adequate to either use one-hop or multi-hop.

Finally, we compared numerical and Monte-Carlo simulation results, giving a first validation to our model. These comparisons show a big similitude between the developed model and the Monte-Carlo simulation. In addition, it was possible to analyse the behaviour of the SNIR and BER by varying important parameters of the network, such as, transmission frequency, number of nodes and sphere radius among others. From the obtained results it was prove that the SNIR decreases with an increase from the number of nodes and the sphere radius, but increases with the transmission power. The End-to-End BER has an contrary behavior with the SNIR.

SUMMARY

INDEX OF FIGURES

INDEX OF TABLES

LIST OF SYMBOLS

Acronyms and Abbreviations

EM	Electromagnetic
RF	Radio-Frequency
FSO	Free-Space Optical
UW-AC	Underwater Acoustic Communications
UAN	Underwater Acoustic Network
SNIR	Signal to Noise plus Interference Ratio
SNR	Signal to Noise Ratio
BER	Bit Error Rate
MAC	Medium Access Control
BC	Before Christ
AC	Alter Current
RV	Random Variable
AUV	Autonomous Underwater Vehicles
TDMA	Time Division Multiple Access
FDMA	Frequency Division Multiple Access
CDMA	Code Division Multiple Access
CSMA	Carrier Sense Multiple Access
ADC	Analogical to Digital Converter
DAC	Digital to Analogical Converter
AM	Amplitude Modulation
PM	Phase Modulation
FM	Frequency Modulation
NRZ	Not Return to Zero
RZ	Return to Zero
AWGN	Additive White Gaussian Noise
OOK	On Off Keying Modulation
MPSK	M-Phase Shift Keying Modulation
DSSS	Direct-Sequence Spread-Spectrum Modulation
OFDM	Orthogonal Frequency-Division Multiplexing Modulation

MIMO	Multiple-Input Multiple-Output modulation	
p.d.f	power density function	
c.d.f	cumulative density function	
INI	Inter Nodal Interference	

Units

m	meters
s	seconds
$Mbps$	Mega bits per second
^0C	Celsius degrees
g	grams
J	Joule
Pa	Pascal
W	Watts
dB	decibels
Hz	Hertz
$nots$	nots
rad	radians
pck	packages
$bits$	bits

Parameters

T	Temperature	^0C
S	Salinity	ppt
d	Depth	m
c	Sound speed	m/s
t	Time unit	s
Z_{imp}	Acoustic impedance	kg/m^2
ρ_A	Density of the medium	kg/m^3
ρ_{A_0}	Density of the medium without sound present	kg/m^3
ρ_{tot}	Total density	kg/m^3
ρ_{dist}	Infinitesimal acoustic density disturbance	kg/m^3
E_{AC}	Acoustic energy	J
$E_{potential}$	Potential energy	J
$E_{kinetic}$	Kinetic energy	J
V	Volume	m^3
A_r	Unit area perpendicular to the propagation direction	m^2

r_{out}	Radius along the acoustic wave front from the power source	m
$Pres$	Acoustic pressure	Pa
$Pres_{ref}$	Reference acoustic pressure	Pa
P	Acoustic power	W
I	Acoustic intensity	W/m^2
I_{ref}	Reference acoustic intensity	W/m^2
$A(l, f)$	Acoustic path loss	
$A_{AbsLoss}$	Absorption loss	
$A_{SprLoss}$	Spreading loss	
l	Hop distance	m
f	Central transmitting frequency	kHz
Δf	Noise frequency bandwidth	Hz
A_0	Acoustic path loss normalization factor	
$a(f)$	Absorption coefficient	$1/km$
k	Path loss exponent	
R	Sphere radius	km
N	Number of nodes	
N_{TU}	Turbulence Noise	Pa/Hz
N_{SH}	Shipping Noise	Pa/Hz
N_S	Sea movement Noise	Pa/Hz
N_{TH}	Thermal Noise	Pa/Hz
N_T	Total Noise	Pa/Hz
v	Wind speed	$knots$
θ	Maximal aperture angle	rad
ϕ	Real deviation angle	rad
$\overline{n}_h$	Average number of hops	
$E[\mathbf{X}]$	Average length of the reference line	m
$E[\mathbf{Y}]$	Average distance of the hop	m
$E[cos(\theta)]$	Average deviation	rad
λ	Poisson parameter	
ρ_s	Spatial density	
P_{RS}	Power of the received signal	W
P_{TS}	Power of the transmitted signal	W
$E[P_{INT}^{TOT}]$	Total average interference power at the receiver	W
$E[P_{int}^i]$	Average interference power caused by node i to the receiver	W
$\overline{\lambda}$	Average package transmission rate	pck/s
L	Package size rate	$bits$
R_b	Transmission rate	$bits/s$

Chapter 1

Introdução

Este capítulo apresenta a introdução do trabalho. Ele começa com uma contextualização do tema, segue com a definição do problema e os objetivos, e termina com a apresentação do trabalho.

1.1 Contextualização

O presente trabalho é a dissertação de mestrado para o Programa de Pós-Graduação em Engenharia de Sistemas Eletrônicos e de Automação (PGEA) da Faculdade de Tecnología da Universidade de Brasília, Brasil.

O nosso planeta está coberto principalmente por água. Este meio abriga a maior quantidade de espécies vivas, mas tem o maior percentual de área inexplorada. As comunicações acústicas submarinas poderiam ser uma importante ferramenta para a exploração, o estudo, a investigação e o uso do mar. Muitas novas investigações e recursos são destinados ao estudo do mar e fundo marinho. As mais importantes áreas de aplicação são: sistemas de vigilância das costas; operação de veículos autônomos submarinos; análise do fundo marinho, mar e espécies; indústria militar; indústria de petróleo e gás; e transporte marítimo.

As comunicações eletromagnéticas (EM) submarinas são principalmente para curto alcance ($< 100\ m$) ou curtíssimo alcance ($< 1\ m$), devido a sua alta atenuação (redução da intensidade da sinal), mas tem como vantagem que podem ser usadas para comunicações de alta velocidade [4]. Mesmo considerando que as ondas eletromagnéticas não são afetadas pela maioria dos parâmetros que influenciam as ondas acústicas, tais como o ruído acústico ambiente e a perda do caminho acústico, o seu uso é limitado. Além disso, as ondas EM sofrem interferência dos equipamentos a pouca distância, por exemplo, motores de navios [5].

As ondas Ópticas do Espaço Livre (FSO do inglês *Free Space Optical waves*) utilizadas como portadoras de sinal de comunicação sem fio são geralmente limitadas a distâncias curtíssimas, pois a grande absorção da água na banda de frequência óptica e o forte retro-espalhamento a partir de partículas em suspensão. Até mesmo a água mais clara tem 1000 *vezes* a atenuação do ar puro, a água turva tem mais de 100 *vezes* a atenuação da neblina mais densa. No entanto, o FSO submarino, especialmente nos comprimentos de onda azul-verde, oferece uma opção prática para

comunicação de alta largura de banda ($10-150\ Mbps$) ao longo de distâncias moderadas ($10-100$ *metros*). Este alcance de comunicação é muito necessário na inspeção dos portos, manutenção de plataformas de petróleo, e ligando submarinos à terra, apenas para citar algumas das demandas nesta frente.

A comunicação acústica é a técnica mais versátil e amplamente utilizada em ambientes submarinos devido à baixa atenuação do som na água quando comparado ao caso de ondas eletromagnéticas. Isto é especialmente verdadeiro em configurações termicamente estáveis, de águas profundas. Por outro lado, o uso de ondas acústicas em águas superficiais pode ser adversamente afetado por gradientes de temperatura, ruído ambiente da superfície e a propagação multi-caminho, devido à reflexão e refração. A velocidade muito mais lenta da propagação acústica na água, cerca de 1500 m/s, em comparação com a de ondas eletromagnéticas e ópticas, é outro fator limitante para uma comunicação eficiente. No entanto, a comunicação submarina vem amplamente empregando ondas acústicas.

Os objetivos deste trabalho são modelar as comunicações acústica submarinas (UW-AC do inglês Underwater Acoustic Communications), inlcuindo interferência na análise resultando no cálculo e otimização da relação sinal-ruído e interferência (SNIR do inglês Signal-to-Noise plus Interference Ratio) e a taxa de erro de bit (BER do inglês Bit Error Rate) fim-a-fim considerando múltiplos saltos para redes acústicas submarinas (UANs do inglês Underwater Acoustic Networks).

O cálculo da relação sinal-ruído (SNR do inglês Signal-to-Noise Ratio) e a BER em comunicações acústicas submarinas têm sido utilizadas por muitos autores com várias finalidades. O presente trabalho acrescenta a interferência a analise, considerando o protocolo de controle de acesso ao meio (MAC do inglês Medium Access Control) ALOHA, resultando no SNIR e, finalmente, obtém-se a BER fim-a-fim. É desenvolvido um modelo matemático tridimensional que nos permite encontrar e estimar a média para a SNIR e BER fim-a-fim.

Parte dos resultados desta dissertação foram apresentados e publicados no International Telecommunications Workshop, em junho de 2015, na cidade de Santa Rita do Sapucaí, MG, Brasil [6].

1.2 Definição do Problema

É de grande relevância a capacidade de se estimar o comportamento de uma rede acústica submarina (UAN), antes de sua implementação real. A possibilidade de conhecer os possíveis valores da relação sinal-ruído mais interferência (SNIR) e a taxa de erro de bits (BER) fim-a-fim permitem-nos variar os parâmetros e determinar seus valores ideais. Por exemplo, se o protocolo MAC ALOHA é considerado, então a ocorrência de interferência em uma rede com vários transmissores deve ser levada em consideração.

2

1.3 Objetivos do Projeto

O primeiro objetivo desta pesquisa é determinar um modelo matemático que nos permita saber a distância média entre os nós, a distância média para o nó central na rede, a distância média do salto e o número médio de saltos, dentro de uma esfera tridimensional, considerando uma topologia aleatória de nós na rede.

O objetivo seguinte é obter a média da SNIR. Esta medida é calculada com base na distância média do salto entre nós, e deve-se considerar a interferência, no caso com o protocolo MAC ALOHA. Além disso, procurou-se comparar o resultado analítico com simulações Monte-Carlo e as discussões consequentes.

Com a média do SNIR de um salto obtido, o próximo passo é calcular e analisar a média do BER de um salto. Para este propósito, é necessário primeiro selecionar um tipo de modulação.

Finalmente, com a média do BER de um salto e o número médio de saltos, o BER fim-a-fim é calculado. Com esse parâmetro, será possível analisar a UAN e selecionar os valores ótimos de frequência de transmissão, número de nós dentro da esfera tridimensional, raio da esfera, potência transmitida e taxa de transmissão de bits.

Todos os parâmetros obtidos devem ser modelados e comparados com as simulações a fim de validar o estudo.

1.4 Apresentação do manuscrito

O Capítulo 3 mostra as características principais das redes acústicas submarinas. Depois disso, no Capítulo 4 são descritos os esquemas de modulação acústica submarinas e no Capítulo 5 o número médio de saltos e a distância média entre os nós são obtidos. A relação sinal-ruído mais interferência (SNIR) é descrita no Capítulo 6 e no Capítulo 7 a taxa de erro de bits (BER) de um salto e a BER fim-a-fim são encontradas. Finalmente, no Capítulo 8 são mostradas as conclusões da pesquisa e possíveis trabalhos futuros.

Chapter 2

Introduction

This chapter presents the introduction of this work. It begins with a contextualization, and the problem definition and the objectives follow, finishing with the work presentation.

2.1 Contextualization

This work represents the master thesis for the Graduate Program in Electronics and Automation Engineering Systems (PGEA from portuguese Programa de Pós-Graduação em Engenharia de Sistemas Eletrônicos e de Automação), at the Department of Electrical Engineering, at University of Brasilia, Brazil.

Our planet is mainly covered by water. This medium hosts the major quantity of alive species, however it has the biggest percent of unexplored area on earth. The underwater acoustic communications can be an important tool for the exploration, study, investigation and use of the sea. Several new researches are destined to the study of the sea and the seabed. The most important study areas are: coastal surveillance systems; autonomous underwater vehicle (AUV) operation; analysis of the seabed, sea and species; military industry; oil and gas industry; and maritime transportation.

The electromagnetic (EM) underwater communications are mainly for short range ($< 100\ m$) or very short range ($< 1\ m$) due to its high attenuation, but for very high speed communications [4]. Even considering that electromagnetic waves are not affected by most of the parameters that affects the acoustic waves, such as ambient acoustic noise and acoustic path-loss, its use is limited. Also, EM waves suffers interference from near equipments, for example, ship motors [5].

Free-space optical (FSO) waves used as wireless communication carriers are generally limited to very short distances because they suffer from severe water absorption at the optical frequency band and strong backscatter from suspending particles. Even the clearest water has $1000 - times$ the attenuation of clear air, and turbid water has more than $100 - times$ the attenuation of the densest fog. Nevertheless, underwater FSO, especially in the blue-green wavelengths, offers a practical choice for high-bandwidth communication ($10 - 150\ Mbps$) over moderate ranges ($10 - 100 meters$). This communication range is most employed in harbor inspection, oil-rig maintenance, and linking

submarines to land, to just name a few of the demands on this front.

Acoustic communication is the most versatile and widely used technique in underwater environments due to the low attenuation (signal reduction) of sound in water. This is especially true in thermally stable, deep water settings. On the other hand, the use of acoustic waves in shallow water can be adversely affected by temperature gradients, surface ambient noise, and multipath propagation due to reflection and refraction. The much slower speed of acoustic propagation in water, about 1500 m/s, compared with that of electromagnetic and optical waves, is another limiting factor for efficient communication and networking. Nevertheless, the currently favourable technology for underwater communication is upon acoustics.

This work objectives are the study and improvement of Underwater Acoustic Communications (UW-AC), by modeling and calculating the Signal-to-Noise plus Interference Ratio (SNIR) and End-to-End Bit Error Rate (BER) for underwater acoustic networks (UANs).

The calculus of the Signal-to-Noise Ratio (SNR) and the Bit Error Rate (BER) in underwater acoustic communications have been used by many authors for various purposes. This work introduces the interference, considering the ALOHA MAC protocol, as an impairment for the SNIR and finally the End-to-End BER. It is developed a three-dimensional mathematical model which allows us to find and estimate the average End-to-End BER, considering multi-hop for UANs.

Part of the results of this work was presented and published in International Telecommunications Workshop, June 2015, in Santa Rita do Sapucaí, MG, Brazil [6].

2.2 Problem Definition

It is of great importance to be able to estimate the behaviour of an Underwater Acoustic Network (UAN) before its implementation. The possibility to preview the value ranges of the Signal-to-Noise plus Interference Ratio (SNIR) and the End-to-End Bit Error Rate (BER) allow us to variate the parameters and determinate the optimal choices before the real implementation of these networks.

The consideration of the interference in underwater acoustic communications is also very important due to the real situation of possible multiple (simultaneous) source transmissions which can cause interference at receivers. We consider the ALOHA as the MAC protocol due to its simplicity which makes possible the SNIR and BER computation.

2.3 Project Objectives

The first objective of this research is to determinate a mathematical model that allows us to determine the average distance between nodes, the average distance to the central node, the average distance of the hop and the average number of hops inside a three-dimensional sphere, considering a random network topology.

To obtain the average One-Hop Signal-to-Noise plus Interference Ratio (SNIR) is our next objective. This parameter is calculated based on the average distance of the hop where the interference is considered with the ALOHA MAC protocol. Also, it is compared with simulations, and its behaviour must be studied and analysed.

Having the average One-Hop SNIR, the next step is to calculate and analyse the average One-Hop BER. To this propose, it is necessary first to select a type of modulation.

Finally, with the average One-Hop BER and the average number of hops, the End-to-End BER can be calculated. With this parameter, we will be able to analyse the UAN and select the optimal values of transmission frequency, number of nodes inside the network, network radius, transmitted power and transmission bit rate.

All the obtained parameters must be modeled and compared with Monte-Carlo simulations, with the assistance of the software MATLAB. These results allow us to have a better look of the UAN.

2.4   Work Presentation

Chapter 3 shows the fundamentals in underwater acoustic networks. After that, in Chapter 4 the underwater acoustic modulation schemes are described and in Chapter 5 the average number of hops and the average distance between nodes are obtained. The Signal-to-Noise plus Interference Ratio (SNIR) is described in Chapter 6 and the One-Hop Bit Error Rate (BER) and End-to-End BER in Chapter 7. Finally in Chapter 8 the investigation is concluded.

Chapter 3

Fundamentals

This chapter begins with a brief history about the underwater acoustics communication (UW-AC). After this, a description of the fundamentals of the UW-AC and the underwater acoustic channel characteristics are presented. The underwater Medium Access Control (MAC) protocols are presented also in this chapter, choosing one of this protocols for our research. Finally, a summary of the main and new activities and research on this subject is presented.

3.1   Introduction

This chapter begins with a brief history about UW-AC that summarizes the first steps and researches in the area. The next section is about the underwater acoustic communication fundamentals. In this section, the principles of the UW-AC are explained, which will be needed further in this work. The underwater channel characteristics are of great relevance for our work, these are the basis of our analysis, and are explained in this chapter too. The interference modeling is one of the contributions of our work. To such end, it is necessary to select a MAC protocol. In this chapter, the main UW-AC MAC protocols are described and the ALOHA MAC protocol is selected for our investigation. Finally, we summarize the main contributions and researches in the UW-AC area.

3.2   Underwater Acoustic Communications History

Aristotle ($384 - 322\ BC$) was the first to note that sound could be heard in the water as well as in the air. Nearly 2000 years later, Leonardo da Vinci ($1452 - 1519$) made the observation that ships could be heard at great distances by water. Almost 200 years after L. da Vinci's observation, the physical understanding of acoustical process was advancing rapidly with Marin Mersenne and Galileo independently discovering the laws of vibrating strings, which Mersenne published in his work L'Harmonie Universelle in the late $1620's$. Mersenne's remarks regarding

the nature and behavior of sound and his early experimental measurements on the speed of sound in the air during the mid to late $1600's$ are considered to provide the foundation for acoustics. Several decades later, in 1687, Sir Isaac Newton published the first mathematical theory of how sound travels, in his great work, Philosophiae Naturalis Principia Mathematica. Although Newton focused on sound in the air, the same basic mathematical theory applies to sound in water.

In 1743, Abbé J. A. Nollet conducted a series of experiments to settle a dispute about whether sounds could travel through water. With his head underwater, he reported hearing a pistol shot, bell, whistle, and shouts. He also noted that an alarm clock clanging in water could be heard easily by an underwater observer, but not in air, clearly demonstrating sound travels through water.

The first successful measurements of the speed of sound in water were not made until the early $1800's$. Using a long tube to listen underwater, as suggested by L. da Vinci, scientists in 1826 recorded how fast the sound of a submerged bell travelled across Lake Geneva.
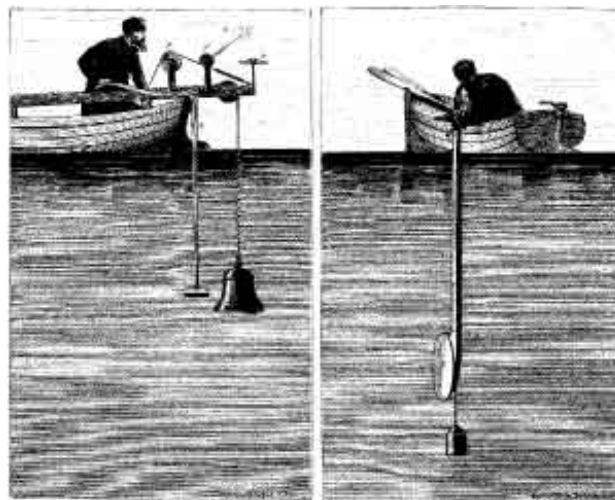
Figure 3.1: First Sound Measure on water [1].

The Submarine Signal Company applied the first practical use of underwater sound in 1901: underwater bells located under lightships or near lighthouses that could be detected by receivers installed on ships. The carbon-granule microphone developed by Thomas Edison and his collaborators for the first telephones was installed in a waterproof container, serving as the hydrophone to receive the underwater bell signals. This mechanism warn ships about the dangers of shallow waters and rocks.

3.3 Underwater Acoustic Communications Fundamentals

Our work purpose is to obtain the Signal-to-Noise plus Interference Ratio (SNIR) and the End-to-End Bit Error Rate (BER) at an Underwater Acoustic Network (UAN), therefore, it is relevant to know some important factors about the acoustic medium, such as, pressure, intensity, acoustic impedance, etc. In this section, these factors and the relationship between them are explained [7], [8], [9].

3.3.1   Sound Speed Profile

The ocean is an acoustic wave guide limited above by the sea surface and below by the sea floor. Sound speed is normally related to density and compressibility. In the ocean, density is related to static pressure, salinity, and temperature. The sound speed in the ocean is an increasing function of temperature (T) in degrees, salinity (S) in parts per thousand, and pressure, the latter being a function of depth (d) in meters [2]. A simplified expression for this dependence is

$$c = 1449.2 + 4.6T - 0.055T^2 + 0.00029T^3 + (1.34 - 0.01T)(S - 35) + 0.016d. \qquad (3.1)$$

Seasonal and diurnal changes affect the oceanographic parameters in the upper ocean. In addition, all of these parameters depend on the geography. Figure 3.2 shows a typical set of sound-speed profiles indicating greatest variability near to the surface as function of season and time of day. In a warmer season (or warmer part of the day), the temperature increases near to the surface and hence the sound speed increases toward the sea surface [2].
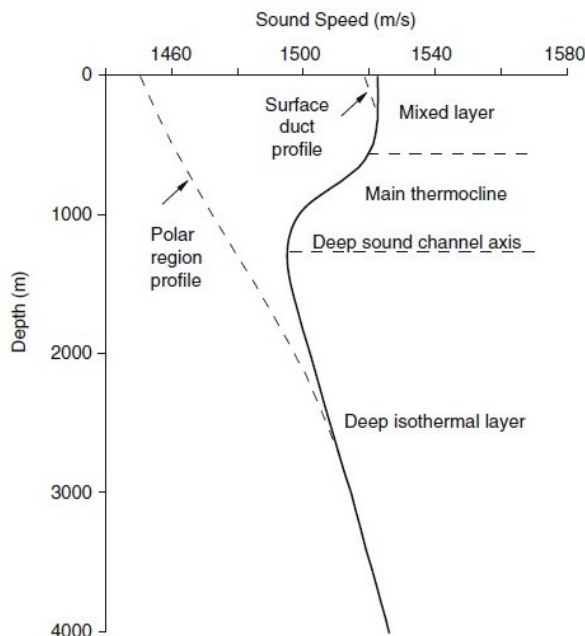
Figure 3.2: Generic Sound Speed Profile [2].

In non-polar regions, the oceanographic properties of the water near the surface result from mixing due to wind and wave activity at the air sea interface. This surface mixed layer has a constant temperature. Hence, in this isothermal mixed layer we have a sound-speed profile which increases with depth because of the pressure gradient effect, the last term in Eq. (3.1). This is the surface duct region, and its existence depends on the surface oceanographic conditions [2].

Below the mixed layer there is the thermocline where the temperature decreases with depth and therefore the sound speed also decreases with depth. Below the thermocline, the temperature is constant (about 2^oC) and the sound speed increases because the increasing pressure. Therefore, between the deep isothermal region and the mixed layer, we must have a minimum sound speed

which is often referred as the axis of the deep sound channel [2].

However, in polar regions, the water is coldest, the surface and hence the minimum sound speed is at the ocean air (or ice) interface as indicated in Figure 3.2. In continental shelf regions (shallow water) with water depth in the order of a few hundred meters, only the upper part of the sound-speed profile in Figure 3.2 is relevant. This upper region depends on season and time of day, which, in turn, affects sound propagation in the water column [2].

Our work considers a seawater with 3.5 percent of salinity, that is the approximate value for this medium, 15^0C of temperature, that is the normal temperature for the used depth that will be less than 1000 m of depth, giving an approximated value of sound speed of 1500 m/s. Those are the used parameters because This will be the sound speed used value for the rest of this work.

3.3.2 Acoustic Transducers

A transducer converts some sort of energy to sound (source or projector) or converts sound to energy (receiver), usually electric. The main transducers used for underwater acoustics are piezoelectric and magnetostrictive [2].

Piezoelectricity: Certain crystalline substances generate electric charges under mechanical stress and conversely experience a mechanical strain in the presence of an electric field. The piezoelectric effect describes a situation where the transducer material senses input mechanical vibrations and produces a charge at the frequency of the vibration. An AC voltage causes the piezoelectric material to vibrate in an oscillatory fashion at the same frequency as the input current. Quartz is the best known single crystal material with piezoelectric properties.

Magnetostriction is the change in dimensions of a ferromagnetic material when it is placed in a magnetic field and the variation in magnetization when the material dimensions change due to an external force.

Some other transduction mechanisms employed are electrodynamic where, for example, sound pressure causes a coil to move through a magnetic field thereby generating an output voltage. This electromagnetic induction is the same principle used in electric generators.

Parametric or finite-amplitude sources are sound projectors which are excited by two high-amplitude primary frequencies. The main disadvantage of parametric sources is that they have low efficiency.

Explosive and air gun sources are high energy wideband types of sources. Actually, the technology is such that their signatures are fairly reproducible. Electric discharge and laser sources are also being used.

Finally, we mention vector sensors. Recall that an acoustic wave in a fluid is a longitudinal wave. That is, the acoustical particle motion is aligned to the direction of propagation. Hence, a small transducer that measures a vector property such as velocity or acceleration will have frequency independent directional properties as opposed to a small pressure sensor that is omni-directional. Particle velocity is proportional to the pressure gradient so that pressure gradient phones also

have this directional property. Such a device has many advantages though one disadvantage is its susceptibility to flow noise.

3.3.3 Acoustics Parameters

The acoustic impedance Z_{imp}, given in units of kilograms per squared meters (kg/m^2), measures the opposition to the flow of sound through the underwater medium. It is given by

$$Z_{imp} = \rho_A c \tag{3.2}$$

where ρ_A is the density of the medium in units of (kg/m^3) and c is the speed of sound in units of meters per second (m/s). For the sea characteristics considered in Section 3.3.1, $\rho_A = 1035\ kg/m^3$ and $c = 1500\ m/s$, resulting that $Z_{imp} = 1559745\ kg/m^2 s$.

The Acoustic Energy is the energy of a sound wave. It is the result of the sum of the kinetic energy ($E_{kinetic}$) and potential energy ($E_{potential}$). The kinetic energy is the energy from the movement of a particle with a certain mass and for fluids it is expressed in terms of density. The used density for the calculus of the kinetic energy is the medium density (ρ_A), related to the total density (ρ_{tot}) and the infinitesimal acoustic density disturbance (ρ_{dist}) by

$$\rho_{tot} = \rho_A + \rho_{dist}. \tag{3.3}$$

The potential energy is caused by the forces of elastic pressure, due to the longitudinally of the sound wave in a fluid [2]. The acoustic energy in units of $1 Joule = 1J = 1\ kgm^2/s^2$ is given by

$$E_{AC} = E_{potential} + E_{kinetic} = \int_V \frac{Pres^2}{2\rho_{A_0}c^2} dV + \int_V \frac{\rho_A v_{part}^2}{2} dV. \tag{3.4}$$

Whereas V is the volume of interest in (m^3), ρ_{A_0} is the density of the medium without sound present in (kg/m^3), v_{part} is the velocity of the particle in (m/s), and $Pres$ is the acoustic pressure in (Pa), due to the deviation of the ambient hydrostatic pressure caused by a sound wave.

The Acoustic Intensity (I) in units of (W/m^2) is defined as the amount of sound that flows through an unit area ($A_r = 4\pi r_{out}^2$) perpendicular to the propagation direction per time unit t, where r_{out} is the radius along the acoustic front wave from the power source which is usually taken as $1\ m$. Accordingly,

$$I = \frac{E_{AC}}{A_r \times t} = \frac{P}{A_r} = \frac{Pres^2}{Z_{imp}} \tag{3.5}$$

or

$$I_{dB} = 10 \log_{10}\left(\frac{I}{I_{ref}}\right) = 20 \log_{10}\left(\frac{Pres}{Pres_{ref}}\right) \tag{3.6}$$

in decibels, where E is the acoustic energy in (J); P is the acoustic power in (W) defined as the energy per second that the acoustic wave conveys, i.e., the quantity of sonic energy transferred (irradiated) within a certain time t; I_{ref} is the reference intensity for acoustic environment equal to 6.41×10^{-19} W/m^2 and $Pres_{ref}$ is the reference pressure for acoustic environment equal to 1 μPa, for $Z_{imp} = 1559745$ $kg/m^2 s$.

Unlike acoustic pressure, acoustic power is neither room dependent nor distance dependent. Acoustic power is the total power produced by the source in all directions within a certain time t.

3.4   Underwater Acoustic Channel Characteristics

3.4.1   Acoustic Path Loss

According to [10], [11] and [12] the path loss, or attenuation equation, found by Urick in 1967, is the combination of the spreading loss and the absorption loss, and it can be given by

$$A(l, f) = A_0 l^k a(f)^l \tag{3.7}$$

or

$$10 \log_{10}(A(l, f)) = 10k \log_{10}(l) + 10l \log_{10}(a(f)) \tag{3.8}$$

in $dBref A_0$, where $a(f)$ is the absorption coefficient of the acoustic signal, depending on the frequency of the signal; k is the path loss exponent that depends on the spreading type; A_0 is a normalization factor; and l is the distance between the source and destination.

Figure 3.3 shows the behavior of the acoustic path loss for the variation of the transmission frequency (a), the network radius (b) and number of nodes (c). Also our model is compared to a Monte-Carlo simulation. The model scenario is for 1 km of radius, 18.5 kHz of central transmitting frequency, 10 nodes and 1.5 as spreading factor, as shown in Table 3.1.

Table 3.1: One-Hop Acoustic path loss. Default parameters

PARAMETER	DEFAULT VALUE
Transmission frequency (f)	18.5 kHz
Number of nodes (N)	10 $Nodes$
Network radius (R)	1 km
Spreading factor (k)	1.5

For the simulation, a sphere with radius R (1 km as default) was created and N nodes (10 as default) were distributed inside randomly and uniformly. Then the path loss from all the nodes to the central one was calculated, considering that it will always be the receiver node, and the average value is found.

The used distance for the model calculus was the average value of the random variable (RV) **X**. This RV represents the distance to the central node and it can be obtained, for a sphere with radius R, as

$$E[\mathbf{X}] = \frac{3R}{4}. \tag{3.9}$$

The procedure to obtain Eq. (3.9) is detailed in Section 5.3.1.

(a) Varying transmission frequency.

(b) Varying network radius.

(c) Varying number of nodes.
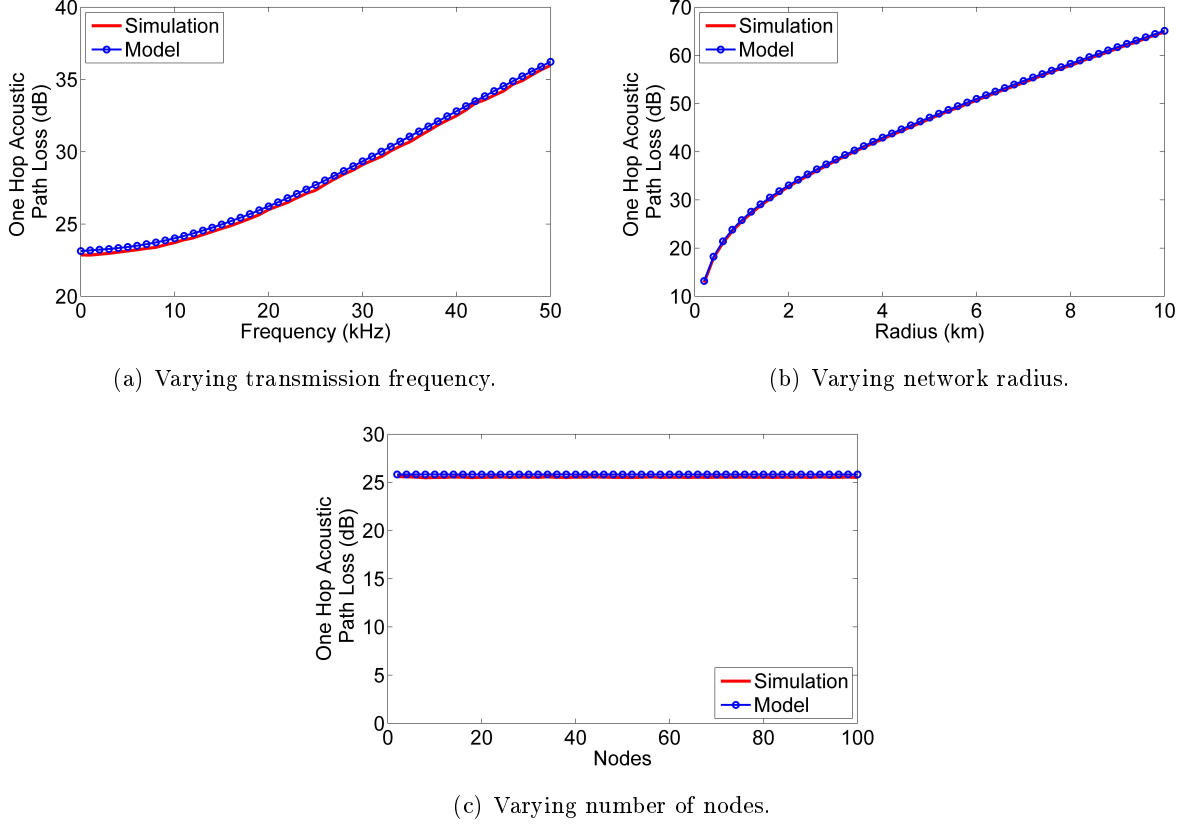
Figure 3.3: Acoustic Path Loss. Simulation versus model. See Table 3.1.

The first thing to note is that the acoustic path loss increases with the transmission frequency. This is caused by the increase of the absorption coefficient $(a(f))$ as we will see further. The acoustic path loss also increases with the network radius, due to the increase of the transmission distance. This behavior is clearly represented in Eq. (3.7) and Eq. (3.8). Finally, Figure 3.3 (c) demonstrates that the number of nodes do not affect the acoustic path loss. The summary of the obtained results from these figures is in Table 3.2.

3.4.2 Absorption Loss and Absorption Coefficient

The absorption losses represent the energy losses in form of heat, due to the viscous friction and ionic relaxation that occur as the sound wave propagates outwards [8]. From Eq. (3.8), the absorption losses can be given by

Table 3.2: Acoustic path loss.

PARAMETER	VARIATION	ONE-HOP ACOUSTIC PATH LOSS
Transmission frequency (f)	Increases	Increases
Number of nodes (N)	Increases	Constant
Network radius (R)	Increases	Increases

$$A_{AbsLoss}(l, f) = 10l \log_{10}(a(f)) \tag{3.10}$$

where $a(f)$ is the absorption coefficient and l is the transmission distance. The absorption coefficient can be calculated by several forms, a good approximation is the Thorp's empirical equation [11], that calculates the absorption coefficient in (dB/km). It is given by

$$a(f) = 0.11\frac{f^2}{1 + f^2} + 44\frac{f^2}{4100 + f^2} + 2.75 \times 10^{-4} f^2 + 0.003 \tag{3.11}$$

for frequencies bigger than hundreds of Hertz and for lower frequencies it is given by

$$a(f) = 0.002 + 0.11\frac{f^2}{1 + f^2} + 0.011f^2. \tag{3.12}$$

Figure 3.4 shows the behavior of the absorption coefficient for different values of central transmission frequency. This coefficient increases rapidly with frequency, imposing a limit on the maximal usable frequency for an acoustic link for a given distance [11].
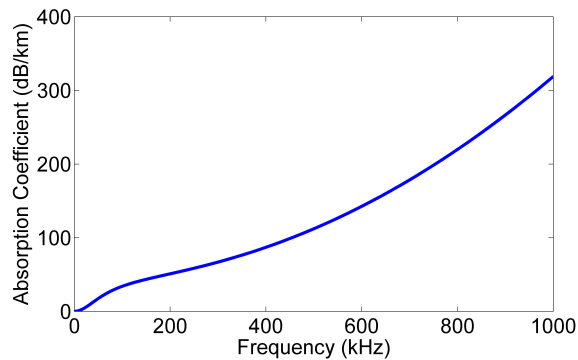
Figure 3.4: Absorption coefficient varying transmission frequency.

3.4.3 Spreading Loss and Spreading Factor

The spreading loss is due to the ever-increasing area covered by the same amount of the sound signal energy, as a wave front moves outward from the source [8], and from Eq. (3.8), it can be given by

$$A_{SprLoss}(l) = 10k \lg l, \tag{3.13}$$

where l is the transmission distance and k is the spreading factor.

The spreading factor represents the spreading type, $k = 1$ for spherical spreading, $k = 2$ for cylindrical spreading and $k = 1.5$ for practical spreading. The spherical spreading describes the decrease in level when a sound wave propagates away from a source uniformly in all directions. This situation occurs generally for a sound source at mid-depth in the ocean. In Figure 3.5 it is possible to see an example of spherical spreading where the sound generated by a sound source (shown as a white dot) at mid-depth in the ocean is radiated equally in all directions. Sound levels are therefore constant on spherical surfaces surrounding the sound source. Sound levels decrease rapidly as sound spreads out from a sphere with a radius of r_0 to a larger sphere with a radius r [1].
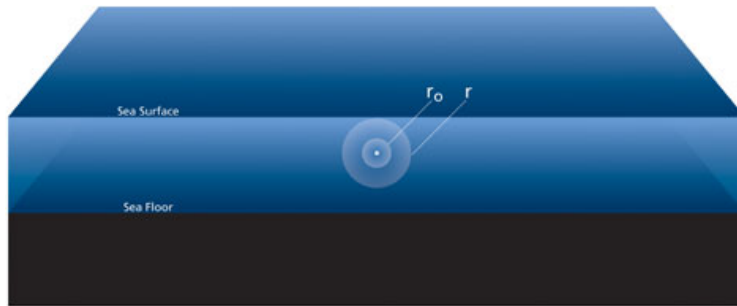
Figure 3.5: Spherical spreading [1].

In the cylindrical spreading, the sound cannot propagate uniformly in all directions from a source in the ocean forever. Beyond some range the sound will hit the sea surface or sea floor. A simple approximation for spreading loss in a medium with upper and lower boundaries can be obtained by assuming that the sound is distributed uniformly over the surface of a cylinder having a radius equal to the range r and a height H equal to the depth of the ocean. In Figure 3.6 it is possible to see an example of cylindrical spreading where the sound generated by a source (shown as a white dot) in mid-ocean cannot continue to spread uniformly in all directions once it reaches the sea surface or sea floor. Once the sound is trapped between the top and bottom of the ocean it gradually begins to spread cylindrically, with sound radiating horizontally away from the source. Sound levels decrease more slowly as sound spreads from a cylinder with a radius of r_0 to a larger cylinder with radius r, compared to the rate of decrease for spherical spreading [1].

The practical spreading is a very used term by the authors [10], [11], [12], where a middle value between spherical and cylindrical spreading is used. The use of the practical spreading is appropriate without losing generality. In this work we use this spreading factor, i.e., $k = 1.5$.

3.4.4 Multipath

The multipath propagation is usually a problem in acoustic communication links. This effect is caused by the replicas of the transmitted signal that reach the receiver, this replicas travel
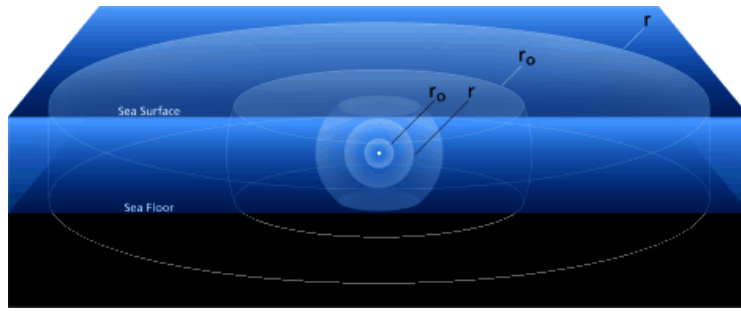
Figure 3.6: Cylindrical spreading [1].

by different path and therefore have different attenuations and delays, possibly causing severe inter-symbol interference (ISI) for acoustic communication.

The reflection and/or refraction are the main causes of the underwater multipath. The reflection of an acoustic wave happens when the wave bounce with the surface or the bottom and reach the receiver, being most probable in shallow water, see Figure 3.7. The refraction is more common in deep water, when the wave speed (sound speed) changes with the depth. Our case of study, as will be explained further, considers a middle depth, more than 1 km from the surface and the bottom, which is deep enough to not consider reflection, but not enough to consider refraction. Therefore, the multipath effect will not be considered in this work.
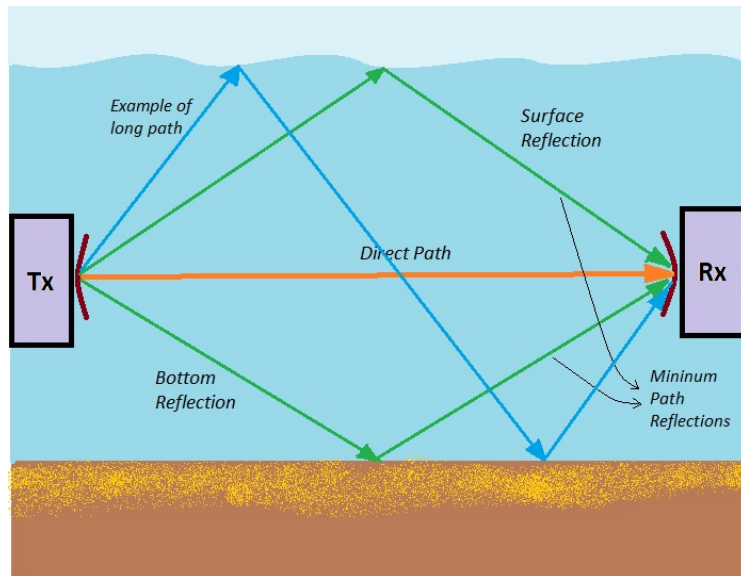
Figure 3.7: Acoustic multipath in a transmission [3].

3.4.5 Doppler Effect

In underwater communications, for short range links, the Doppler effect is irrelevant [3]. This effect is bigger and can be seen more often in Autonomous Underwater Vehicles (AUV), where we have two possible forms of Doppler distortion at the receiver. The Doppler Shifting caused by an apparent shift of frequency with the movement of the vehicles towards or away from each other,

and the Doppler Spreading, that measures the time varying nature of the frequency dispersiveness in the Doppler Spectrum.

In our network topology, which will be explained further, the nodes are fixed and do not move, therefore, we do not consider the Doppler Effect.

3.4.5.1 Noise

Underwater Acoustic Networks (UANs) have many elements that affect the acoustic communication between two nodes, depending on the transmission frequency. A very important impairment is the underwater environmental noise which is caused by several sources. According to [11], [12] and [13] almost all the ambient noise sources can be described as static and continuum Gaussian power spectral density (p.s.d.). The main noise sources p.s.d. in units of $dBre1\mu Pa$ per Hz are: the turbulence (N_{TU}), the ship movement (N_{SH}), the sea movement (N_S) depending on the wind speed (v) in units of ($knots$), and the thermal noise (N_{TH}). These noises are given by

$$10 \log_{10}(N_{TU}(f)) = 30 - 30 \log_{10}(f), \qquad (3.14)$$

$$10 \log_{10}(N_{SH}(f)) = 10 \log_{10}\left(\frac{3 \times 10^8}{1 + 10^4 f}\right), \qquad (3.15)$$

$$10 \log_{10}(N_S(f)) = 40 + 10 \log_{10}\left(\frac{v^2}{1 + f^{\frac{5}{3}}}\right), \qquad (3.16)$$

$$10 \log_{10}(N_{TH}(f)) = -15 + 20 \log_{10}(f). \qquad (3.17)$$

With these equations it is possible to calculate the total noise p.s.d. in ($dBre1\mu Pa$ per Hz) by

$$10 \log_{10}(N_T(f)) = 10 \log_{10}\left(10^{0.1N_T} + 10^{0.1N_{SH}} + 10^{0.1N_S} + 10^{0.1N_{TH}}\right). \qquad (3.18)$$

Figure 3.8 shows the noise p.s.d. behavior for different values of central transmission frequency and 20 $knots$ of wind speed. It is possible to see that depending on the frequency region, one source will have more relevance than the other. Noise caused by turbulence, Eq. (3.14), only might be considered for very low frequencies values ($f < 10Hz$). Shipping noise, Eq. (3.15), is dominant for the $10Hz < f < 100Hz$ region. The bigger impairment for the $100Hz < f < 100kHz$ region is the sea movement noise, Eq. (3.16), that depends on the wind speed, and it is important to highlight that it is the operating region used by the majority of acoustic systems. For frequencies higher than $100kHz$ the thermal noise, Eq. (3.17), is the main one. Table 3.3 summarizes the obtained results.
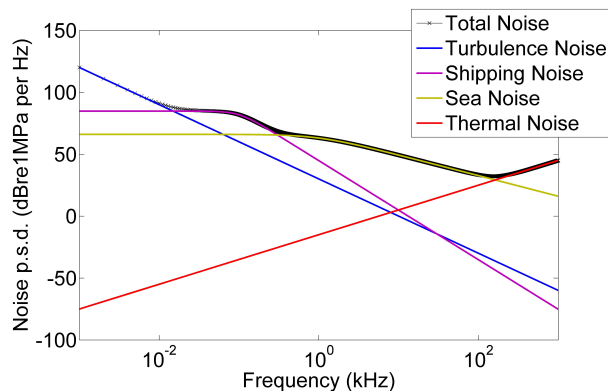
Figure 3.8: Underwater noise p.s.d. varying transmission frequency.

Table 3.3: Noise.

FREQUENCY BAND	MAIN NOISE	EQUATION
$f < 10Hz$	Turbulence	3.14
$10Hz < f < 100Hz$	Shipping	3.15
$100Hz < f < 100kHz$	Sea movement	3.16
$f > 100kHz$	Thermal	3.17

3.5   Underwater Medium Access Control (MAC) Protocols

Medium Access Control (MAC) protocols manage the access to the communication medium. Its main objective is to avoid collision, but also deal with other factors, such as energy consumption, scalability and latency [9].

The two classical schemes that MAC protocols can be divided (contention-free and contention-based schemes) are still valid in UANs.

Contention-free schemes assign different frequency bands, time slots or codes to different users of the communication medium. Because of that, nodes do not compete in order to obtain access to the channel. The three basic types of this scheme are: time-division multiple access (TDMA), frequency-division multiple access (FDMA) and code-division multiple access (CDMA) [9], see Figure 3.9

Contention-based MAC protocols avoid the pre-allocation of resources, and the nodes must compete with each other to gain access to the channel. This type of protocols usually relies on random access to distribute transmissions and normally also includes some recovery mechanism in case a collision occurs.

Figure 3.10 shows a classification of MAC protocols obtained from [9]. This classification do not consider that there exists some protocols that have characteristics of contention-based and contention-free schemes.
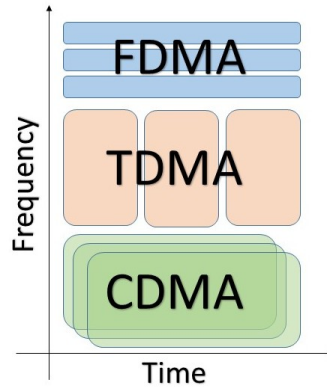
Figure 3.9: Contention-free MAC protocols.
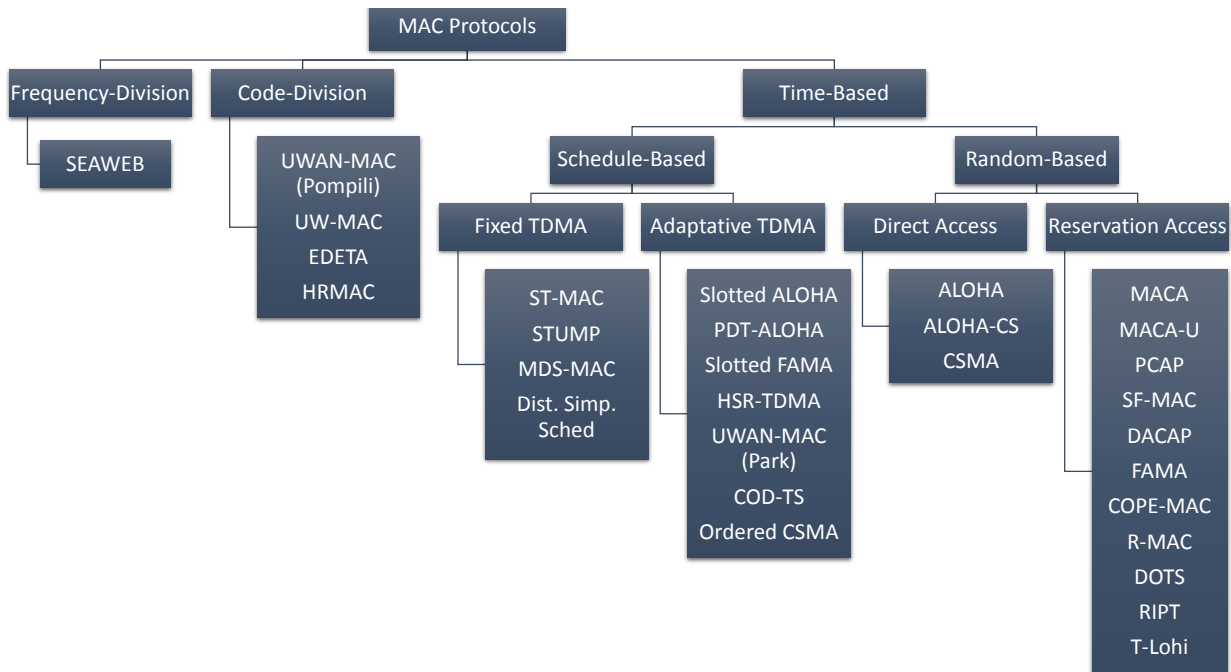
Figure 3.10: MAC protocols.

3.5.1 MAC Protocols for Underwater Acoustic Sensor Networks

Because the long propagation delays of underwater transmissions, these networks suffer from space uncertainty, and it is necessary to consider the location of the receivers and their possible interference. Communications based on radio-frequency (RF) for the air medium do not consider these aspects, because the transmission speed is very fast (light speed) and it is possible to say that all the receptors are at the same distance from the transmitter, therefore, it is only important to consider the time uncertainty (transmission time). Acoustic communications are slower, travel at the sound speed velocity (1500 m/s approximately for an underwater acoustic wave), causing the space uncertainty which is a very important factor, along with the time uncertainty. This problem is common known as the space-time or space-temporal uncertainty, [9] and [14].

The long propagation delays in UANs induce also spatial unfairness, i.e, the packet reception time depends on the distance to the transmitter, then, the channel becomes free first at the transmitter and later on at the receiver. Hence, nodes closer to the transmitter are able to gain access to the channel before nodes located closer to the receiver [9].

3.5.2 ALOHA MAC Protocol

Traditional MAC protocols try to handle the temporal uncertainty using several mechanisms: synchronizing the transmission (Slotted-ALOHA), unique transmission slot (TDMA), or sensing the channel before transmitting (CSMA). All the mechanism are considered at the transmitter, assuming that they are also valid for the receptor. Disregarding the space uncertainty, this is true for RF communication in air medium as explained in Section 3.5.1, but it is not the case for underwater acoustic communications [14].

ALOHA MAC protocol [15], unlike, Slotted-ALOHA [16], does not consider the temporal uncertainty and as proved in [14] it is important to consider both (temporal and space) uncertainty. In ALOHA the analysis is centered at the transmitter assuming that all the receivers are at the same distance, and the total offered load to the network is a combination of Poisson arrivals and exponential retransmissions, and it is a Poisson process with parameter G.

Figure 3.11 shows the ALOHA behavior, where $V.I.$ is the vulnerability interval, i.e., time interval relative to a sender's transmission within each other node's transmission causes collision [14] and T is the packet transmission time. Therefore, for ALOHA, the vulnerability time ($V.I.$) is equal to $2T$. The throughput of ALOHA is given by

$$TH_{ALOHA} = Ge^{-2G}. \qquad (3.19)$$
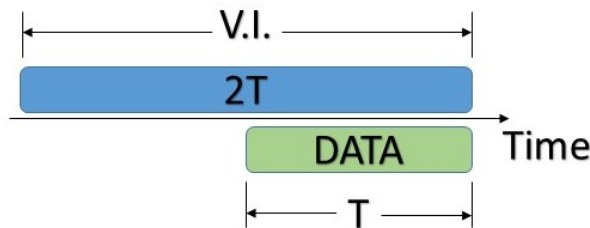
Figure 3.11: ALOHA MAC Protocol.

If the spatial uncertainty is consider in ALOHA, the throughput is the same because if we focus at the receptor side, the packet arrivals is still a Poisson process, with the same parameter. Moreover, when latency is not present, we do not have changes in the collision probability. That is, to not consider the spatial uncertainty (propagation delays) do not affect the behavior of the ALOHA MAC protocol, because its duality with the temporal uncertainty which is neither considered [14]. This issue together with the protocol simplicity make us to use ALOHA. Note that

the purpose of this work is not the study of the propagation delay at UANs neither how it affects the acoustic communication.

3.6 Underwater Acoustic Sensor Networks Overview and Research

In [11] Stojanovic realizes that the path loss in an acoustic channel not only depends on the transmission distance, but also on the frequency of the signal, resulting that the useful bandwidth depends on the transmission distance. With this result it is possible to show that a better throughput is achieved with multiple short hops, instead of a single long hop. Stojanovic uses a pre-specified SNR to obtain the necessary transmission power and quantifies the channel bandwidth and capacity.

In [17] Stefanov and Stojanovic consider the behavior of underwater acoustic ad hoc networks in the presence of interference. They assume an uniform distribution of the nodes inside a limited area and study the sustainable number of hops through the network, the end-to-end frame error probability, the power consumption and the bandwidth allocation. The authors demonstrate also that the desired connectivity level can be achieved by a judicious selection of the operating frequency.

Felambam et al. in [18] investigate the optimal node location for an initial underwater wireless sensor network. The authors formulate the problem as a non-linear mathematical program with the objectives of minimizing the transmission loss for a given number of nodes inside a volume. The obtained solution was the location of each node represented as a truncated octahedron to fill out the 3D space.

In [9] Climent et al. make a survey of the advances and future trends in Physical, MAC and Routing layers in underwater acoustic wireless sensor networks. This work shows an overview of the current research on this area, analysing the state of the art. This paper also summarizes their security threads and surveys the currently proposed studies.

Zhu et al. in [19] investigate two critical issues found in the commercial modem-based real systems: low transmission rates and long preambles. These impairments drastically reduce the throughput of the existing MAC protocols in practical world. The article analyses the impact of the two newly found modem characteristics on the random access-based MAC and handshake-based MAC. The author believes based on the analysis in the paper, that time sharing-based MAC protocols is very promising and proposes a time sharing-based MAC protocol and calculate its nodal throughput, resulting in a better performance.

Murugan and Natarajan in [20] simulate an underwater acoustic communication using passive time reversal (PTR) technique with transmitted and receiver nodes separated in range by 4 km in 120 m deep water. The PTR system is simulated for single-user and multi-user. The authors transmit through the underwater channel using Quadrature Phase Shift Keying (QPSK) modulation. The system performance was analysed with the implementation of the PTR system, archiving a better Bit Error Rate (BER). Also, BER is found to vary with the distance among the users and

with the number of users.

However, previous works did not analysed the SNIR with interference caused by other concurrent transmission nodes employing a random medium access control protocol like ALOHA as function of network radius, transmission frequency, number of nodes and transmission power. Accordingly, interference depends on the MAC scheme employed and on the network parameters. Our paper investigates the SNIR and BER for underwater acoustic networks using the ALOHA MAC protocol as a function of such important network parameters.

3.7   Conclusions

A brief history about UW-AC and its fundamentals that will allow us to relate the different variables of the medium, i.e., intensity, power, pressure and others, were presented in this chapter. After that, the characteristics of the acoustic channel were described, reporting the main parameters of the medium, such as acoustic path loss, absorption loss, spreading loss and noise. With the purpose to validate the Urickťs model and study its behavior, it was modeled and compared with a Monte-Carlo simulation. The same was done for the Thorpťs empirical equation.

Also, it was discussed the medium access control (MAC) protocols for underwater acoustic networks, explaining the behavior of the space-temporal uncertainty that is present at UANs, and the relationship between both, where we choose to work with ALOHA MAC protocol due to its simplicity and generality, remarking that in this case is not necessary to consider the spatial uncertainly, because time uncertainty does not affect the ALOHA operation. Finally, a brief summary of the main investigations and results from the area researches about UANs was shown.

Chapter 4

Underwater Acoustic Modulation Schemes

This chapter briefly reviews the analog and digital modulation schemes. It explains also the differences between the non-coherent and coherent modulations, discussing the advantages and disadvantages of each one. After that, it briefly summarizes the latest modulation techniques and its advantages for the underwater medium. Finally, we discuss our choice for the Binary Phase Shift Keying (BPSK) modulation.

4.1 Introduction

The modulation of a signal is the transformation of one or more parameters (amplitude, phase or frequency) of a periodic waveform (carrier signal) from another signal (modulating signal) which contains the information to be transmitted. The modulated signal spectrum must match with the communication channel characteristics. The modulation process must be reversible, such that the receiver can recover the information by demodulation.

Considering that the available bandwidth at an underwater acoustic channel is limited, it is important to pursue the maximal spectral efficiency. Other important aspect to consider is the energy consumption, because in almost all cases, the position of the node is unreachable, which implies that the node dies with battery depletion. Considering these aspects, several works have been developed trying to find the optimal modulation scheme [9].

This chapter begins explaining the analog and digital modulations. Inside the digital modulations, it explains the non-coherent and the coherent types. Finally, it describes a brief summary of the latest modulations techniques that can be used for underwater acoustic networks (UANs) and selects a modulation technique to use in our research.

4.2 Analog and Digital Modulations

The modulation of a signal can be analog for analog (continuum) modulating signals, or digital when the modulating signal is discrete. The analog modulation usually occupies less bandwidth, but the digital one is more robust. In addition, the analog to digital converter (ADC) allows us to transform an analog signal to a digital one and recover it with a digital to analogic converter (DAC), as a result, an all digital network is obtained.

In analog modulations the carrier is a sinusoidal signal and its amplitude, phase or frequency may vary proportionally to the information message signal. Therefore, it is possible to have Amplitude Modulation (AM) as in Figure 4.1, Phase Modulation (PM) and Frequency Modulation (FM) as in Figure 4.2. The digital modulations will be explained in the following sections.
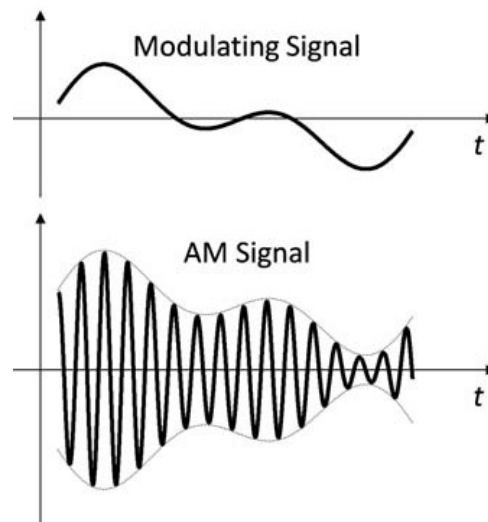
Figure 4.1: Conventional AM.
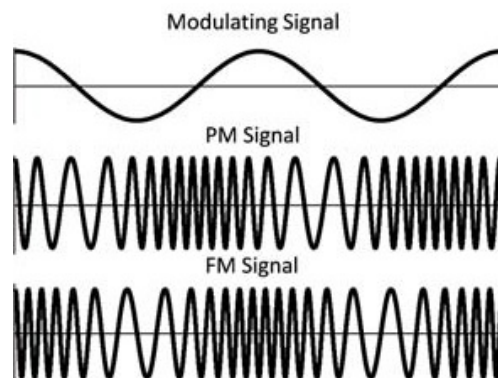
Figure 4.2: Conventional PM and FM.

4.3 Non-Coherent Modulation Schemes

The earliest developed works in acoustic communications were mainly focused on non-coherent modulation methods based on energy detection, particularly [9]. Non-coherent systems do not need carrier phase information and use methods like square law (push detection or energy detection) to recover the transmitted data at the receiver end. Several non-coherent modulations schemes were developed, such as: *On-Off Keying* (OOK) [21] and [3], with not return to zero (NRZ) with a relationship between the Bit Error Rate (BER) and the Signal-to-Noise Ratio (SNR) given by

$$BER_{NC-NRZ-OOK} = \frac{1}{2}erf\left(\frac{1}{2\sqrt{2}}\sqrt{SNR}\right) \tag{4.1}$$

and with return to zero (RZ) by

$$BER_{NC-RZ-OOK} = \frac{1}{2}erf\left(\frac{1}{2}\sqrt{SNR}\right). \tag{4.2}$$

Another non-coherente shceme is *Frequency Shift Keying* (FSK), [22] and [23] which BER is given by

$$BER_{NC-FSK} = \frac{1}{2}e^{-\frac{SNR}{2}}. \tag{4.3}$$

This type of modulation has as advantage its simplicity and reliability; therefore, the modems do not need high resource processors with higher power consumption. However, the spectral efficiency is low, due to the inter-symbol and inter-carrier interferences generated by Doppler and multipath spread [9].

4.3.1 Coherent Modulation Schemes

In the coherent systems, carrier phase information at the receiver is needed, and it uses matched filters to detect and decode the transmitted data. With the purpose to increase the spectral efficiency and the communication range, several alternatives have been explored, such as *On-Off Keying* (OOK) [3], with a relationship between BER and SNR, when an Additive White Gaussian Noise (AWGN) is assumed [24] and [25], given by

$$BER_{C-RZ-OOK} = Q(\sqrt{SNR}). \tag{4.4}$$

Another scheme is *Frequency Shift Keying* (FSK) [3] given by

$$BER_{C-FSK} = Q(\sqrt{SNR}). \tag{4.5}$$

In addition, *Phase Shift Keying* (M-PSK) [3] and [26], is another technique, in which BER is given by

$$BER_{BPSK} = BER_{QPSK} = Q(\sqrt{2SNR}), \tag{4.6}$$

or

$$BER_{8-PSK} = 2Q\left(\sqrt{2SNR} \times sin\left(\frac{\pi}{8}\right)\right), \tag{4.7}$$

or

$$BER_{16-PSK} = 2Q\left(\sqrt{2SNR} \times sin\left(\frac{\pi}{16}\right)\right) \tag{4.8}$$

for M=2 and M=4 , M=8, and M=16, respectively. The M-PSK modulation schemes are shown in Figure 4.3. Other type of coherent modulation is the *Quadrature Amplitude Modulation* (QAM) with a relationship between BER and SNR given by

$$BER_{M-QAM} = \frac{4}{k}\left(1 - \frac{1}{\sqrt{M}}\right)Q\left(\sqrt{\frac{3\overline{k}}{M-1}SNR}\right) \tag{4.9}$$

where $\overline{k}$ is the number of bits/symbol and it is given by

$$\overline{k} = \log M. \tag{4.10}$$

$Q(x)$ represents the Q function and can be expressed as

$$Q(x) = \int_x^\infty \frac{1}{\sqrt{2\pi}}e^{-\frac{t^2}{2}}\,dt. \tag{4.11}$$

These modulation schemes have a bigger communication rate and spectral efficiency, but the modem complexity and energy consumption increase as well.

The obtained BER for BPSK is the same as that for QPSK with the advantage that for the same bandwidth it is possible to have a double of transmission bit rate for the QPSK case. However, for our analysis, we select the BPSK modulation due to its simplicity, robustness and and because it is very used by the underwater acoustic modems.

4.3.2   Special Modulation Schemes

In order to achieve a better use of the bandwidth, it is possible to use different advanced modulation schemes such as: *Direct-Sequence Spread-Spectrum* (DSSS), [27]; *Orthogonal Frequency-Division Multiplexing* (OFDM), [28]; and *Multiple-input-Multiple-output* (MIMO), [29].

The most used scheme among these is the OFDM. This modulation scheme is considered robust when multipath effects are present, and it is very common for underwater channels. The OFDM divides the available usable spectrum into many narrowbands, and each one can be modulated using various modulation formats (BPSK, QPSK, QAM).

(a) BPSK Modulation.

(b) QPSK Modulation.

(c) 8-PSK Modulation.
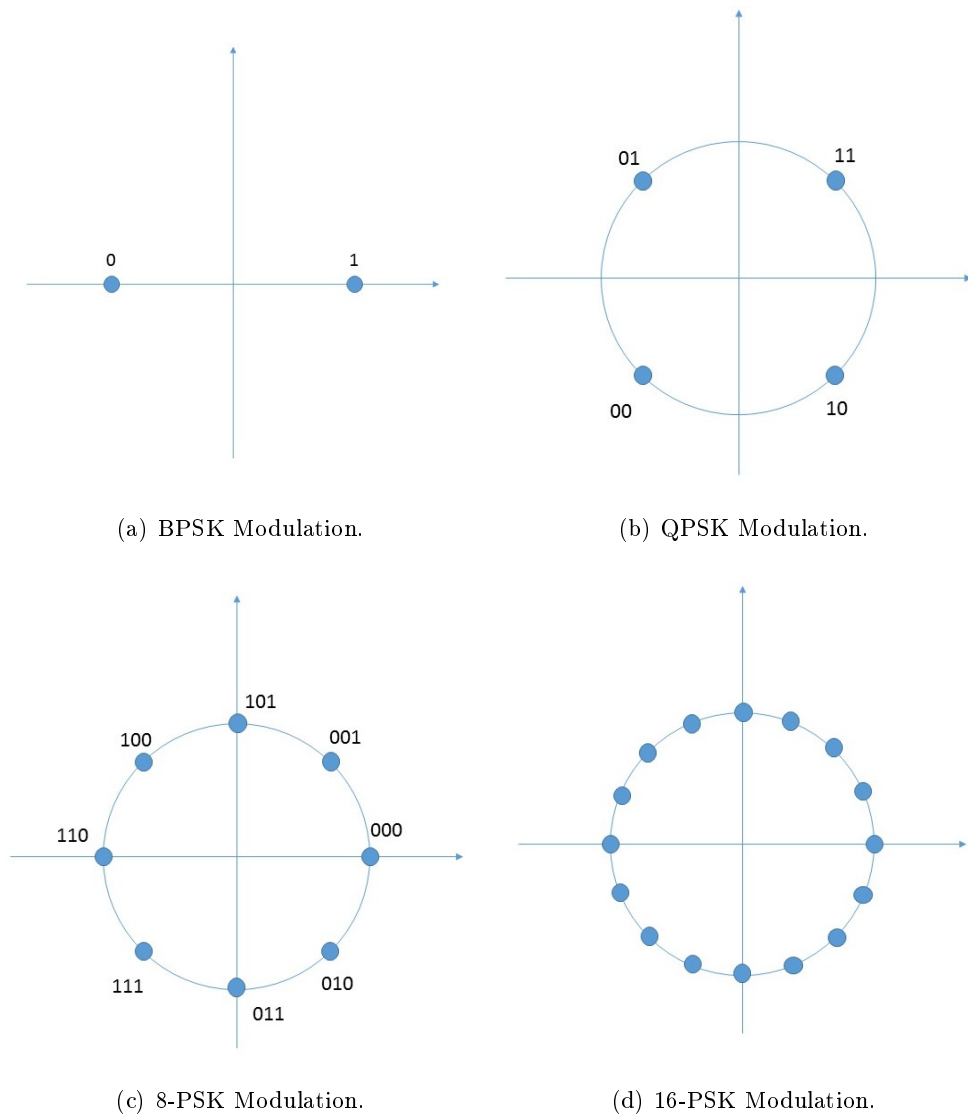
(d) 16-PSK Modulation.

Figure 4.3: M-PSK Modulation.

4.4   Conclusions

A brief summary about the modulation techniques was given in this chapter. The difference between analog and digital modulation was explained, specifying the advantages of each one. Furthermore, the types of modulations that can be used for UANs was detailed, and the Binary Phase Shift Keying (BPSK) was selected for our research.

Chapter 5

Network Modeling

This chapter begins by explaining the routing strategy selected for our network. The average number of hops, the average distance between nodes and the central node (receiver node), the average distance of the hop according to the selected routing strategy, the average distance between nodes and the average deviation are obtained. Finally, the behavior of the average number of hops with the variation of the transmission frequency, the number of nodes, the network radius and the maximal aperture angle are analysed, and the simulation is compared to the model.

5.1 Introduction

It is of great relevance to understand the network topology assumed in this work, based on that we can obtain the average number of hops in a route. This is the objective of this chapter. We will be able to obtain further in this work the End-to-End Bit Error Rate (BER) and analyse the behavior of the underwater acoustic networks (UANs) with the variation of the network's main parameters, such as number of nodes, transmission frequency, network radius, maximal aperture angle and transmitted power, from the average number of hops.

Our network will consist in a three dimensional sphere with radius R and N nodes distributed randomly and uniformly. Therefore, to obtain the average number of hops it is necessary to first calculate the average distance between the nodes inside the sphere and the central node (assuming that it is always the receiver node), the average distance of the hop according to the routing strategy and the average deviation. The probability density function (p.d.f.) of the random variable that represents the distance between two nodes inside the sphere, is another important parameter obtained in this chapter. All of these elements are of great relevance in our work, and will be very useful further to obtain the Signal-to-Noise plus Interference Ratio (SNIR) and the End-to-End BER.

5.2 Network Topology and Routing Strategy

This work considers the network topology from [30] and [31], but here it is adapted to a three-dimensional space which is more appropriate to model the underwater environment. Accordingly, N nodes are randomly and uniformly distributed inside a sphere with radius R. Therefore it is assumed that a node is likely located anywhere within the sphere and the position of one node is independent of the position of the other nodes.

It is assumed, as in [30], that the communication path between the source and the destination node is determined during the discovery phase of the route. The selection of the routing protocol may vary depending on what is intended to achieve, for example, the route can be selected in order to achieve the minimum number of hops or the largest energy savings. In our case, the routing strategy consists of a sequence of hops through intermediate nodes, each one with the minimum possible length, towards the direction of the destination node, in order to reduce the interference caused by other transmitting nodes improving the Signal-to-Noise plus Interference Ratio (SNIR).

To this end, a reference line between the source node and the destination node (assumed at the center of the sphere) is drawn. The transmitting node selects for the next hop the nearest neighbour node within a sector of angle θ centered on the reference line, as shown in Figure 5.1. Therefore, the angle θ determines how the path can deviate from the reference line and how long the hop can be. If θ is very large, it is more likely that the route deviates more from the reference line, but the hop can be smaller, and vice-versa. Figure 5.1 shows an example of the route, where the angle ϕ represents how much the path is actually deviated from the reference line.
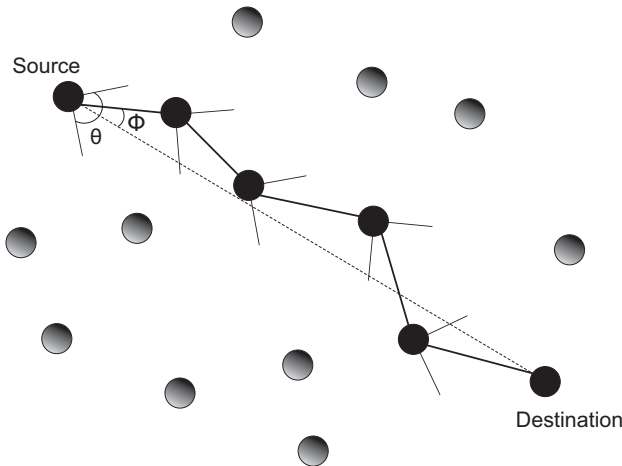
Figure 5.1: Routing strategy.

5.3 Average Number of Hops

The average number of hops $(\overline{n}_h)$ in the route should be inversely related to the average length of the hop. With the routing strategy described in Section 5.2, it is possible to project each hop over the reference line and to approximate $\overline{n}_h$ as

$$\overline{n}_h = \frac{E[\mathbf{X}]}{E[\mathbf{Y}]E[cos(\phi)]}, \tag{5.1}$$

where $E[\mathbf{X}]$ is the average length of the reference line, i.e., it is the average distance between a node and the receiver node (assumed at the center of the sphere), $E[\mathbf{Y}]$ is the average hop distance according to that described in Section 5.2 routing strategy, and $E[cos(\phi)]$ is the average deviation, ϕ represents the real deviation from the reference line.

5.3.1   Average Length of the Reference Line

The average distance between any node and the receiver node within a sphere of radius R (average length of the reference line) can be determined by

$$E[\mathbf{X}] = \int_0^R x f_{\mathbf{X}}(x) dx \tag{5.2}$$

where the receiver node is located in the center of the sphere. In Eq. (5.2) the random variable (RV) $\mathbf{X}$ represents the distance between any node to the central node (receiver).

The cumulative density function (c.d.f.) of the RV $\mathbf{X}$ represents the probability that the distance from any node, within a sphere of radius R, to a node located at the center of the sphere, is less than or equal to a certain value x, i.e., the probability of knowing that the destination node is at the center of the sphere, the source node is within the sphere with center at B and radius x, as in Figure 5.2. This analysis is possible because the node's location is uniformly distributed in the topology described in Section 5.2. Accordingly, considering that $V_E(x)$ is the volume of the sphere with radius x and $V_E(R)$ is the sphere with radius R, it is possible to determine the c.d.f. of $\mathbf{X}$ as

$$F_{\mathbf{X}}(x) = \begin{cases} \frac{V_E(x)}{V_E(R)} & 0 < x < R \\ 0 & \text{otherwise} \end{cases} = \begin{cases} \frac{x^3}{R^3} & 0 < x < R \\ 0 & \text{otherwise} \end{cases}. \tag{5.3}$$

With the c.d.f. of the RV $\mathbf{X}$ obtained by Eq. (5.3), it is possible to calculate its probability density function (p.d.f.) by differentiating it, therefore

$$f_{\mathbf{X}}(x) = \begin{cases} \frac{3x^2}{R^3} & 0 < x < R \\ 0 & \text{otherwise} \end{cases}. \tag{5.4}$$

Finally by substituting Eq. (5.4) into Eq. (5.2), we obtain that the average distance between any node and the central one, inside a sphere with radius R, i.e., the average length of the reference line is given by

$$E[\mathbf{X}] = \frac{3R}{4}. \tag{5.5}$$
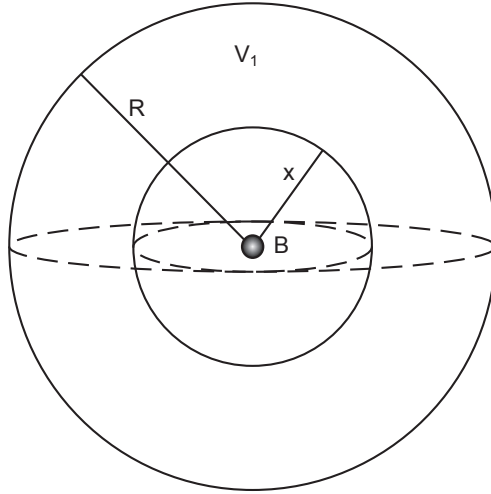
Figure 5.2: Average length of the reference line.

5.3.2 Average Hop Distance

With the network's topology described in Section 5.2, it is possible to determine the average hop distance, i.e., the mean of the random variable (RV) $\mathbf{Y}$, as follows. Considering that the probability of the RV $\mathbf{Y}$ be greater than some distance y equals to the probability of not having any nodes inside a volume of radius y, and angle θ, (V_2 in Figure 5.3), this probability is given by

$$P\{\mathbf{Y} > y\} = 1 - P\{\mathbf{Y} \leqslant y\} = 1 - F_{\mathbf{Y}}(y). \qquad (5.6)$$

Then, we are able to deduce the cumulative density function (c.d.f.) of the RV $\mathbf{Y}$ as

$$F_{\mathbf{Y}}(y) = 1 - P\{\mathbf{Y} > y\} \qquad (5.7)$$
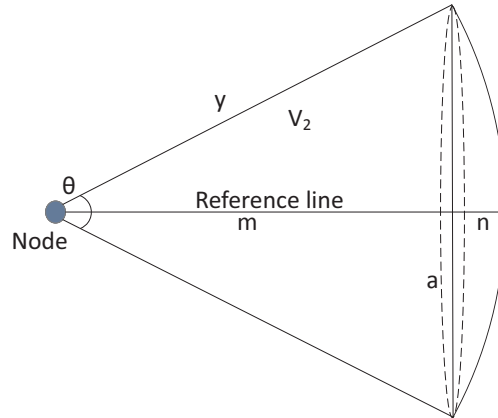
Figure 5.3: Average distance of the hop.

Considering that the node's position is independent and uniformly distributed, the amount of nodes inside a volume has the same behavior as a Poisson distribution with parameter λ and

spatial density ρ_s. We need to know the case for zero nodes inside the region V_2 in the Figure 5.3, given by

$$P\{\mathbf{Y} > y\} = P\{Z = 0\} = e^{-\lambda}\frac{\lambda^0}{0!} = e^{-\lambda}, \tag{5.8}$$

where the RV $\mathbf{Z}$ represents the amount of nodes inside V_2 in Figure 5.3. The parameter λ depends on the relationship between the number of nodes (N) and the sphere's volume (V_1) in Figure 5.2, i.e., the spatial density (ρ_s), and the volume of the region (V_2) in Figure 5.3. Therefore, it can be obtained by

$$\lambda = \rho_s V_2 = \frac{N}{V_1}V_2. \tag{5.9}$$

The volume (V_1) of the sphere in Figure 5.2 is given by

$$V_1 = \frac{4}{3}\pi R^3. \tag{5.10}$$

The volume of the region (V_2) in Figure 5.3 depends on y and the θ angle, and it is given by

$$V_2 = \frac{1}{3}(\pi a^2 m) + \frac{\pi n^2}{3}(3y - n) = \frac{1}{3}\pi y^3[\cos(\theta/2) - \cos^3(\theta/2)] + \frac{1}{3}y^3[2 - 3\cos(\theta/2) + \cos^3(\theta/2)], \tag{5.11}$$

therefore

$$V_2 = \frac{2}{3}\pi y^3[1 - \cos(\theta/2)]. \tag{5.12}$$

Using Eq. (5.8) and Eq. (5.12) to Eq. (5.7), it is possible to obtain the c.d.f. of the RV $\mathbf{Y}$ as

$$F_{\mathbf{Y}}(y) = 1 - e^{-\frac{2}{3}\pi\rho_s[1-\cos(\theta/2)]y^3} \tag{5.13}$$

Thus, differentiating Eq. (5.13) with respect to y, we obtain the probability density function (p.d.f.) of the RV $\mathbf{Y}$, given by

$$f_{\mathbf{Y}}(y) = \frac{\partial F_{\mathbf{Y}}(y)}{\partial y} = 2\pi\rho_S y^2[1 - \cos(\theta/2)]e^{-\frac{2}{3}\rho_s\pi y^3[1-cos(\theta/2)]}. \tag{5.14}$$

Because we are working with a sphere of radius R, it is necessary to normalize the p.d.f. of $\mathbf{Y}$. With that purpose we obtain first the normalization factor by

$$NF = \int_0^R f_{\mathbf{Y}}(y)dy = 1 - e^{-\frac{2}{3}\rho_s\pi R^3[1-cos(\theta/2)]}. \tag{5.15}$$

Therefore the normalize p.d.f. of $\mathbf{Y}$ is given by

$$f_{\mathbf{Y}_N}(y) = \frac{2\pi\rho_s y^2[1 - \cos(\theta/2)]e^{-\frac{2}{3}\rho_s\pi y^3[1-cos(\theta/2)]}}{1 - e^{-\frac{2}{3}\rho_s\pi R^3[1-cos(\theta/2)]}}. \tag{5.16}$$

Finally, it is possible to calculate the average hop distance as

$$E[\mathbf{Y}] = \int_0^R y f_{\mathbf{Y}_N}(y)dy. \tag{5.17}$$

It is important to remark that this integral does not have a close solution, only a numerical solution.

5.3.3 Average Deviation From The Reference Line

The real deviation angle from the reference line (ϕ) is uniformly distributed in the interval $(\frac{-\theta}{2};\frac{\theta}{2})$, because θ is the maximal allowed deviation angle from the reference line. Considering this, it is possible to obtain its p.d.f. as

$$f_\Phi(\phi) = \frac{1}{\frac{\theta}{2} - \frac{-\theta}{2}} = \frac{1}{\theta} \tag{5.18}$$

and its mean as

$$E[cos(\phi)] = \int_{-\frac{\theta}{2}}^{\frac{\theta}{2}} cos(\phi)f_\Phi(\phi)d\phi = \int_{-\frac{\theta}{2}}^{\frac{\theta}{2}} cos(\phi)\frac{1}{\theta}d\phi = \frac{2}{\theta}sin\left(\frac{\theta}{2}\right). \tag{5.19}$$

5.4 Average Distance Between Nodes

Consider $\mathbf{D}$ as the random variable (RV) that represents the distance between nodes 1 and 2 in Figure 5.4. Also, consider the RV $\mathbf{X}$ representing the distance between node 1 and the center of the sphere (Point B) (length of the reference line), obtained in Section 5.3.1, with p.d.f. given by Eq. (5.4). Noting that $f_{\mathbf{D}|\mathbf{X}}(d|x)$ is the conditional probability that node 2 is located at a distance d from node 1, given that node 1 is at a distance x from the center of the sphere with radius R. Then, the probability density function (p.d.f.) of the RV $\mathbf{D}$ can be expressed as

$$f_{\mathbf{D}}(d) = \int_0^R f_{\mathbf{D}|\mathbf{X}}(d|x)f_{\mathbf{X}}(x)dx \tag{5.20}$$

We compute the p.d.f. of the RV $\mathbf{D}$ separately for the two possible cases: $0 \leq d \leq R$ and $R \leq d \leq 2R$.

Case 1: $0 \leq d \leq R$.

For this case, there exists two regions of x where $f_{\mathbf{D}|\mathbf{X}}(d|x)$ has a different behavior: $0 \leq x \leq R - d$ and $R - d \leq x \leq R$. Let's examine each one separately.

Case 1.1: $0 \leq x \leq R - d$.
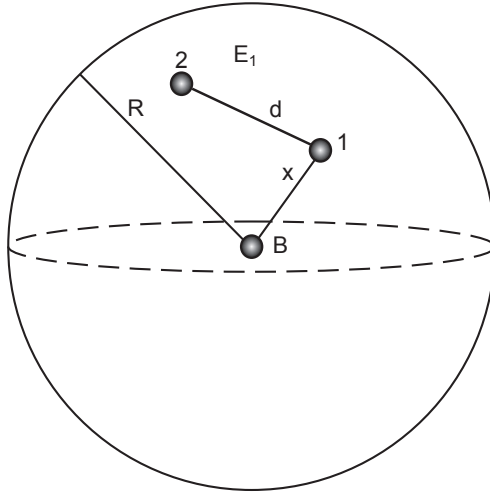
Figure 5.4: Average distance between nodes.

Figure 5.5 shows that the entire region is inside the sphere $E1$, the distance between node 1 and the center of the sphere cannot be larger than the sphere radius minus the distance between nodes 1 and 2. In this case, due to the uniform distribution of the nodes, the conditional probability $f_{\mathbf{D}|\mathbf{X}}(d|x)$ is the relationship between the area of the Region 1 (R_1) and the volume of the sphere, given by

$$f_{\mathbf{D}|\mathbf{X}}(d|x)_{1.1} = \frac{A_{R_1}}{V_{E_1}} = \frac{4\pi d^2}{\frac{4}{3}\pi R^3} = \frac{3d^2}{R^3}. \tag{5.21}$$
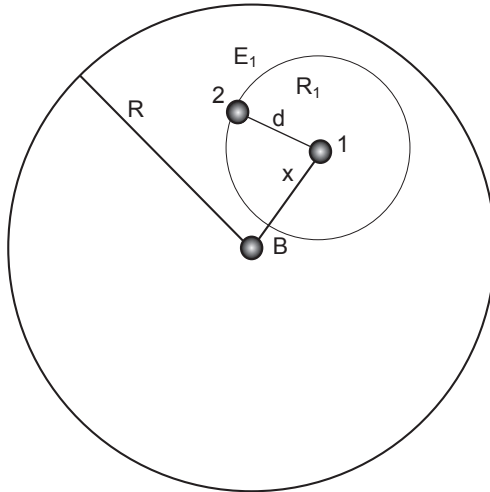
Figure 5.5: Region $0 \leq x \leq R - d$.

Case 1.2: $R - d \leq x \leq R$.

Figure 5.6 shows that in this case part of the region is outside the sphere. This is because the distance from node 1 to the center of the sphere can vary from $R - d$ to the sphere radius. Therefore, the area of the region R_2 inside the sphere is given by

34

$$A_{R_2} = d^2 \int_0^{2\pi} d\phi' \int_0^{\theta} \sin(\theta') d\theta' = 2\pi d^2 \left(1 - \frac{x^2 + d^2 - R^2}{2xd} \right), \tag{5.22}$$

where θ represents the angle between d and x, and it was used trigonometric identities to obtain the final result. Therefore, the conditional probability $f_{\mathbf{D}|\mathbf{X}}(d|x)$ can be obtained as

$$f_{\mathbf{D}|\mathbf{X}}(d|x)_{1.2} = \frac{A_{R_2}}{V_{E_1}} = \frac{2\pi d^2 \left(1 - \frac{x^2 + d^2 - R^2}{2xd} \right)}{\frac{4}{3}\pi R^3} = \frac{3d^2}{2R^3} \left(1 - \frac{x^2 + d^2 - R^2}{2xd} \right). \tag{5.23}$$
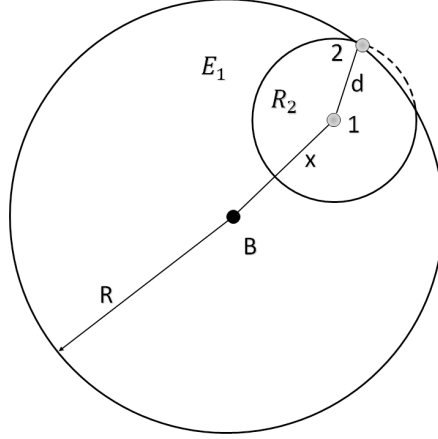
Figure 5.6: Region $R - d \leq x \leq R$.

Therefore, with Eq. (5.21) and Eq. (5.23) the conditional probability $f_{\mathbf{D}|\mathbf{X}}(d|x)_1$ for the region $0 \leq d \leq R$ is given by

$$f_{\mathbf{D}|\mathbf{X}}(d|x)_1 = \begin{cases} \frac{3d^2}{R^3} & 0 \leq x \leq R - d \\ \frac{3d^2}{2R^3} \left(1 - \frac{x^2 + d^2 - R^2}{2xd} \right) & R - d \leq x \leq R \end{cases}. \tag{5.24}$$

and the p.d.f. of the RV $\mathbf{D}$ for the same region is obtained as

$$f_{\mathbf{D}}(d) = \int_0^{R-d} f_{\mathbf{D}|\mathbf{X}}(d|x)_{1.1} f_{\mathbf{X}}(x) dx + \int_{R-d}^{R} f_{\mathbf{D}|\mathbf{X}}(d|x)_{1.2} f_{\mathbf{X}}(x) dx = \frac{3d^2}{R^3} - \frac{9d^3}{4R^4} + \frac{3d^5}{16R^6}. \tag{5.25}$$

Case 2: $R \leq d \leq 2R$.

For this case, we have also two regions for x where $f_{\mathbf{D}|\mathbf{X}}(d|x)$ has a different behavior: $0 \leq x \leq d - R$ and $d - R \leq x \leq R$. Again, let's examine each one separately as in **Case 1**.

Case 2.1: $0 \leq x \leq d - R$.

Figure 5.7 shows that the shell $(R3)$ is outside the sphere. This is because the distance from node 1 to the center of the sphere can vary from zero to $(d - R)$; therefore, the conditional probability $f_{\mathbf{D}|\mathbf{X}}(d|x)$ is zero, i.e.,

$$f_{\mathbf{D}|\mathbf{X}}(d|x)_{2.1} = 0. \tag{5.26}$$
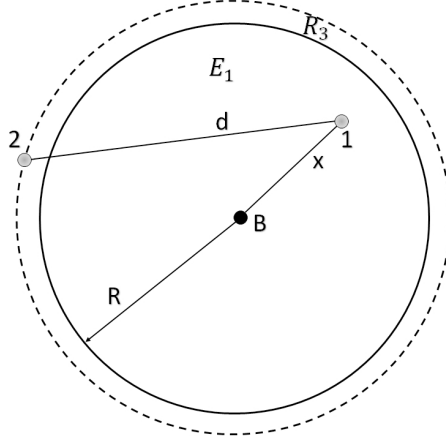
Figure 5.7: Region $0 \leq x \leq d - R$.

Case 2.2: $d - R \leq x \leq R$.

This case is similar to the *Case 1.2.*, the shell intersect the sphere, therefore, we have some region inside the sphere and some region outside the sphere, and the conditional probability $f_{\mathbf{D}|\mathbf{X}}(d|x)$ is equal to Eq. (5.23), so that

$$f_{\mathbf{D}|\mathbf{X}}(d|x)_{2.2} = \frac{A_{R_4}}{V_{E_1}} = \frac{3d^2}{2R^3} \left(1 - \frac{x^2 + d^2 - R^2}{2xd} \right). \tag{5.27}$$
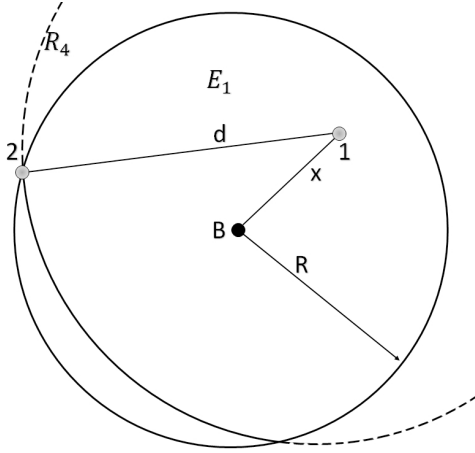
Figure 5.8: Region $d - R \leq x \leq R$.

For the second region of d, using Eq. (5.26) and Eq. (5.27) we have that the conditional probability $f_{\mathbf{D}|\mathbf{X}}(d|x)_2$ is given by

$$f_{\mathbf{D}|\mathbf{X}}(d|x)_2 = \begin{cases} 0 & 0 \leq x \leq d - R \\ \frac{3d^2}{2R^3} \left(1 - \frac{x^2 + d^2 - R^2}{2xd} \right) & d - R \leq x \leq R \end{cases}. \tag{5.28}$$

and the p.d.f. of the RV $\mathbf{D}$ for the region $R \leq d \leq 2R$ is given by

$$f_{\mathbf{D}}(d) = \int_0^{d-R} f_{\mathbf{D}|\mathbf{X}}(d|x)_{2.1} f_{\mathbf{X}}(x) dx + \int_{d-R}^{R} f_{\mathbf{D}|\mathbf{X}}(d|x)_{2.2} f_{\mathbf{X}}(x) dx = \frac{3d^2}{R^3} - \frac{9d^3}{4R^4} + \frac{3d^5}{16R^6}. \quad (5.29)$$

It is possible to see that, for both regions (**A1** and **A2**), the p.d.f. of the RV **D** is the same. Therefore,

$$f_{\mathbf{D}}(d) = \frac{3d^2}{R^3} - \frac{9d^3}{4R^4} + \frac{3d^5}{16R^6} \qquad (0 \le d \le 2R). \qquad (5.30)$$

5.5   Results

With the purpose to give a first validation to the mathematical model developed in this chapter, Monte-Carlo simulations were performed using the software MATLAB and the results were compared to previously obtained by the model. Also, using the simulation it was possible to obtain the biggest number of hops for each run. Simulation and model employed 10 randomly distributed nodes inside a 1 km sphere, with a maximal aperture angle (θ) of ($\pi/18$) rad, all summarized in Table 5.1.

Table 5.1: Average number of hops. Default parameters.

PARAMETER	DEFAULT VALUE
Transmission frequency (f)	18.5 kHz
Number of nodes (N)	10 $Nodes$
Network radius (R)	1 km
Maximal aperture angle (θ)	($\pi/18$) rad

The simulation in MATLAB for the distance from any node (transmitted node) to the center of the sphere (receiver node), consists of creating a 1 km sphere with N randomly distributed nodes inside it. Then, the distance from all the nodes to the center node is calculated and the average value is found. The process is repeated 100 times and averaged to obtain the final result. This final result is compared to the model. For simulation of the distance of the hop, the process is similar, but, the calculated distance is according to the routing strategy described in Section 5.2. From these values, the number of hops is obtained.

Figure 5.9 shows the behavior of the average number of hops by varying the transmission frequency, the number of nodes, the network radius, and the maximal aperture angle.

These figures show that the average number of hops do not vary with the transmission frequency. This is an expected result based on the equations developed in this chapter. In addition, the average number of hops increases linearly with the number of nodes, i.e., for the same radius, more nodes results in a bigger density of nodes, therefore more hops, as Figures 5.9 (a), (b) and (d) illustrate.
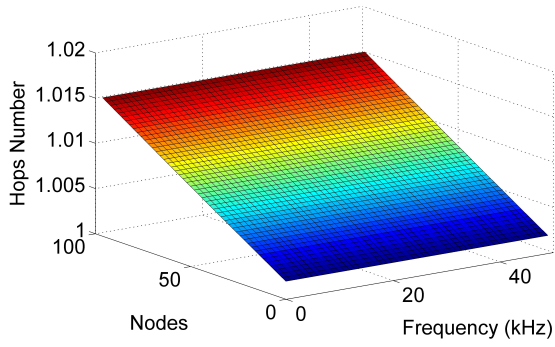
(a) Varying transmission frequency and number of nodes.
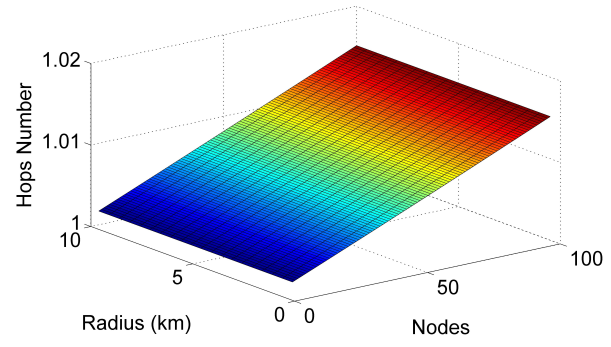
(b) Varying number of nodes and network radius.
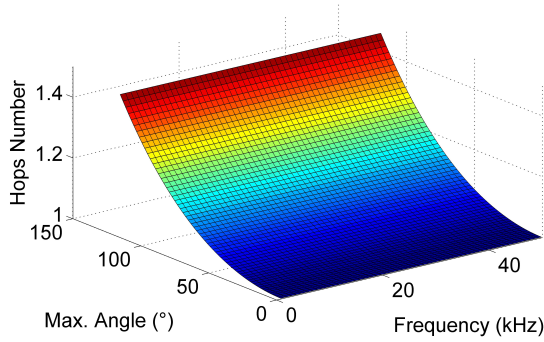
(c) Varying transmission frequency and maximal aperture angle.
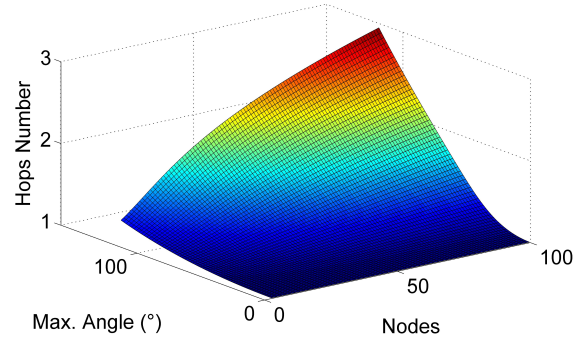
(d) Varying number of nodes and maximal aperture angle.
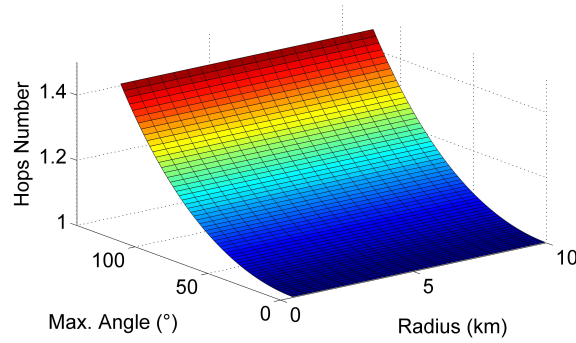
(e) varying network radius and maximal aperture angle

Figure 5.9: Average number of hops. Model. See Table 5.1.

The average number of hops increases for higher angle values as it is possible to see in Figures 5.9 (c) and (e), because according to the network topology described in Section 5.2, if the maximal aperture angle is bigger the node will select for the next hop the nearest node, consequently, the number of hops will increase.

Finally, Figures 5.9 (b) and (e) allow us to conclude that the average number of hops does not depend on the radius, because regardless of the size of the sphere (network) the node will select the nearest node inside the maximal aperture angle, i.e., the length of the reference line will increase with the radius, as Eq. (5.5), but the hop distance will decrease as well, see Eq. (5.17), compensating the variation.

Table 5.2 summarizes the obtained results for the average number of hops by varying the central transmission frequency, the number of nodes, the network radius and the maximal aperture angle.

Table 5.2: Average number of hops.

PARAMETER	VARIATION	NUMBER OF HOPS
Transmission frequency (f)	Increases	Constant
Number of nodes (N)	Increases	Increases
Network radius (R)	Increases	Constant
Maximal aperture angle (θ)	Increases	Increases

Figure 5.10 shows a comparison between the simulations and the developed model. It also shows the biggest number of hops for each run, varying the number of nodes and the maximal aperture angle. From this figure we can conclude two things. First, the great similitude between the model and the simulation, giving a first validation to our model; the second aspect to conclude is that even when the average number of hops is small, we have cases where the maximum archived number of hops is larger, reaching five hops for more than 100° for example.
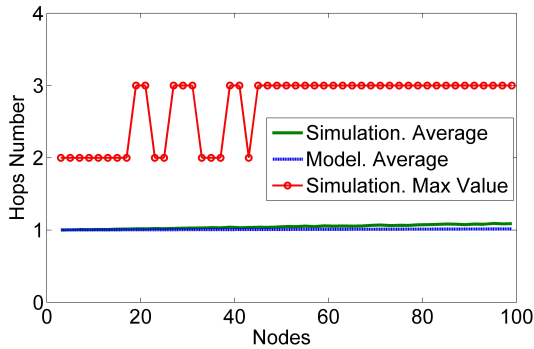
(a) Varying number of nodes.
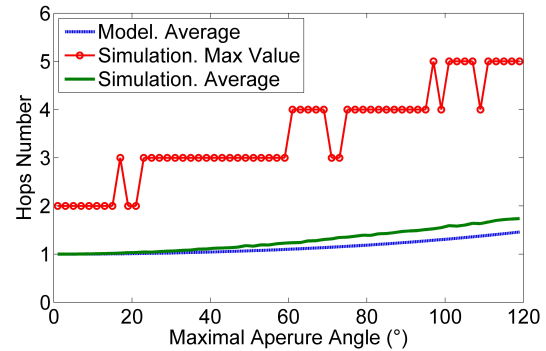
(b) Varying maximal aperture angle.

Figure 5.10: Number of hops. Simulation versus model and maximal value. See Table 5.1.

5.6 Conclusions

This chapter focus on explaining the adopted network topology in this work and develops a mathematical model to obtain the average number of hops and the distance between nodes for Underwater Acoustic Networks (UANs) formed by N nodes uniformly distributed inside a sphere with radius R.

In order to obtain the average number of hops, it was necessary first to obtain the average distance of the hop based on the network strategy, the average distance of the reference line (average distance between any node inside the sphere and the central node) and the average deviation. Some of the developed equations will be used further in this work, for example, to

obtain the received power in one hop. The distance between any nodes inside the sphere will be used to obtain the average interference in a communication link.

Finally Monte-Carlo simulation and model results were compared to give a first validation to the developed model and to show the behavior of the average number of hops. It was made for the variation of the transmission frequency, the number of nodes, the network radius and the maximal aperture angle. The Monte-Carlo simulations and model allow us to conclude two things: first, the model has good accuracy, and second, the average number of hops depends only on the number of nodes and the maximal aperture angle.

Chapter 6

Signal-to-Noise plus Interference Ratio

This chapter develops a mathematical model to obtain the Signal-to-Noise plus Interference Ratio (SNIR) for underwater acoustic networks (UANs). In order to achieve this purpose, it was necessary first to obtain the received signal power and the received interference. The noise was obtained early in this work. Simulation and model were compared to give a first validation to the analysis and to see the behavior of the received signal, the interference, the SNR and the SNIR.

6.1 Introduction

The SNIR is a measure that can provide a lot of information about the channel in wireless communication systems (upper bounds on channel capacity, rate of information transfer, etc.). It can be used to measure the quality of the link as well. Starting from the SNR (Signal-to-Noise Ratio) we include in this work the interference as an additional impairment for the communication, considering the use of the ALOHA MAC protocol.

In this chapter we develop a mathematical model that allows us to calculate the SNIR for one hop in underwater acoustic networks (UANs) with the described topology in Chapter 5. The SNIR is defined as the relationship between the received signal power and the noise power plus interference. Defining P_{RS} as the power of the received signal in units of Watt (W), obtained in Section 6.2, Δf as the frequency bandwidth in units of Hertz (Hz), N_T as the total noise power spectral density in units of Watt per Hertz (W/Hz) obtained in Section 3.4.5.1, and $E[P_{INT}^{TOT}]$ as the average total power interference at the receiver, in units of Watt (W) obtained in Section 6.3, the SNIR at the destination node at a distance $\bar{Y}$ from the source node can be obtained as

$$SNIR = \frac{P_{RS}}{N_T \Delta f + E\left[P_{INT}^{TOT}\right]} \tag{6.1}$$

or in units of decibels (dB) as

$$SNIR_{dB} = 10 \log_{10}(P_{RS}) - 10 \log_{10}\left(N_T \Delta f + E\left[P_{INT}^{TOT}\right]\right). \tag{6.2}$$

6.2 Utile Received Signal

The power of the received signal P_{RS} for a given transmission power (P_{TS}) and acoustic path loss $A(l, f)$, i.e., given distance (l) and frequency (f), is given by

$$P_{RS} = \frac{P_{TS}}{A(l, f)}. \tag{6.3}$$

The received signal power decreases with the distance and it depends also on the frequency of the signal due to the acoustic path loss $A(l, f)$ obtained in Section 3.4.1. The parameter l represents the distance between the transmitter and receiver and it is treated in our model as the mean of the RV $\mathbf{X}$ when is analysed the one-hop communication, this value was obtained in Section 5.3.2. If the analysed communication is multi-hop, it is necessary to treat the parameter l as the mean RV $\mathbf{Y}$ obtained in Section 5.3.2.

Figure 6.1 and 6.2 represent the behavior of the received signal power versus the variation of the transmission frequency, the number of nodes, the transmitted power and the network radius. From the modem Teledyne Benthos ATM9XX [9], a central transmission frequency of 18.5 kHz and 20 W of transmission power were used as default parameters, in addition to a radius of 1 km, 10 nodes and maximal aperture angle (θ) of $\pi/18$ rad. The first figure shows the behavior of the received signal power for one-hop ($l = E[\mathbf{X}]$) and the second one for multi-hop ($l = E[\mathbf{Y}]$). The default parameters are shown in Table 6.1.

Table 6.1: Received signal. Default parameters.

Modem	Teledyne Benthos ATM9XX
PARAMETER	DEFAULT VALUE
Transmission frequency (f)	18.5 kHz
Number of nodes (N)	10 $Nodes$
Network radius (R)	1 km
Maximal aperture angle (θ)	($\pi/18$) rad
Transmitted power (P_{TS})	20 W

It is possible to see in these figures that the received signal power decreases transmission frequency increases, which is due to an increase of the path loss (increase of the absorption coefficient).

Also, the received signal power for one-hop consideration does not depend on the number of nodes, this is because $l = E[\mathbf{X}]$. For multi-hop, the used average distance $l = E[\mathbf{Y}]$ and therefore the received signal power increases with the number of nodes.
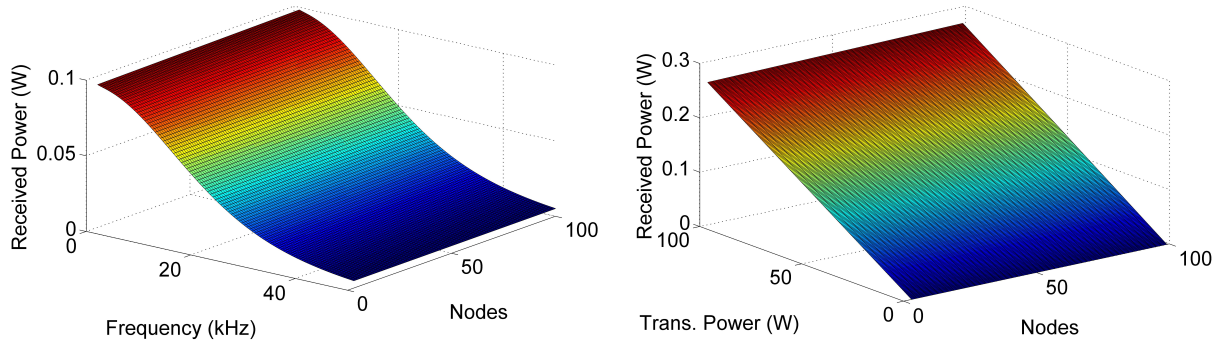
(a) Varying transmission frequency and number of nodes.

(b) Varying number of nodes and transmitted power.
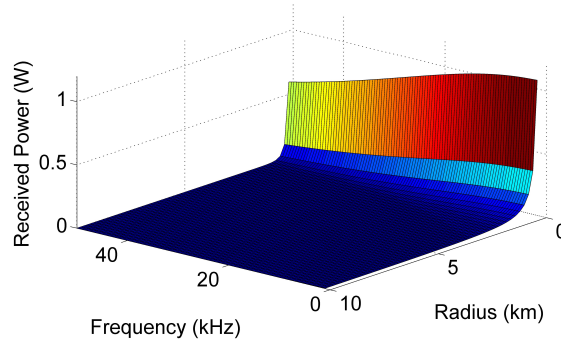
(c) Varying transmission frequency and network radius.

Figure 6.1: Received signal for One-Hop. Model. See Table 6.1.

From Figure 6.1 (b) and Figure 6.2 (b) we can say that the received signal power increases linearly with the transmitted power, this is clearly reflected in Eq. (6.3). Finally, Figure 6.1 (c) and Figure 6.2 (c) show that the strength of the signal is lower for a bigger radius, and it is logical, because for a bigger radius the resulting distance of the hop is also bigger (for both scenarios), and consequently the path loss increases.

Table 6.2 summarizes the behavior of the received signal strength varying the transmission frequency, the number of nodes, the network radius and the transmitted power.

Table 6.2: Received Signal.

PARAMETER	VARIATION	REC SIGNAL (O-HOP)	REC SIGNAL (M-HOP)
Transmission frequency (f)	Increases	Decreases	Decreases
Number of nodes (N)	Increases	Constant	Increases
Network radius (R)	Increases	Decreases	Decreases
Transmitted Power (P_{TS})	Increases	Increases	Increases

43
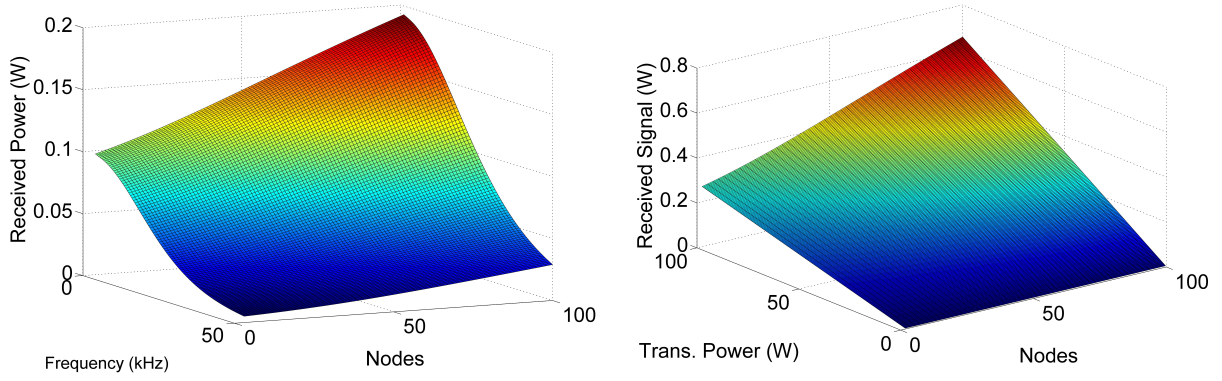
(a) Varying transmission frequency and number of nodes.

(b) Varying number of nodes and transmitted power.
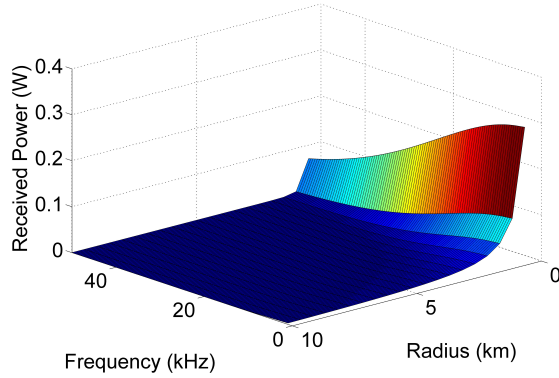
(c) Varying transmission frequency and network radius.

Figure 6.2: Received signal for Multi-Hop. Model. See Table 6.1.

6.3 Interference

Substituting Eq. (3.7) to Eq. (6.3) it is possible to say that the received power by a node is giving by

$$P_{RS} = \frac{P_{TS}}{A_0 l^k a(f)^l},$$ (6.4)

that depends on the distance between nodes (l), the spreading factor (k) and the absorption coefficient ($a(f)$).

Because the acoustic communication medium is shared by all network nodes, there exists a probability that two or more nodes try to transmit at the same time, causing interference. The average interference caused by one node can be calculated by Eq. (6.4). Nevertheless, because of the random topology of the network, the distance between two nodes (l) is random as well, and it should be treated as the random variable (RV) **D**, whose c.d.f. and p.d.f. were determined in Section 5.4. Accordingly, the average interference caused by the node i to the receiver node is given by

$$E\left[P_{int}^i\right] = E\left[\frac{P_{TS}}{A_0 d^k a(f)^d}\right] = \frac{P_{TS}}{A_0} E\left[\frac{1}{d^k a(f)^d}\right]. \tag{6.5}$$

From the p.d.f. of the RV $\mathbf{D}$ given by Eq. (5.30), it follows that

$$E\left[\frac{1}{d^k a(f)^d}\right] = \int_0^{2R} \frac{1}{d^k a(f)^d} f_{\mathbf{D}}(d) dd. \tag{6.6}$$

It is important to remark that Eq. (6.6) does not have a closed solution, only a numerical one.

Substituting Eq. (6.6) to Eq. (6.5) it is possible to obtain the final expression for the average interference caused by node i to the receiver node, as

$$E\left[P_{int}^i\right] = \frac{P_{TS}}{A_0} \int_0^{2R} \frac{1}{d^k a(f)^d} f_{\mathbf{D}}(d) dd. \tag{6.7}$$

In a real network the probability that one node transmission coincides with another communication depends on the used MAC protocol. For this case, we use an ALOHA without re-transmission protocol, because of its simplicity and generality, and since it is not necessary to consider the propagation delay, as explained Section 3.5. Therefore, according to [30] and [32] the total average interference power experienced by the receiver node can be written as

$$E\left[P_{INT}^{TOT}\right] = \left(1 - e^{-\frac{\overline{\lambda}L}{R_b}}\right) \sum_{i=1}^{N-2} E\left[P_{int}^i\right]. \tag{6.8}$$

that depends on the average packet transmission rate for one node in units of packets per second (pkt/s) following a Poisson distribution, $\overline{\lambda}$; the packet size in units of bits, L; and the transmission rate in units of bits per second ($bits/s$), R_b.

In Eq. (6.8) the factor $\left(1 - e^{-\frac{\overline{\lambda}L}{R_b}}\right)$ represents the probability that a node causes interference to another transmission independently of its location [30]. The other factor, $\left(\sum_{i=1}^{N-2} E[P_{int}^i]\right)$, is the average interference power caused by a node concurrently transmitting with another node. Here we consider that all the nodes in the network experiment the same inter-nodal interference (INI).

In Figure 6.3, it is possible to see the behavior of the interference as a function of the number of nodes, the transmission frequency, the network radius and the transmitted power. This was made for the modem Teledyne Benthos ATM9XX [9] with a central transmission frequency of 18.5 kHz, 5 kHz of frequency bandwidth, 20 W of transmitted power and 2400 $bits/s$ of transmission rate as default values; placed at an UAN with an average packet transmission rate for one node of 1 pkt/s, 768 $bits$ of packet size, 1 km radius and 10 nodes. Table 6.3 shows the default values used for modeling the interference.

From Figure 6.3 we note that the interference slowly decreases with frequency due to the fact that as frequency increases the path loss also increases; therefore, the interference will be lower.

Table 6.3: Received interference. Default parameters.

Modem	Teledyne Benthos ATM9XX
PARAMETER	DEFAULT VALUE
Transmission frequency (f)	18.5 kHz
Frequency bandwidth (Δf)	5 kHz
Number of nodes (N)	10 $Nodes$
Network radius (R)	1 km
Maximal aperture angle (θ)	($\pi/18$) rad
Transmitted power (P_{TS})	20 W
Transmission rate (R_b)	2400 $bits/s$
Average packet transmission rate ($\overline{\lambda}$)	1 pkt/s
Packet size (L)	768 $bits$

(a) Interference versus transmission frequency and number of nodes.
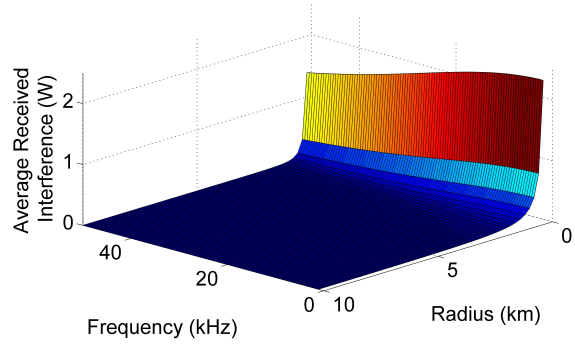
(b) Interference versus transmission frequency and network radius.
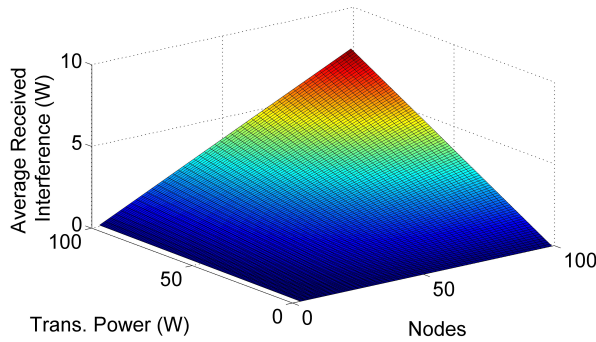
(c) Interference versus number of nodes and transmitted power.

Figure 6.3: Received interference. Model. See Table 6.3.

It is important to also remark that with the increase of the network radius, the interference losses strength, i.e., it has a high attenuation, because for a bigger radius the distance among the

nodes increases and the path loss increases as well, provoking the reduction of the interference, i.e., the received signal by the receiver node will be weaker. Even, for 10 nodes, it is possible to say that for a radius bigger than 5 *km* the interference can be ignored.

Another aspect to consider is the transmitted power. If this parameter increases, the interference also increases since the relationship between these two variables is linear, which is clearly observed from Eq. (6.7).

Finally, if the number of nodes increases, the network will have more nodes with a chance to cause interference in the communication, resulting in more total average interference.

The summary of the behavior of the interference with the variation of the transmission frequency, the number of nodes, the network radius and the transmitted power is shown in Table 6.4.

Table 6.4: Received interference.

PARAMETER	VARIATION	INTERFERENCE
Transmission frequency (f)	Increases	Decreases
Number of nodes (N)	Increases	Increases
Network radius (R)	Increases	Decreases
Transmitted Power (P_{TS})	Increases	Increases

6.4 Received Signal, Interference and Noise Comparison

This section directly compares the behavior of the three involved variables in an acoustic communication: the received signal (for one-hop), the noise and the interference. Figure 6.4 shows the behavior of the three variables, by varying the transmission frequency, the number of nodes, the network radius, and the transmitted power. We employed the default parameters from Table 6.3 and a wind speed (v) of 20 *knots*.

As it is possible to see in Figure 6.4 (a) an increase of the frequency causes the increase of the acoustic path loss, due to an increase of the absorption coefficient. Therefore, the received signal and the interference decrease. Also, for higher frequencies it is possible to observe lower noise values as it was shown in Section 3.4.5.1. Here it is important to analyse the optimal value of frequency, where all these three impairments are minimized. Further in this work, the optimal frequency will be obtained.

The second aspect to note, shown in Figure 6.4 (b), is that only the interference depends on the number of nodes, increasing with it linearly, as it was shown in Section 6.3. Moreover, for less than 10 nodes and $1km$ of radius, the interference is lower than noise. For more than 10 nodes, interference becomes the major impairment in the acoustic communication. Based on this result we can deduce that the optimal number of nodes for the SNIR in our model is the lower possible. It is the quantity of nodes were the lower value of SNIR is obtained

(a) Varying transmission frequency.

(b) Varying number of nodes.

(c) Varying network radius.

(d) Varying transmitted power.
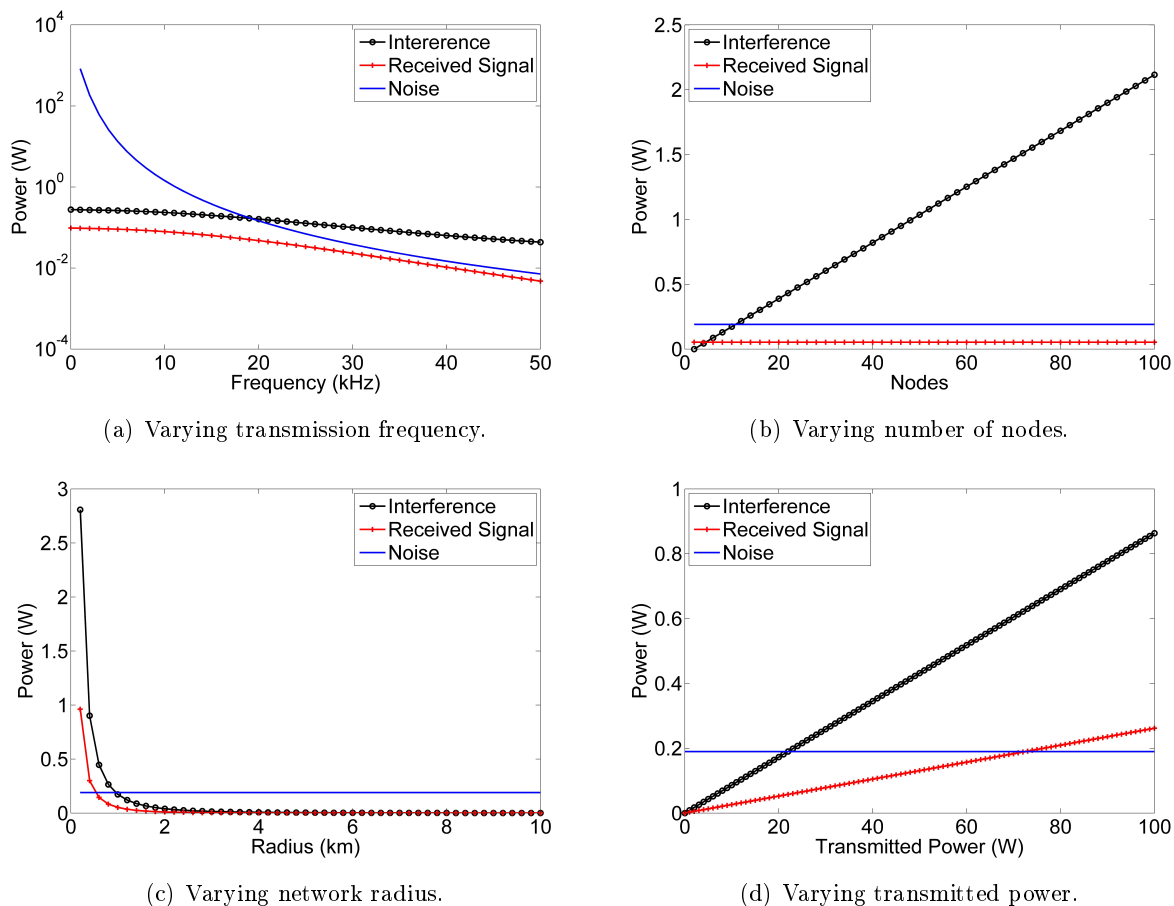
Figure 6.4: Received signal, interference and noise comparison. Model. See Table 6.3.

Figure 6.4 (c) shows that only the noise is radius independent, but more importantly, the increasing of the radius causes an increase in the acoustic path loss, and therefore, a decrease in the received signal and interference. Because the slope of the received signal curve is higher than the interference one, the best possible radius to work is the smaller one (bigger interference and received signal). For a larger radius, the interference will be lower, and it can be even ignored, but the useful signal will be very attenuated by the acoustic path loss as well.

Noise is the only parameter that does not depend on the transmitted power, as Figure 6.4 (d) shows. The increase of the interference and the received signal with the transmitted power is linearly, validating the obtained results in Section 6.3 and Section 6.2.

Table 6.5 summarizes the behavior of the received signal, the interference and the noise, varying the transmission frequency, the number of nodes, the network radius and the transmitted power.

Table 6.5: Received signal, interference and noise variation comparison.

PARAMETER	VARIATION	R. SIGNAL (ONE-HOP)	INTER.	NOISE
Transmission frequency (f)	Increases	Decreases	Decreases	Decreases
Number of nodes (N)	Increases	Constant	Increases	Constant
Network radius (R)	Increases	Decreases	Decreases	Constant
Transmitted Power (P_{TS})	Increases	Increases	Increases	Constant

6.5 Results

6.5.1 Simulation versus Model

With the purpose to give a first validation to the developed SNIR model, using the software MATLAB, we simulate (Monte-Carlo) the UAN and compared it to the model. It was used a scenario with 10 nodes, all employing the modem Teledyne Benthos ATM9XX [9] default parameters, randomly distributed inside a 1 km sphere, with a central transmission frequency of 18.5 kHz, 5 kHz of frequency bandwidth, 20 W of transmitted power, 2400 $bits/s$ of transmission rate, average packet transmission rate of 1 pkt/s and 768 $bits$ of packet size. The used wind speed for noise calculation was 20 $knots$. The used default parameters are shown in Table 6.3. Also, for simplicity, it was considered that the receiver node is located at the center of the sphere (see Figure 6.5).

For the simulation we create a 1 km radius sphere with 10 nodes randomly distributed. One of these nodes is the receiver node, and it is located at the center of the sphere. Then, the distance from a node to the center is measured and with this value the received power is calculated by Eq. (6.3). In order to obtain the interference experimented by the receiver node, the distance from all the nodes to the center is measured as well, and with these values the interference caused by each node is obtained (except the transmitter node and the receiver node), and the total interference according to the MAC protocol from Eq. (6.8) is obtained as well. Therefore, with the total noise (obtained by the model equations), the interference and the received power, the SNIR is obtained. The process is repeated for all the nodes and the average SNIR is obtained. This process is again repeated 100 times and the final average SNIR for the simulation is calculated. This value is compared to the developed model.

In Figure 6.6 it is possible to see the behavior of the SNIR simulated (Monte-Carlo) and the SNIR obtained from the model, varying the transmission frequency, the number nodes, the network radius and the transmitted power.

The first thing to note is the great similitude between the simulation and the model, giving a first validation to our model. Analysing Figure 6.6 (a) we can see that SNIR increases with frequency until it reaches an optimal value, and this value depends mainly on the compensation between the interference and the received signal, i.e., path loss, analysed in Section 3.4.1. This optimal value of frequency will be obtained further in this work.
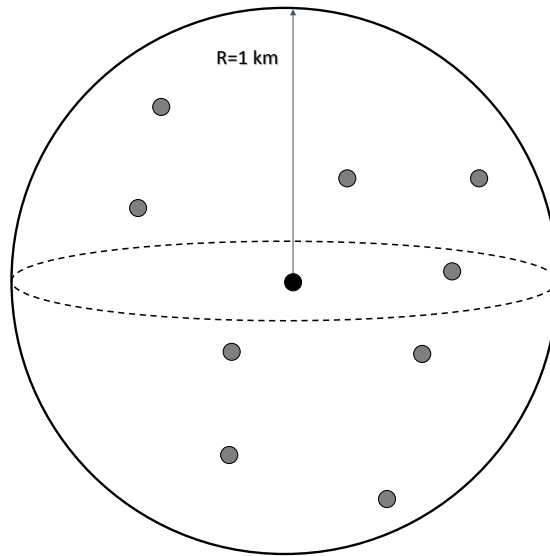
Figure 6.5: Nodes distribution inside the network sphere.
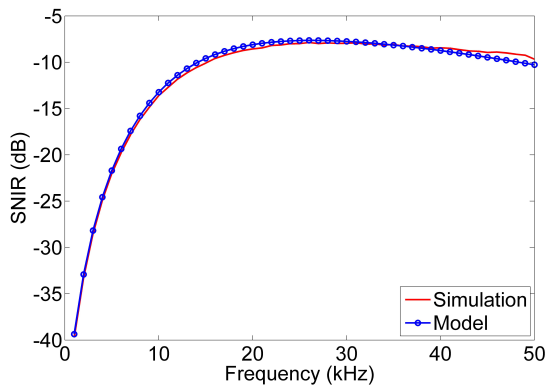
(a) Varying transmission frequency.
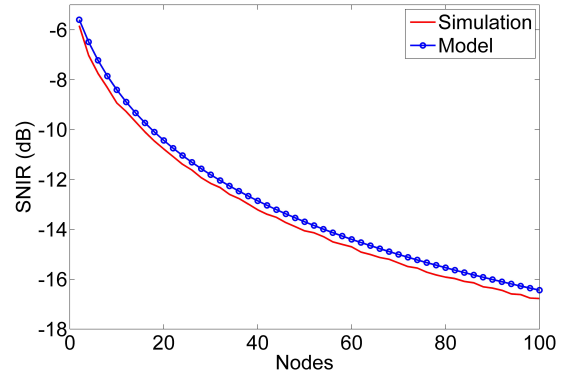
(b) Varying number of nodes.
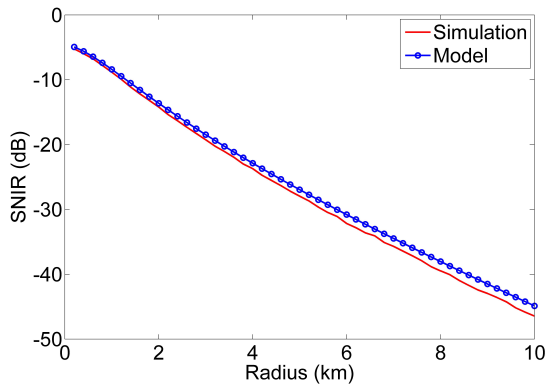
(c) Varying network radius.
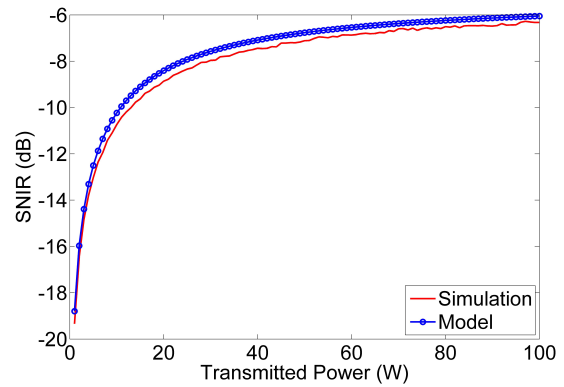
(d) Varying transmitted power.

Figure 6.6: SNIR. Simulation versus Model. See Table 6.3.

Figure 6.6 (b) validates the results in Section 6.4 in which the best values of SNIR occur for the lowest possible number of nodes. This is when the interference is lower, knowing that the received signal and the noise do not depend on the number of nodes, as it was demonstrated previously.

Figure 6.6 (c) also confirms the conclusions from Section 6.4, that the best value of SNIR happens for the smaller possible radius, because in such case the acoustic path loss is minimum (the distance between the nodes is minimal), i.e., the effective received signal and the interference are maximal, remarking that the received signal is stronger than the interference.

Finally, in Figure 6.6 (d) we can see that an increase of the transmitted power causes an increase in SNIR. For higher values of transmitted power a higher value of received signal and interference results. However, once again, the strength of the utile received signal is greater than the interference.

Table 6.6 shows the behavior of the SNIR for the variation of the transmission frequency, the number of nodes, the network radius and the transmitted power.

Table 6.6: SNIR.

PARAMETER	VARIATION	SNIR
Transmission frequency (f)	Increases	Increases until optimal and decreases
Number of nodes (N)	Increases	Decreases
Network radius (R)	Increases	Decreases
Transmitted Power (P_{TS})	Increases	Increases

6.5.2 SNIR versus SNR

From our point of view, one of the more important contributions of our work is to include the interference (considering the ALOHA MAC protocol) in the calculus of Signal-to-Noise Ratio (SNR), becoming Signal-to-Noise plus Interference Ratio (SNIR). In order to demonstrate the relevance of the interference, we model and compare the two cases, varying the transmission frequency, the number of nodes, the network radius and the transmitted power. The results are shown in Figure 6.7.

The first thing to note is that for all the cases, the values of the SNIR are lower than the values of SNR, demonstrating that the interference is a considerable impairment in the acoustic communication if ALOHA MAC protocol is used. This difference can be noted in Figures 6.7 (a), 6.7 (b) and 6.7 (d). By varying the number of nodes inside the sphere, we can see that the value of SNR is constant, because if interference is not considered, there is only noise and utile received signal, and these parameters do not depend on the number of nodes. On the other hand, the SNIR decreases with the increase in N as shown in previous section.

Figure 6.7 (c) confirms another conclusion from Section 6.3 in this chapter, that the influence of the interference is reduced with the increase of the network radius. Moreover, for the used scenario, for a radius larger than 5 km the interference can be ignored. The SNR curve also decreases with R, due to an increase of the acoustic path loss, i.e., reduction of the received signal.

The increase of the transmitted power produces an increase in both SNR and SNIR. Here it is
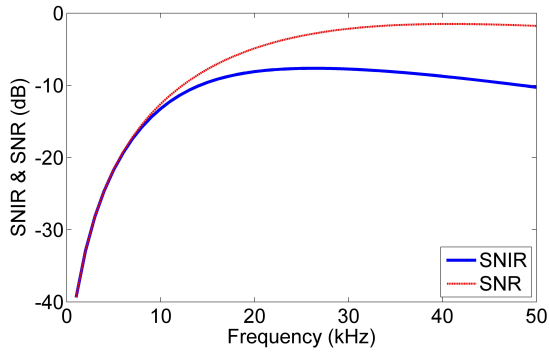
(a) Varying transmission frequency.
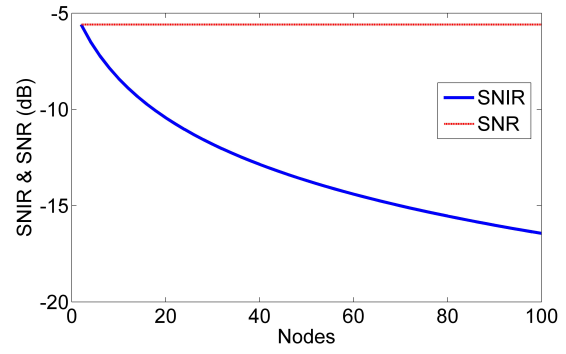
(b) Varying number of nodes.
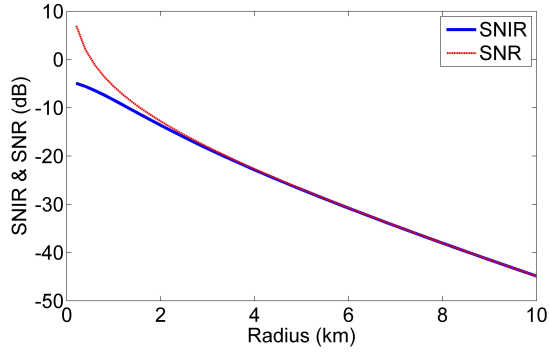
(c) Varying network radius.
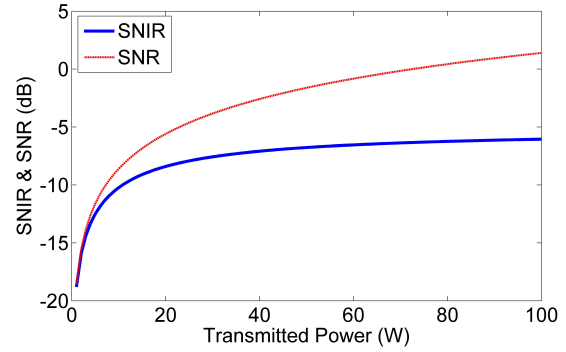
(d) Varying transmitted power.

Figure 6.7: SNIR versus SNR. Model. See Table 6.3.

important to remark that the slope of the SNR curve is bigger than the SNIR, which is due to the lack of interference in the SNR case, causing a faster increasing. A similar effect occurs by varying the transmission frequency up to a maximum value and after that SNR and SNIR decreases.

6.6 Conclusions

In this chapter was developed a mathematical model that allow us to calculate the Signal-to-Noise plus Interference Ratio (SNIR) of a link at an Underwater Acoustic Network (UAN), using the ALOHA MAC protocol and considering the interference as a remarkable impairment .

In order to have a first validation of this model, we performed Monte-Carlo simulations using the software MATLAB and compare it with the results obtained from the model. The comparison shows good agreement between the model and the simulation, by varying the transmission frequency, number of nodes, transmitted power and network radius.

Finally, with the purpose of demonstrating the relevance of the interference by employing an ALOHA MAC protocol, we model two scenarios: considering the interference (SNIR) and without interference (SNR). The results prove that the interference is a very important impairment and influences directly on the acoustic communication.

The obtained results in this chapter allow us to calculate at a predetermined scenario of an

UAN, the expected SNIR for one hop, and configure it to obtain a measure of quality in the communication link. Also, for a given modulation, we can now obtain the Bit Error Rate (BER) for one hop. Furthermore, based on the obtained results in this chapter, it is possible to obtain the optimal transmission frequency for an underwater acoustic communication link.

Chapter 7

One-Hop and End-to-End Bit Error Rate of a Route

In this chapter the End-to-End BER is obtained based on the previous results. In order to achieve this purpose it is necessary first to derive the One-Hop BER, calculated from the SNIR and the selected modulation scheme. Simulation is carried out to validate the model and analyse the behavior of the End-to-End BER, comparing the cases with and without interference. Also, the optimal transmission frequency for End-to-End BER is obtained. Finally, it is compared the One-Hop BER with the End-to-End BER discussing when it is more adequate the use of each one.

7.1 Introduction

In a digital transmission, the number of bit errors is the number of received bits of a data stream over a communication channel that has been altered due to noise, interference, distortion or bit synchronization errors. The Bit Error Rate (BER) is the relationship between the number of bit errors and the total number of transferred bits during the transmission time interval. The BER is an unitless performance measure, usually expressed as a number between zero and one or as a percentage value.

Another objective of this research is to develop a mathematical model that allows us to calculate the End-to-End BER in Underwater Acoustic Networks (UANs), based on the Signal-to-Noise plus Interference Ratio (SNIR) described in Chapter 6 and using one of the modulation scheme described in Chapter 4. For our study we select the Binary Phase Shift Keying (BPSK) modulation. The End-to-End BER permits is to evaluate the behavior of the network, considering interference using the ALOHA MAC protocol.

Another important aspect to consider from our study is that it allows us to find the opti-

mal communication frequency. This value of frequency will give the optimal value of SNIR and, therefore, the optimal End-to-End BER, improving the performance of the entire network.

7.2 One-Hop BER

In order to obtain the End-to-End BER it is necessary to calculate first the BER of one hop. Considering that the modulations scheme used is BPSK, described in Section 4.3.1 and according to [3] and [26], the One-Hop BER can be expressed as

$$BER_H = Q\left(\sqrt{2SNIR}\right),\tag{7.1}$$

where SNIR was obtained in Chapter 6 and $Q(x)$ represents the Q function given by Eq. (4.11) in Chapter 4. Figure 7.1 shows the One-Hop BER behaviour for various types of modulation, varying the transmission frequency, the number of nodes, the network radius and the transmitted power.

(a) Varying transmission frequency.

(b) Varying number of nodes.

(c) Varying network radius.

(d) Varying transmitted power.
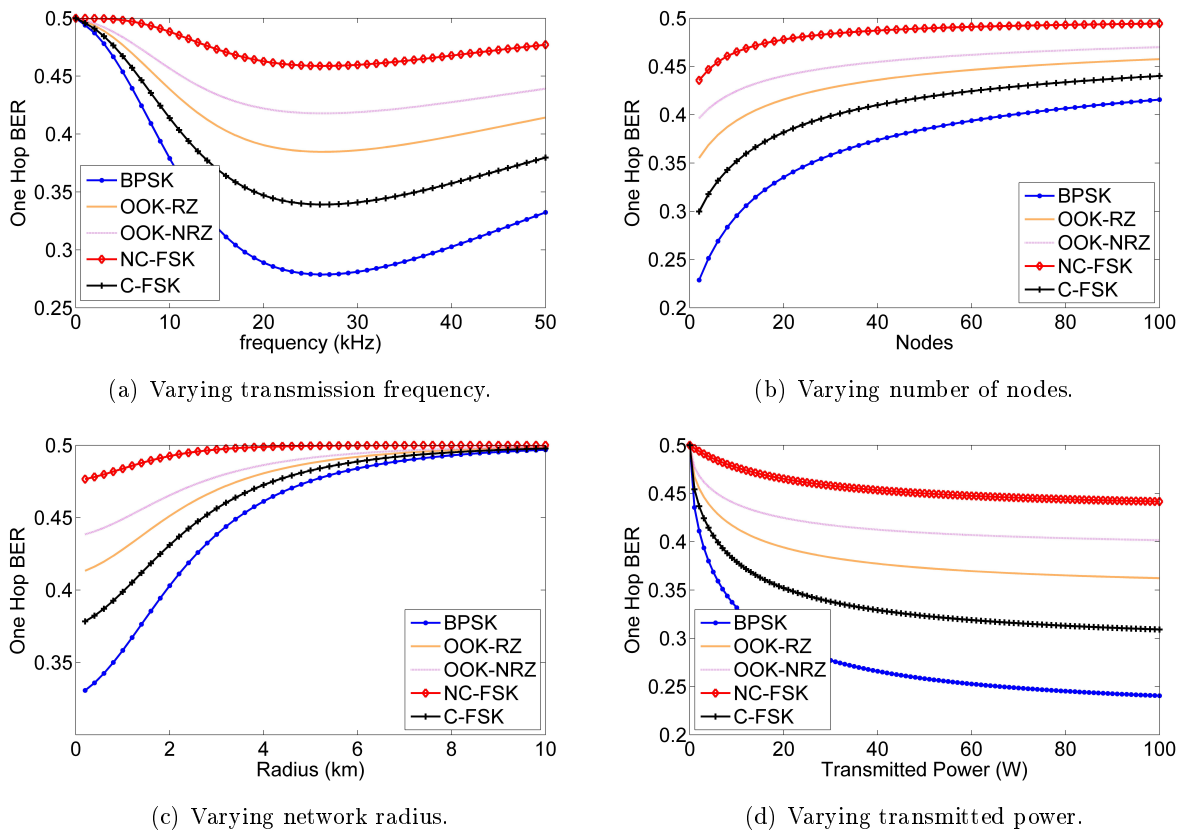
Figure 7.1: One-Hop BER modulations. Model. See Table 6.3.

From these figures it is possible to conclude that the BPSK modulation is the most robust modulation between those analysed.

The One-Hop BER give us a first look to the network throughput. We employed a scenario formed by 10 nodes using the Teledyne Benthos ATM9XX modem [9] parameters with a central transmission frequency of 18.5 kHz, 5 kHz of frequency bandwidth, 20 W of transmitted power

and 2400 *bits/s* of transmission bit rate; placed at an UAN with an average packet transmission rate of 1 *pkt/s*, 768 *bits* of packet size and 1 *km* of network radius, similar to the one described in Figure 6.5. Table 7.1 summarizes the used default parameters for the One-Hop BER model.

Table 7.1: One-Hop BER. Default parameters.

Modem	Teledyne Benthos ATM9XX
Modulation	BPSK
PARAMETER	DEFAULT VALUE
Transmission frequency (f)	18.5 kHz
Frequency bandwidth (Δf)	5 kHz
Number of nodes (N)	10 $Nodes$
Network radius (R)	1 km
Maximal aperture angle (θ)	($\pi/18$) rad
Transmitted power (P_{TS})	20 W
Transmission rate (R_b)	2400 $bits/s$
Average packet transmission rate ($\overline{\lambda}$)	1 pkt/s
Packet size (L)	768 $bits$
Wind speed (v)	20 $knots$

Figure 7.2 shows the behavior of the One-Hop BER when transmission frequency is varied, the number of nodes, the maximal aperture angle, the transmitted power and the network radius. It is important to remark that because it is the One-Hop BER, the used distance for the received power calculation will be $l = E[\mathbf{X}]$, i.e., the average distance from any node to the receiver node at the center of the sphere.

The first aspect to note is that the behavior of the One-Hop BER is opposite to the SNIR, i.e., for a higher SNIR, we get a lower BER.

The increase of the transmission frequency causes a decrease of the One-Hop BER, until the optimal (minimum) value. After this, point the value of the One-Hop BER increases. It is important to remark that the optimal transmission frequency for the One-Hop BER is very similar to the value obtained for the SNIR in Chapter 6.

From Figures 7.2 (a), (e), (f) and (g) we see that the One-Hop BER increases with an increase in the of the number of nodes. Therefore, the optimal value of nodes is the minimum possible for network operation. This result is similar to the one obtained for the SNIR in Chapter 6. The reason for the increase of the One-Hop BER with the number of nodes is the same as in the reduction of the SNIR, i.e., due to the increase of the interference.

The analysis of the maximal aperture angle became important for the One-Hop BER due to the developed mathematical model. Figures 7.2 (b), (e) and (h) show that the One-Hop BER
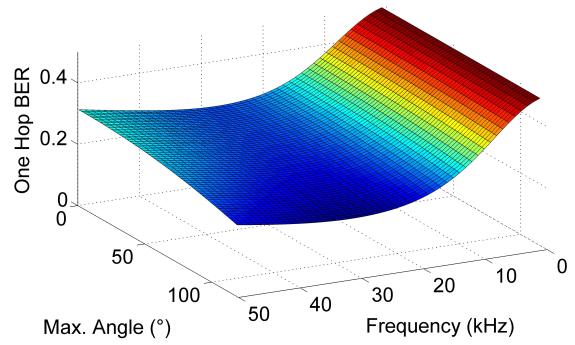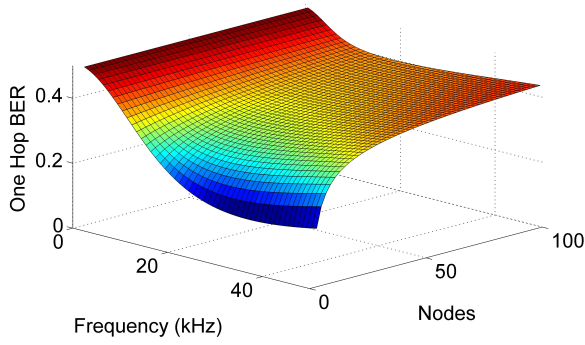
(a) Varying transmission frequency and number of nodes.

(b) Varying transmission frequency and maximum aperture angle.
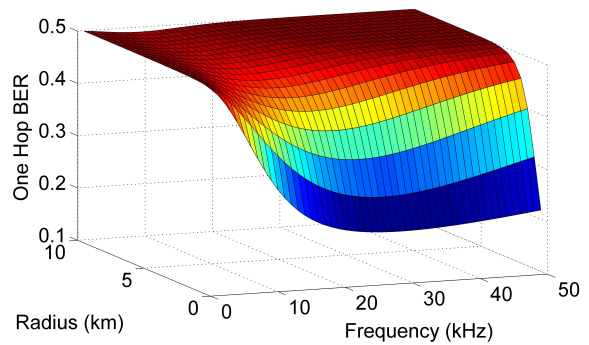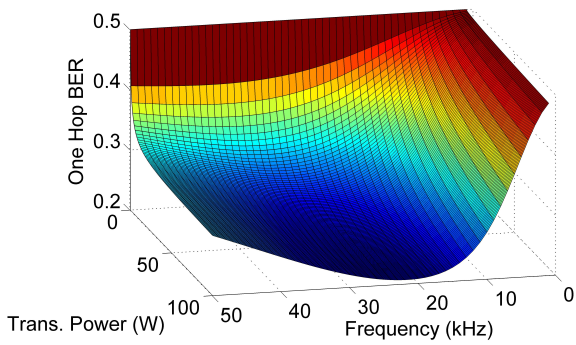
(c) Varying transmission frequency and transmitted power.

(d) Varying transmission frequency and network radius.
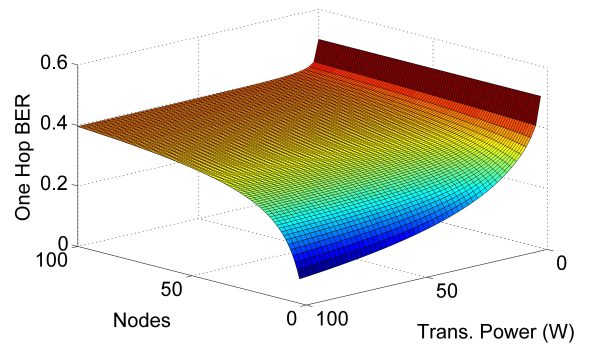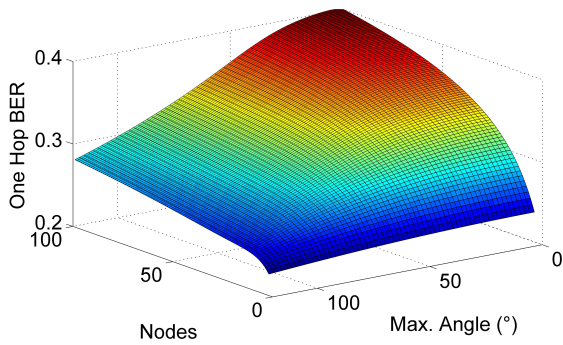
(e) Varying number of nodes and maximal aperture angle.

(f) Varying number of nodes and transmitted power.
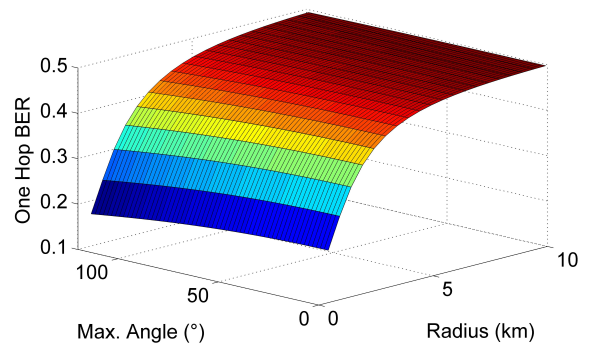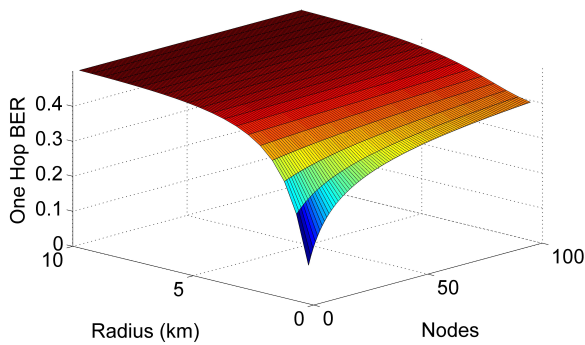
(g) Varying number of nodes and network radius.

(h) Varying network radius and maximal aperture angle.

Figure 7.2: One-Hop BER. Model. See Table 7.1.

decreases with the increase of θ, hence, the optimal angle is the largest one possible to use. The explanation to this behavior is that as θ increases the chances to find a closer neighbor node also increases which improves the SNIR for such a short link, that is, the hop length tends to be small which causes less path loss and results a stronger received signal.

The increase of the transmitted power causes, as in the SNIR case, a better One-Hop BER performance, i.e., when the P_{TS} increases the received signal increases as well, resulting in a lower One-Hop BER.

Finally, Figures 7.2 (d), (g) and (h) show that the increase of the network radius causes an increase of the One-Hop BER since the distance among nodes increases. In addition, note that if the radius is bigger than 5 km the interference can be ignored.

As in the SNIR case, for the One-Hop BER, simulations were made with the software MATLAB to analyse the behavior with and without interference, comparing with the developed model. Figure 7.3 shows the obtained results, by varying the transmission frequency, the number of nodes, the transmitted power and the network radius.

(a) Varying transmission frequency.

(b) Varying number of nodes.

(c) Varying transmitted power.

(d) Varying network radius.
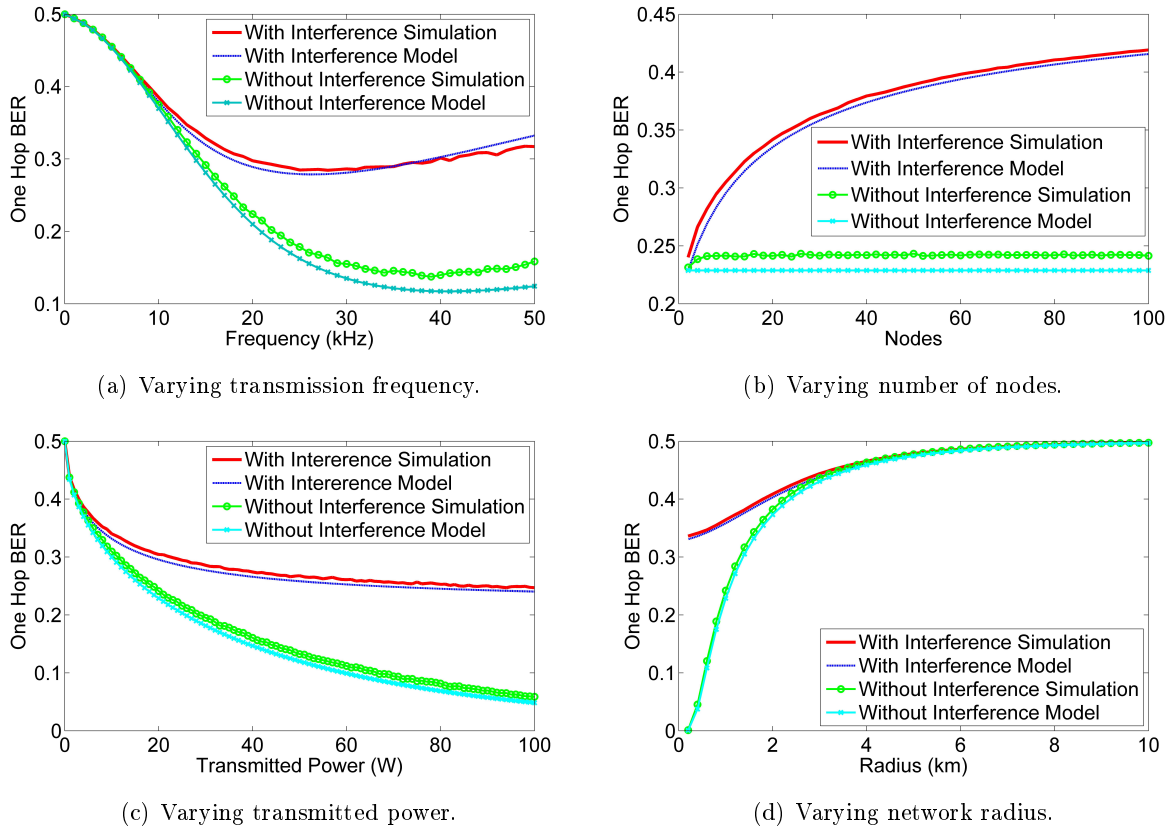
Figure 7.3: One-Hop BER with and without interference. Simulation versus model. See Table 7.1.

As in Chapter 6, from Figure 7.3, model and simulations present good agreement. it is possible to see that the interference is a big impairment if ALOHA MAC protocol is used, and the analysis of underwater wireless networks cannot be disregarded. Table 7.2 summarizes the One-Hop BER behavior variation.

Table 7.2: One-Hop BER.

PARAMETER	VARIATION	ONE-HOP BER
Transmission frequency (f)	Increases	Decreases until optimal and increases
Number of nodes (N)	Increases	Increases
Network radius (R)	Increases	Increases
Transmitted power (P_{TS})	Increases	Decreases
Maximal aperture angle (θ)	Increases	Decreases

7.3 End-to-End BER

To further compare the performance of underwater acoustic communication, we extend our analysis to consider a multi-hop network in which the receiver node will be in the center of a sphere with radius R, and the transmitter node inside this sphere, as explained in Section 5.2. Accordingly, a sender node communicates to the destination node (located at the center of network sphere) through intermediate nodes which will relay the data packet along the route to destination. For such a case, one measure of performance is the End-to-End BER, which computes the probability of bit error considering the entire path route. Our final model allows to analyse a possible network scenario before its real implementation, contributing to obtain in advance the best values of transmission frequency, number of nodes, network radius, etc., which helps the planing and design of such UANs.

Considering that the links at the route are independent, and errors at each link are accumulated until the destination, it is possible to say that the End-to-End BER (under the Gaussian assumption for the interference noise [24], [25]) at the route is given by [33].

$$BER_R = 1 - \prod_{j=1}^{\overline{n}_h} (1 - BER_j) \tag{7.2}$$

where $\overline{n}_h$ is the average number of hops, obtained in Chapter 5, and BER_j is the Bit Error Rate at hop j, obtained from Section 7.2.

We model the End-to-End BER for an UAN formed by 10 nodes employing the Teledyne Benthos ATM9XX modem [9] default parameters, i.e., transmission frequency of 18.5 kHz, 5 kHz of frequency bandwidth, 20 W of transmitted power and 2400 $bits/s$ of transmission rate; placed at an UAN with an average packet transmission rate of 1 pkt/s, 768 $bits$ of packet size, 1 km of network radius and with a maximal aperture angle (θ) of ($\pi/18$) $radians$, similar to the one described previously and summarized in Table 7.1. It is important to remark that the used distance for the received signal calculation for this cases (end-to-end) will be the average distance of the hop, obtained as $E[\mathbf{Y}]$.

Figure 7.4 shows numerical results for the model of the End-to-End BER, varying the transmission frequency, the number of nodes, the maximal aperture angle, the network radius and the

transmitted power.

From these figures we can see that the variation of the transmission frequency causes in the End-to-End BER the same effect as in the One-Hop BER, i.e., there is an optimal value of transmission frequency which can be explained by Eq. (7.2) that inherits the One-Hop BER from Eq. (7.1) and noting that the average number of hops does not depend on f.

Figures 7.4 (a), (e), (f) and (g) show that an increase in the number of nodes increases the End-to-End BER. In previous sections and chapters we saw that the increase in the number of nodes increases the One-Hop BER and the average number of hops, therefore, the higher value of the End-to-End BER is justified from Eq. (7.2). Also, we observe that for End-to-End BER the optimal number of nodes is the minimal possible. Consequently, it is better to have less nodes causing interference and provoking a lower number of hops, but with hops having larger distances.

The maximal aperture angle also affects the End-to-End BER. Figures 7.4 (b), (e) and (h) show an important difference between the One-Hop BER and the End-to-End BER. For the first case, as observed in previous section, an increase in the maximal aperture angle causes a decrease in the One-Hop BER. But for the End-to-End BER the behavior is opposite, i.e., increasing the maximal aperture angle causes an increase in the End-to-End BER. This is due to the average number of hops, as it was observed in Chapter 5. The number of hops is increased if the maximal aperture angle decreases. Therefore, the effect in the average number of hops, exponential in Eq. (7.2), dominates the effect on the One-Hop BER.

The increase in network radius, as observed in previous sections, increases the One-Hop BER and do not affect the average number of hops. Therefore, as seen in Figures 7.4 (c), (g) and (h), for a bigger radius a bigger End-to-End BER is obtained. Thus, we conclude again that the optimal radius is the minimal possible.

The other analysed parameter, the transmitted power, behaves as expected. If the transmitted power increases, the One-Hop BER decreases, as explained in previous sections, and do not affect the average number of hops. Therefore, the End-to-End BER also decreases.

In order to validate our final result, using the software MATLAB we simulate (Monte-Carlo) an UAN, creating a scenario with N nodes employing the parameters from a Teledyne Benthos ATM9XX [9] modem (10 as default) randomly distributed inside a sphere with radius R (1 km as default). The default parameters are shown in Table 7.1. With the network created, varying the transmission frequency, the number of nodes, the network radius, the maximal aperture angle and the transmitted power, the BER was obtained for each hop of the route from each node to the central node (receiver node), based on the network topology described in Section 5.2. After that, using Eq. (7.2), the End-to-End BER for each route and the average End-to-End BER was obtained. This process was repeated 100 times and the final average End-to-End BER was derived. Figure 7.5 shows the comparison between simulation and model.

These figures confirm the previously obtained results: the increase of the End-to-End BER with the number of nodes, the network radius and the maximal aperture angle. Also, the figures validate our mathematical model, due to the good agreement between model and simulation. Table
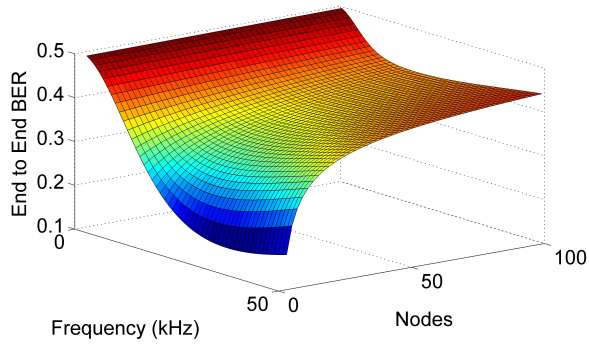
(a) Varying transmission frequency and number of nodes.
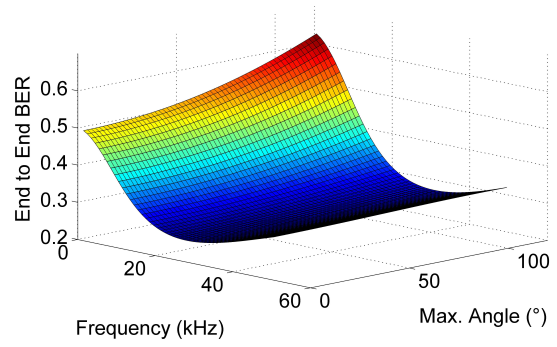
(b) Varying transmission frequency and maximal aperture angle.
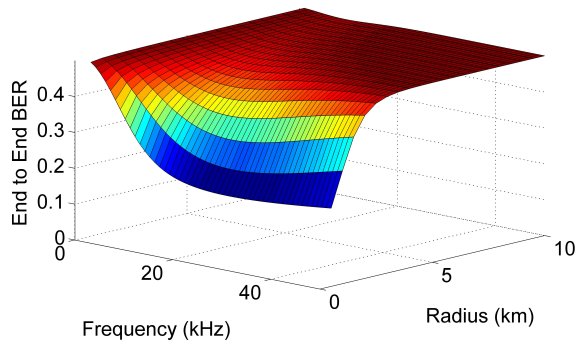
(c) Varying transmission frequency and network radius.
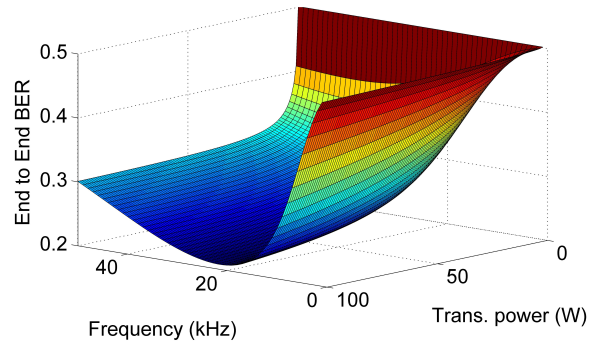
(d) Varying transmission frequency and transmitted power.
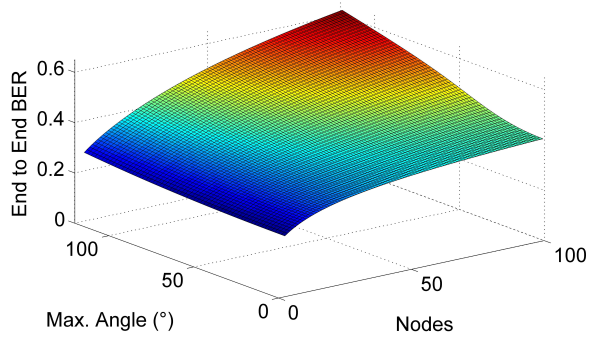
(e) Varying number of nodes and maximal aperture angle.
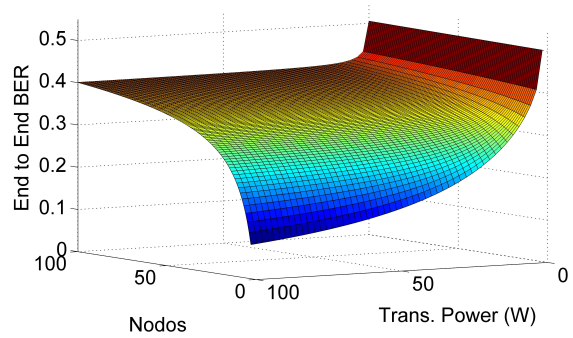
(f) Varying number of nodes and transmitted power.
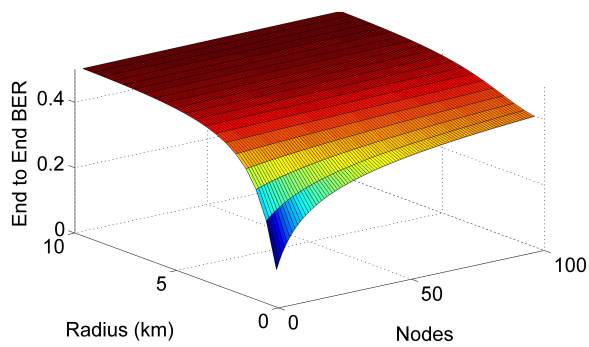
(g) Varying number of nodes and network radius.
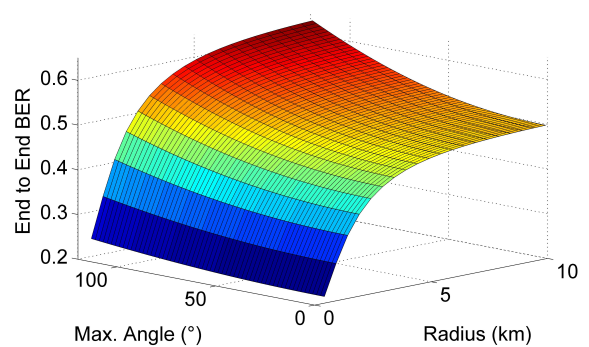
(h) Varying network radius and maximal aperture angle.

Figure 7.4: End-to-End BER. Model. See Table 7.1.

(a) Varying transmission frequency.

(b) Varying number of nodes.

(c) Varying transmitted power.

(d) Varying network radius.

(e) Varying maximal aperture angle.
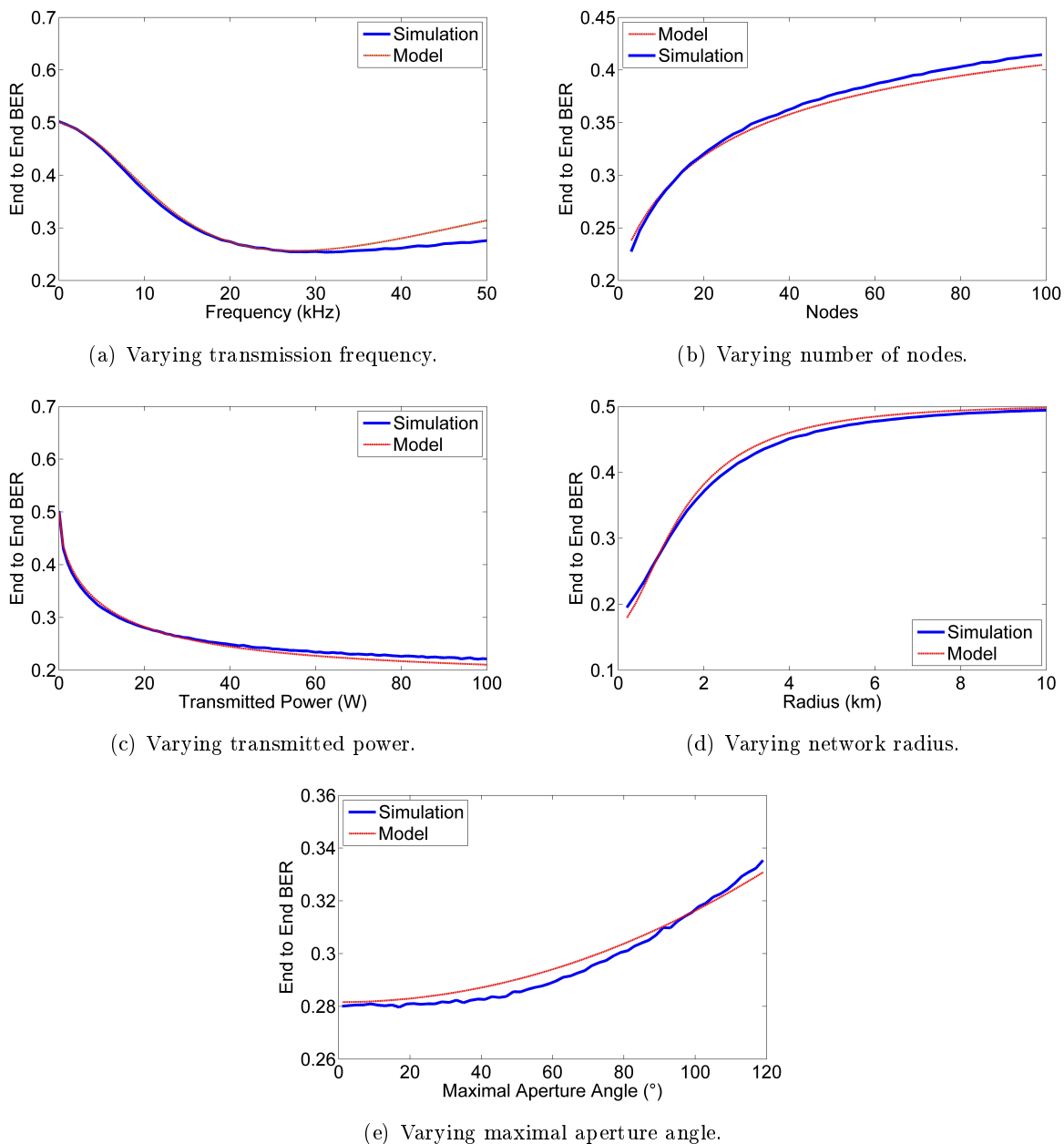
Figure 7.5: End-to-End BER. Simulation versus model. See Table 7.1.

7.3 summarizes the behavior of the End-to-End BER.

7.4 Optimal Values

The optimal transmission frequency is that value which minimizes the End-to-End BER. Figure 7.6 shows the optimal frequency for the End-to-End BER by varying the number of nodes, the maximal aperture angle, the transmitted power, the network radius and the transmission bit rate. The used values for the other parameters are shown in Table 7.1. The optimal values were obtained using the optimization function $fminbnd$ from MATLAB. This function minimize the End-to-End

Table 7.3: End-to-End BER.

PARAMETER	VARIATION	ONE-HOP BER
Transmission frequency (f)	Increases	Decreases until optimal and increases
Number of nodes (N)	Increases	Increases
Network radius (R)	Increases	Increases
Transmitted power (P_{TS})	Increases	Decreases
Maximal aperture angle (θ)	Increases	Increases

BER based on the developed mathematical model and receives as input the network parameters. Appendix I.5 shows the MATLAB code for the optimal transmission frequency varying the number of nodes.

Figure 7.6 (a) shows that the optimal transmission frequency for the End-to-End BER decreases with the number of nodes if the analysis considers interference, i.e., obtained by the SNIR. If the interference is not considered, the optimal frequency will increase very slow (almost constant) with the number of nodes. In Section 6.5.2, it was proved that the SNR does not depend on the number of nodes. Note that an increase in the number of nodes causes an increase in the interference, as Figure 6.3 (a), Section 6.3, shows. Therefore the optimal frequency is a trade-off among the received signal, the interference and the noise. A decrease of the frequency leads to a decrease of the attenuation coefficient, i.e., the path loss, and an increase of the utile received signal strength and the interference as Figure 6.4 (a) shows, but the effect on the utile received signal is more relevant than the effect on the interference.

An increase of the maximal aperture angle causes that the optimal frequency increases in both cases, with and without interference, as in Figure 7.6 (b). Note that if the maximal aperture angle increases, the End-to-End BER also increases, as Figure 7.5 (e) illustrates.

The transmitted power affects the interference as Figure 6.3 (c) shows. Therefore, it impacts the optimal transmission frequency as it is illustrated in Figure 7.6 (c). If the End-to-End BER does not consider interference, the optimal frequency is constant.

From Figure 7.6 (d), for network radius above 2 Km, the optimal transmission frequency varies in the same way with or without interference.

If End-to-End BER does not consider interference, the variation of the bit rate does not affect the optimal frequency, as in Figure 7.6 (e).

7.5   One-Hop BER versus End-to-End BER

In order to know when it is more efficient to transmit the information in only one-hop or in multi-hop by considering the BER performance, we make a comparison between these two cases by varying the transmission frequency, the number of nodes, the network radius and the transmitted

(a) Varying number of nodes.

(b) Varying maximal aperture angle.

(c) Varying transmitted power.

(d) Varying network radius.

(e) Varying bit rate.
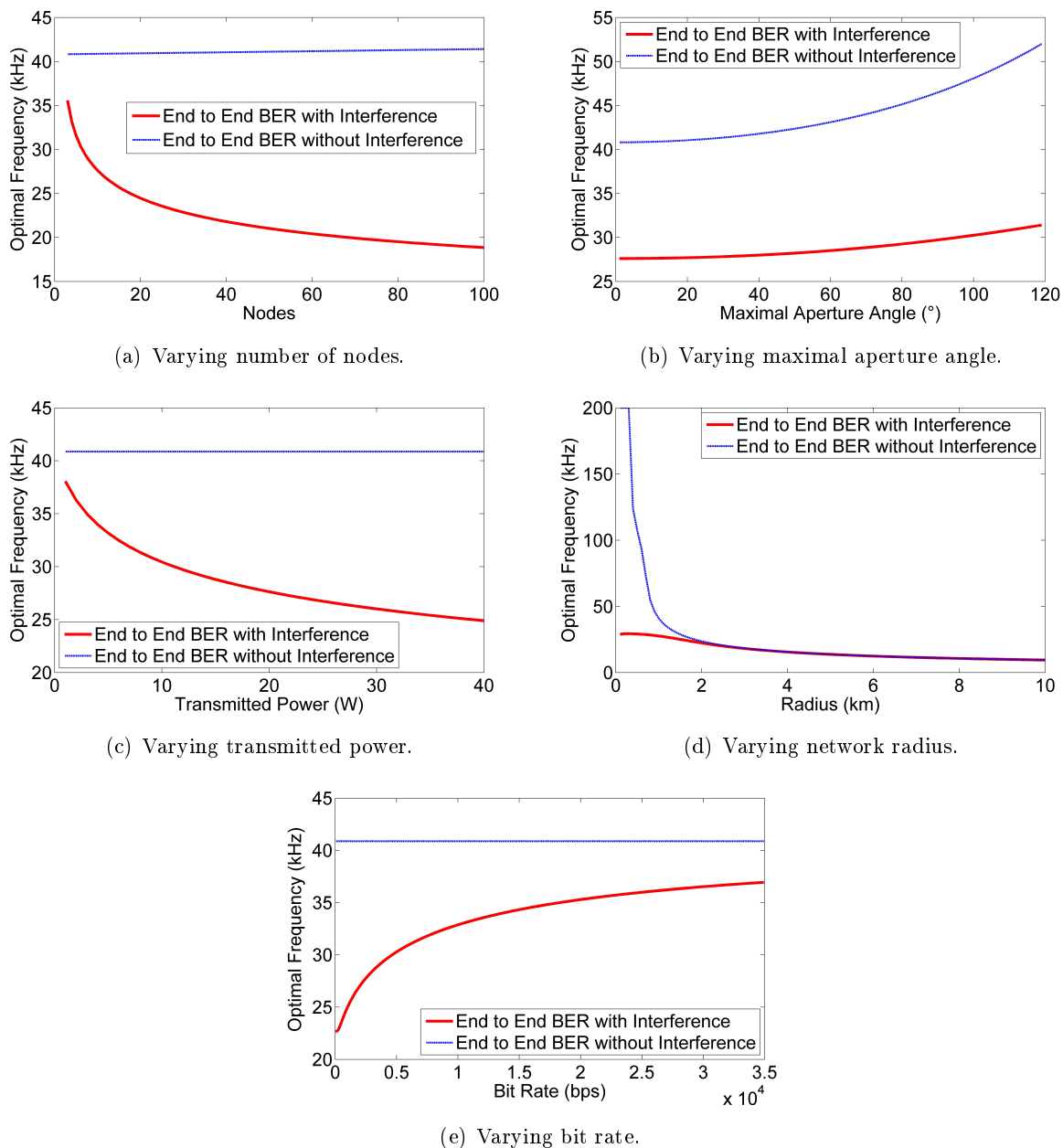
Figure 7.6: Optimal transmission frequency for the End-to-End BER. Model. See Table 7.1.

power.

Figure 7.7 shows the obtained results by varying those parameters and for different maximal aperture angles. The used default values are shown in Table 7.1. In some scenarios, the obtained One-Hop BER is lower than the End-to-End BER.

Figure 7.7 shows that for $\theta = 10^o$ it is better to transmit in a multi-hop fashion. However, for higher values of maximal aperture angle, like 60° or 90° depending on the value of the network parameter (f, R, and N), it is better to transmit using a single-hop, if the BER is the measure of interest. For these cases, bigger angles, the transmitting node based on the network topology will transmit to a node closest to him, but more far from the reference line.

64
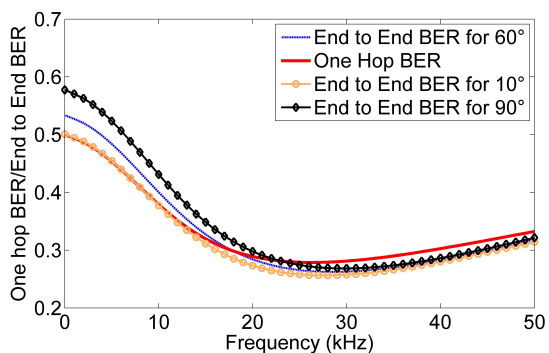
(a) Varying transmission frequency and maximal aperture angle.
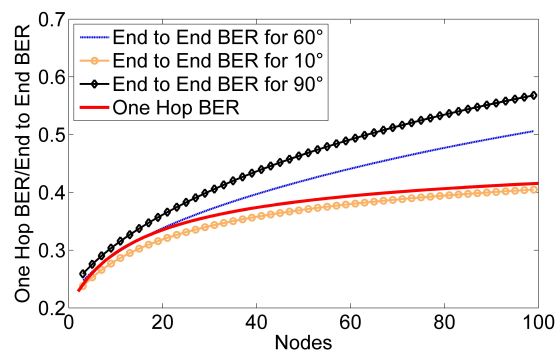
(b) Varying number of nodes and maximal aperture angle.
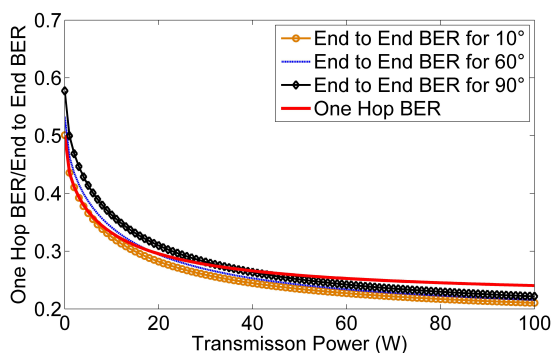
(c) Varying transmitted power and maximal aperture angle.
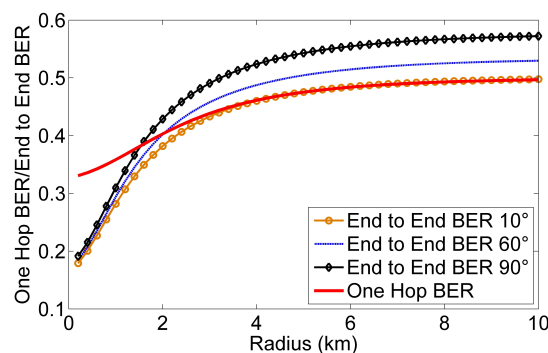
(d) Varying network radius and maximal aperture angle.

Figure 7.7: One-Hop BER versus End-to-End BER. Model. See Table 7.1.

7.6 Conclusions

This chapter was the final step of this research, obtaining the End-to-End BER of an UAN, based on our developed mathematical model. First, it was obtained the One-Hop Bit Error Rate, considering a BPSK modulation, SNIR. The End-to-End BER was calculated with the average number of hops and the One-Hop BER. Monte-Carlo simulations and model were compared and the agreement of the results validates our analysis.

In addition, it was obtained the optimal transmission frequency, varying the maximal aperture angle, the transmitted power, the bit rate, the number of nodes and the network radius. We found that the optimal number of nodes, network radius and maximal aperture angle are the smallest possible. The optimal transmitted power is the highest possible.

Finally, it was compared the One-Hop BER to the End-to-End BER, analysing the scenarios where is more efficient to each one.

It is possible to conclude also that the behaviour of the One-Hop BER and the End-to-End BER has a big relationship with the used network topology.

Chapter 8

General Conclusions and Future Works

This work began presenting the fundamentals of the UANs. It introduces the subject with some history. After that were described and relation the used parameters for this type of network, such as acoustic impedance, acoustic intensity, acoustic power and acoustic pressure among others. The characteristics of the acoustic channel were described also, explaining the acoustic path loss, the absorption loss, the spreading loss and the noise. It was justified why this work does not consider the multipath and the Doppler effect. In addition, the MAC protocols for UANs were discussed and was selected for our study the ALOHA MAC protocol. This MAC protocol does not consider the temporal uncertainly, therefore, as was shown, the consideration of the spatial uncertainly does not change the behavior of the protocol.

Another important element analysed in this work was the modulations for UANs. It explain the characteristic of the digital and analog modulations, specification the advantages of each one. Was selected for our investigation the BPSK modulation, because it is robust, simple and very widely used by underwater acoustic modems.

In chapter 5 was explained the adopted network topology and was developed a mathematical model to obtain the average number of hops and the p.d.f. for the distance between two nodes inside the network. In order to obtain the average number of hop it was necessary to obtain before the average distance from any node inside the network to the central node (assumed as the receiver node). In addition was necessary to obtain the average distance of the hop based on the selected network strategy and the average deviation from the reference line.

After that, was obtained a mathematical model that allow us to calculate the SNIR of a link at an UAN, using ALOHA MAC protocol and considering the interference as an important and determinant impairment. This result will permit to calculate at a predetermined scenario the expected SNIR for one-hop. Therefore we will be able to configure it to obtain a better measure of quality in the communication link.

Finally based on the previous results, was obtained the One-Hop BER and the End-to-End BER for the entire path. With this model we also was able to determine, based on a MATLAB function, the optimal frequency to get the optimal End-to-End BER.

The obtained results from this research could be an important tool for the study and analysis of the underwater acoustic communications. In addition, allow us to preview the behavior of the network before its implementation. Also, was included into the analysis of the Signal-to-Noise Ratio, the interference, and was proved that if ALOHA MAC protocol is consider, it is an important element to consider.

Numerical and Monte-Carlo simulation results presented good agreement which validates our modeling. The results were presented as a function of important network parameters as transmission frequency, total number of nodes inside the network, network radius, etc.

Future research topics might consider other MAC protocols, studying the behavior of the interference in other scenarios. In addition, the effects of acoustic fading and mobility are of importance, as well. Also, the analysis of the multi-path and the Doppler effect could be very interesting and can improve our developed model. Another important research area is the study of the impact of the SNIR and BER behavior in higher layers underwater network protocols.

REFERENCES

[1] S. Authors. Accessed: 2014-08-10. [Online]. Available: http://www.dosits.org/science/sciencesummary/

[2] F. Jensen, W. Kuperman, M. Porter, and H. Schmidt, *Computational Ocean Acoustics*. Springer, 2011.

[3] J. Miranda, "Modulation Analysis for an Underwater Communication Channel," Master's thesis, Universidade do Porto, Portugal, 2012.

[4] A. Zoksimovski, D. Sexton, M. Stojanovic, and C. Rappaport, "Underwater Electromagnetic Communications Using Conduction-Channel Characterization," *WUWNet*, vol. 56, November 2012.

[5] Y. K. Zahedi, F. Yunes, and S. H. S. Ariffin, "A Survey of Existing Medium Access Control (MAC) for Underwater Wireless Sensor Networks (UWSN)," *Fourth Asia International Conference on Mathematical/Analytical Modelling and Computer Simulations. IEEE Computer Society.*, pp. 544–549, 2010.

[6] R. Ortega and R. M. de Moraes, "Signal-to-Noise and Interference Ratio Analysis for ALOHA Underwater Acoustic Networks," *IWT 2015, Santa Rita de Sapucai, Brazil*, pp. 180–185, June 2015.

[7] L. Berkhovskikh and Y. Lysanov, *Fundments of Ocean Acoustics*. Springer, 1982.

[8] X. Lurton, *An Introduction to Underwater Acoustic. Principles and Application.* Springer, 2010.

[9] S. Climent, A. Sanchez, J. Capella, N. Meratnia, and J. Serrano, "Underwater Acoustic Wireless Sensor Networking: Advances and Future Trends in Physical, MAC and Routing Layers," *Sensors*, vol. 14, pp. 795–833, January 2014.

[10] K. Saraswathi, K. A. Netravathi, and S. Ravishankar, "A Study on channel modeling of underwater acoustic communication," *International Journal of Research in Computer and Communication Technology*, vol. 3, pp. 143–147, January 2014.

[11] M. Stojanovic, "On the Relationship between Capacity and Distance in an Underwater Acoustic Communication Channel," *Mobile Computer and Communication Review*, vol. 11, pp. 34–43, 2006.

[12] M. Stajanovic and J. Presing, "Underwater Acoustic Communication Channels: Propagation Models and Statical Characterization," *IEEE Communications Magazine*, vol. 47, pp. 84–89, January 2009.

[13] R. Coates, *Underwater Acoustic Systems*. Wiley, 1989.

[14] A. Syed, W. Ye, B. Krishnamachari, and J. Heidemann, "Understanding Spatio-Temoral Uncertainty in Medium Access with ALOHA protocols," *WuWNet*, pp. 41–48, September 2007.

[15] N. Abramson, "The ALOHA System: Another Alternative for Computer Communications," *Fall Joint Computer Conference*, pp. 281–285, November 1970.

[16] R. Lawrence, "ALOHA Packet System With and Without Slots and Capture," *ACM SIG-COMM Computer Communication Review*, vol. 5, pp. 28–42, April 1975.

[17] A. Stefanov and M. Stojanovic, "Communication Theoretic Analysis of Underwater Ad-Hoc Networks in the Presence of Interference," *IEEE Globecom 2010 Workshop on Heterogeneous, Multi-hop Wireless and Mobile Networks*, pp. 186–190, 2010.

[18] M. Felamban, B. Shihada, and K. Jamshaid, "Optimal Node Placement in Underwater Wireless Sensor Networks," *IEEE 27th International Conference on Advanced Information Networking and Applications*, pp. 492–499, March 2013.

[19] Y. Zhu, Z. Jiang, Z. Peng, M. Zuba, J. Cui, and H. Chen, "Toward Practical MAC Design for Underwater Acoustic Networks," *IEEE INFOCOM*, pp. 683–691, April 2013.

[20] S. Murugan and V. Natarajan, "Performance Analysis of Signal to Noise Ratio and Bit Error Rate for Multiuser using Passive Time Reversal Technique in Underwater Communication," *International Conference on Wireless Communication and Sensor Computing, 2010. ICWCSC 2010*, pp. 1–4, January 2010.

[21] T. Elganimi, "Performance Comparison between OOK, PPM and PAM Modulation Schemes for Free Space Optical (FSO) Communication Systems: Analytical Study," *International Journal of Computer Application*, vol. 79, pp. 22–27, November 2016.

[22] B. Benson, "Design of a Low-cost Underwater Acoustic Modem for Short-Range Sensor Networking Application," Ph.D. dissertation, University of California, San Diego, CA, USA, 2010.

[23] J. Willis, W. Ye, and J. Heidemann, "Low-Power Acoustic Modem for Dense Underwater Sensor Networks", journal = "WUWNet, Los Angeles, California, USA," pp. 22–27, September 2013.

[24] N. Parrish, L. Tracy, S. Roy, P. Arabshahi, and W. L. J. Fox, "System Design Considerations for Undersea Networks: Link and Multiple Access Protocols," *IEEE Journal on Selected Areas in Communications*, vol. 26, pp. 1720–1730, December 2008.

[25] B. Borowski and D. Duchamp, "Measurement-based Underwater Acoustic Physical Layer Simulation," *IEEE OCEANS 2010*, pp. 1–8, September 2010.

[26] A. Valentine, "Performance of Maximal-Ratio Diversity Systems in a Correlated Nakagami-Fading Environment," *IEEE Transactions on Communications*, vol. 43, pp. 2360–2369, August 1995.

[27] M. Stojanovic and L. Freitag, "Multichannel detection for wideband underwater acoustic CDMA communications," *IEEE Journal of Oceanic Engineering*, vol. 31, pp. 685–695, July 2006.

[28] H. Yan, S. Zhou, Z. J. Shi, and B. Li, "A DSP Implementation of OFDM Acoustic Modem," *WuWNet, Montreal, Quebec, Canada*, pp. 89–92, September 2007.

[29] S. Roy, V. MacDonald, and J. Proakis, "High-rate communication for underwater acoustic channels using multiple transmitters and space-time coding: Receiver structures and experimental results," *IEEE Journal of Oceanic Engineering*, vol. 32, pp. 663–688, July 2007.

[30] S. Panichpapiboon, G. Ferrari, and O. K. Tonguz, "Sensor Networks with Random Versus Uniform Topology: MAC and Interference Considerations," *IEEE VTC, Milan, Italy*, vol. 4, pp. 2111 – 2115, May 2004.

[31] O. K. Tonguz and G. Ferrari, *Ad Hoc Wireless Networks: A Communication-Theoretic Perspective*. Jhon Wiley and Sons, 2006.

[32] P. C. Ghobad and R. M. de Moraes, "Ber analysis with an appropriate friis formula for multi-hop aloha dense ad hoc networks," *Vehicular Technology Conference (VTC Fall), 2012 IEEE*, pp. 1–5, September 2012.

[33] G. Ferrari and O. K. Tonguz, "Impact of Mobility on the BER Performance of Ad Hoc Wireless Networks," *IEEE Transaction on Vehicular Technology*, vol. 56, pp. 271–286, January 2007.

APPENDIX

I. MATLAB CODES FOR SIMULATION AND MODEL

I.1 One-Hop Matlab Simulations and Model varying Central Transmitting Frequency

```matlab
%Ruben  Ortega  Blanco
%Simulation  and  Model  varying  Central  Transmitting  Frequency  of:
    %One-Hop  Received  Signal
    %One-Hop  Interference
    %Noise
    %One-Hop  Acoustic  Path  Loss
    %One-Hop  Signal-to-Noise  Ratio  (SNR)
    %One-Hop  Signal-to-Noise  Interference  Ratio  (SNIR)
    %One-Hop  Bit  Error  Rate  (BER)  with  and  without  interference
%Post-Graduation  Program  in  Electronics  and  Automation  Engineering  Systems  (PGEA)
%Electric  Engineering  Department
%University  of  Brasilia
%Brazil

clc
clear

%Parameters
N=10;                      %Number  of  Nodes
R=1;                       %Sphere  Radius(km)
k=1.5;                     %Spreading  factor
A0=10^(0.1*25);            %Unit-normalizing  constant  for  Acoustic  Path  Loss
Pt=20;                     %Transmission  Power  (W)
Pa=1035;                   %Sea  density(kg/m^3)
c=1507;                    %Sound  Speed(m/s)
r=1;                       %Output  reference  radius(m)
v=20;                      %Wind  Speed  (knots)
DF=5*(10^3);               %Noise  Frequency  Bandwith(Hz)
T=1;                       %Average  rate  of  paq.  trans.  for  a  node  (pck/sec)
L=768;                     %Paq.  Size  (bits)
Rb=2400;                   %Data  transm.  rate  (bits/sec)
Phi=pi/3;                  %Max.  aperture  angle  (rad)

%frequency  values
beg=1;                     %beginning  value
step=1;                    %steps
finish=50;                 %last  value
p=0;

m=0;                       %Iterations
rep=100;                   %number  of  iterations
```

```matlab
%Matrix to store values
for f=beg:step:finish
    p=p+1;
end
SNR_m_W=zeros(p);                   %Store SNR model
SNR_m_W_Log=zeros(p);               %Store SNR model decibels
SNR_s_av_W=zeros(p);                %Store SNR simulation
SNR_s_W_Log=zeros(p);               %Store SNR simulation decibels
SNIR_m_W=zeros(p);                  %Store SNIR model
SNIR_m_W_Log=zeros(p);              %Store SNIR model decibels
SNIR_s_av_W=zeros(p);               %Store SNIR simulation
SNIR_s_av_W_Log=zeros(p);           %Store SNIR simulation decibels
BER_m_BPSK_W=zeros(p);              %Store BER model without inter. for BPSK
BER_int_m_BPSK_W=zeros(p);          %Store BER model with inter. for BPSK
BER_m_OOK_RZ_W=zeros(p);            %Store BER model without inter. for OOK-RZ
BER_int_m_OOK_RZ_W=zeros(p);        %Store BER model with inter. for OOK-RZ
BER_m_OOK_NRZ_W=zeros(p);           %Store BER model without inter. for OOK-NRZ
BER_int_m_OOK_NRZ_W=zeros(p);       %Store BER model with inter. for OOK-NRZ
BER_m_NC_FSK_W=zeros(p);            %Store BER model without inter. for FSK-NC
BER_int_m_NC_FSK_W=zeros(p);        %Store BER model with inter. for FSK-NC
BER_m_C_FSK_W=zeros(p);             %Store BER model without inter. for FSK-C
BER_int_m_C_FSK_W=zeros(p);         %Store BER model with inter. for FSK-C
BER_s_av_W=zeros(p);                %Store BER sim. without inter. for BPSK
BER_int_s_av_W=zeros(p);            %Store BER sim. with inter. for BPSK
REC_SIN_sim_W=zeros(p);             %Store Received Signal
INT_s_av=zeros(p);                  %Store Interference simulated
INT_m_W=zeros(p);                   %Store Interference model
INT_m_dB=zeros(p);                  %Store Interference model decibels
Noise=zeros(p);                     %Store Total Noise
Noise_lin_W=zeros(p);               %Store Noise times freq bandwith in Watts
Path_loss_mod=zeros(p);             %Store Path loss model in decibels
Path_loss_mod_lin=zeros(p);         %Store Path loss model
Path_loss_s_av=zeros(p);            %Store Path loss simulation
REC_SIN_W=zeros(p);                 %Store Received Signal Model
REC_SIN_W_dB=zeros(p);              %Store Received Signal Model decibels
X=zeros(3,N);                       %Store the uniforms and random points
p=0;


Imp=Pa*c;                           %Acoustic Impedance
Area=4*pi*(r)^2;                    %Output Reference Area
Z=(3/4)*R;                          %Dist. to central node model


%ITERATIONS VARYING FREQUENCY
for f=beg:step:finish
    p=p+1;

    %Absortion Coeficient for frequency values bigger than 0.1kHz
    a = 10^(0.1*((0.11*((f.^2)./(1+f.^2))+44*((f.^2)./(4100+f.^2))+((2.75*10^-4)*f
        .^2)+0.003)));

    %NOISE
```

```matlab
Ntur=30−30*log10(f);                          %Turbulency
Ntr=10*log10((3*10^8)./(1+(10^4)*f.^4));  %Trafic
Nsea=40+10*log10((v.^2)./(1+f.^(5/3)));    %Sea movement
Nth=−15+20*log10(f);                          %Thermal
%Total Noise in Pascal/Hz
Nt=(10.^(0.1*(Ntr))+10.^(0.1*(Ntur))+10.^(0.1*(Nsea))+10.^(0.1*(Nth)))*10^(−6);
%Total Noise in Watts
Nt_W=((Nt*DF)^2)*Area/Imp;


%INTERFERENCE MODEL
I=log(a)^(−2+k)*R*(log(a)^(−1−k)*R^(−1−k)*(k−3)*(−2+k)*(log(a)*R)^((1/2)*k)*exp
    (−(1/2)*log(a)*R)*whittakerM(−(1/2)*k,−(1/2)*k+1/2,log(a)*R)/(−k+3)+log(a)
    ^(−1−k)*R^(−1−k)*(log(a)*R−k+2)*(k−3)*(log(a)*R)^((1/2)*k)*exp(−(1/2)*log(a)
    *R)*whittakerM(−(1/2)*k+1,−(1/2)*k+1/2,log(a)*R)/(−k+3));
Ecal=(3*Pt/(A0*R^3))*I;
P_int_mod=(1−exp((−T*L)/Rb))*(N−2)*Ecal;


%ACOUSTIC PATH LOSS
A_path_mod=A0*(Z^k)*(a^Z);
A_path_mod_dB=10*log10(A_path_mod);


%RECEIVED SIGNAL
P_rec_mod=Pt/A_path_mod;


%Store values of each iteration of simulation
SNR_steps_av_W=zeros(rep,1);          %Store SNR
SNIR_steps_av_W=zeros(rep,1);         %Store SNIR
INT_sim_av=zeros(rep,1);              %Store Interference
P_rec_i=zeros(rep,1);                 %Store Received Signal
BER_steps_av_W=zeros(rep,1);          %Store BER without Interference
BER_int_steps_av_W=zeros(rep,1);      %Store BER with Interference
Path_loss_steps_av=zeros(rep,1);      %Store Path loss
m=1;
%SIMULATION
for m=1:rep
    i=0;
    %Filling nodes inside the sphere
    while i < N
        x = 2*R*rand(3, 1) − R;   %Storing random posit of node (i+1)
        if norm(x) <= R           %Delimiting x vec. to sphere of rad R
            i = i + 1;
            X(:, i) = x;
        end
    end
    %Store values for each node inside the sphere
    SNR_W=zeros(N,1);             %Store SNR
    SNIR_W=zeros(N,1);            %Store SNIR
    BER_int_W=zeros(N,1);         %Store BER without Interference
    BER_W=zeros(N,1);             %Store BER with Interference
    INT_sim_W=zeros(N,1);         %Store Interference
    P_rec_W=zeros(N,1);           %Store Received Power
    Path_loss_i=zeros(N,1);       %Store Path loss
```

```matlab
    %Calculating for each node
    for i = 1:N
        l=norm(X(:,i));            %Distance to node i
        %INTERFERENCE RECEIVED BY NODE I
        P_int=0;
        for j=1:N
            l_node=norm(X(:,j));
            l_node_j_i=abs(norm(X(:,i)-X(:,j)));
            if l_node_j_i~=0
                E=Pt/(A0*(l_node^k)*(a^l_node));
                P_int=P_int+(1-exp((-T*L)/Rb))*E;
            end
        end
        INT_sim_W(i)=P_int;        %Tot inter. received by node i

        %ACOUSTIC PATH LOSS FOR TRANSMISSION TO NODE I
        A_path=A0*(l^k)*(a^l);
        A_path_dB=10*log10(A_path);
        Path_loss_i(i)=A_path_dB;

        %RECEIVED SIGNAL BY NODE I
        P_rec=Pt/A_path;
        P_rec_W(i)=P_rec;

        %SNR IN TRANSMISSION TO NODE I
        SNR_i_W=P_rec/(Nt_W);
        SNR_W(i)=SNR_i_W;

        %SNIR IN TRANSMISSION TO NODE I
        SNIR_i_W=P_rec/(Nt_W+P_int); %SNIR for Hop to node i for Watts
        SNIR_W(i)=SNIR_i_W;

        %BER IN TRANSMISSION TO NODE I (BPSK)
        BER_int_W(i)=qfunc((2*SNIR_i_W)^0.5);    %With Interference
        BER_W(i)=qfunc((2*SNR_i_W)^0.5);         %Without Interference
    end

    %Saving values in matrix
    P_rec_i(m)=(sum(P_rec_W))/N;
    INT_sim_av(m)=(sum(INT_sim_W))/N;
    SNR_steps_av_W(m)=(sum(SNR_W))/N;
    SNIR_steps_av_W(m)=(sum(SNIR_W))/N;
    BER_steps_av_W(m)=(sum(BER_W))/N;
    BER_int_steps_av_W(m)=(sum(BER_int_W))/N;
    Path_loss_steps_av(m)=(sum(Path_loss_i))/N;
end

%RESULTS
%MODEL
SNR_model_W=P_rec_mod/(Nt_W);   %for Watts
SNR_m_W(p)=SNR_model_W;
SNR_m_W_Log(p)=10*log10(SNR_model_W);
```

```matlab
SNIR_model_W=P_rec_mod/(Nt_W+P_int_mod);    %For Watts
SNIR_m_W(p)=SNIR_model_W;
SNIR_m_W_Log(p)=10*log10(SNIR_model_W);


INT_m_W(p)=P_int_mod;
INT_m_dB(p)=10*log10(P_int_mod*(10^6)/DF);


REC_SIN_W(p)=P_rec_mod;
REC_SIN_W_dB(p)=10*log10(P_rec_mod);


BER_model_BPSK_W=qfunc((2*SNR_model_W)^0.5);
BER_m_BPSK_W(p)=BER_model_BPSK_W;
BER_model_OOK_RZ_W=(1/2)*erfc((1/2)*((SNR_model_W)^0.5));
BER_m_OOK_RZ_W(p)=BER_model_OOK_RZ_W;
BER_model_OOK_NRZ_W=(1/2)*erfc((1/(2*(2^0.5)))*((SNR_model_W)^0.5));
BER_m_OOK_NRZ_W(p)=BER_model_OOK_NRZ_W;
BER_model_NC_FSK_W=(1/2)*exp(-SNR_model_W/2);
BER_m_NC_FSK_W(p)=BER_model_NC_FSK_W;
BER_model_C_FSK_W=qfunc(SNR_model_W^(0.5));
BER_m_C_FSK_W(p)=BER_model_C_FSK_W;


BER_int_model_BPSK_W=qfunc((2*SNIR_model_W)^0.5);
BER_int_m_BPSK_W(p)=BER_int_model_BPSK_W;
BER_int_model_OOK_RZ_W=(1/2)*erfc((1/2)*((SNIR_model_W)^0.5));
BER_int_m_OOK_RZ_W(p)=BER_int_model_OOK_RZ_W;
BER_int_model_OOK_NRZ_W=(1/2)*erfc((1/(2*(2^0.5)))*((SNIR_model_W)^0.5));
BER_int_m_OOK_NRZ_W(p)=BER_int_model_OOK_NRZ_W;
BER_int_model_NC_FSK_W=(1/2)*exp(-SNIR_model_W/2);
BER_int_m_NC_FSK_W(p)=BER_int_model_NC_FSK_W;
BER_int_model_C_FSK_W=qfunc(SNIR_model_W^(0.5));
BER_int_m_C_FSK_W(p)=BER_int_model_C_FSK_W;


Path_loss_mod(p)=A_path_mod_dB;
Path_loss_mod_lin(p)=A_path_mod;


Noise(p)=10*log10(10.^(0.1*(Ntr))+10.^(0.1*(Ntur))+10.^(0.1*(Nsea))+10.^(0.1*(
    Nth)));
Noise_lin_W(p)=Nt_W;


%SIMULATION
SNR_sim_av_W=(sum(SNR_steps_av_W))/rep;
SNR_s_av_W(p)=SNR_sim_av_W;
SNR_sim_W_Log=10*log10(SNR_sim_av_W);
SNR_s_W_Log(p)=SNR_sim_W_Log;


SNIR_sim_av_W=(sum(SNIR_steps_av_W))/rep;
SNIR_s_av_W(p)=SNIR_sim_av_W;
SNIR_s_av_W_Log(p)=10*log10(SNIR_sim_av_W);


BER_sim_av_W=(sum(BER_steps_av_W))/rep;
BER_s_av_W(p)=BER_sim_av_W;
```

```matlab
    BER_int_sim_av_W=(sum(BER_int_steps_av_W))/rep;
    BER_int_s_av_W(p)=BER_int_sim_av_W;

    INT_sim_ave=(sum(INT_sim_av))/rep;
    INT_s_av(p)=INT_sim_ave;

    REC_SIN_s_W=(sum(P_rec_i))/rep;
    REC_SIN_sim_W(p)=REC_SIN_s_W;

    Path_loss_sim_av=(sum(Path_loss_steps_av))/rep;
    Path_loss_s_av(p)=Path_loss_sim_av;
end

%PRINTING
% plot(beg:step:finish,INT_s_av,'g',beg:step:finish,INT_m_W,'-b');
% plot(beg:step:finish,REC_SIN_sim_W,'g',beg:step:finish,REC_SIN_W,'-b');
% plot(beg:step:finish,SNIR_s_av_W,'-k',beg:step:finish,SNIR_m_W,'-b');
% plot(beg:step:finish,SNIR_s_av_W_Log,'-k',beg:step:finish,SNIR_m_W_Log,'-b');
% plot(beg:step:finish,SNR_s_av_W,'-k',beg:step:finish,SNR_m_W,'-b');
% plot(beg:step:finish,SNR_s_W_Log,'-k',beg:step:finish,SNR_m_W_Log,'-b');
% plot(beg:step:finish,BER_int_s_av_W,'-k',beg:step:finish,BER_int_m_BPSK_W,'-b');
% plot(beg:step:finish,BER_s_av_W,'-k',beg:step:finish,BER_m_BPSK_W,'-b');
% plot(beg:step:finish,BER_m_BPSK_W,'-r',beg:step:finish,BER_int_m_BPSK_W,'b',beg:
     step:finish,BER_m_OOK_RZ_W,'-k',beg:step:finish,BER_int_m_OOK_RZ_W,'-g',beg:step
     :finish,BER_m_OOK_NRZ_W,'-y',beg:step:finish,BER_int_m_OOK_NRZ_W,'-m',beg:step:
     finish,BER_m_NC_FSK_W,'-b*',beg:step:finish,BER_int_m_NC_FSK_W,'-r*',beg:step:
     finish,BER_m_C_FSK_W,'-c',beg:step:finish,BER_int_m_C_FSK_W,'-k*');
% plot(beg:step:finish,Path_loss_s_av,'-k',beg:step:finish,Path_loss_mod,'-b');
% plot(beg:step:finish,INT_m_W,'-k',beg:step:finish,REC_SIN_W,'g',beg:step:finish,
     Noise_lin_W,'-b');
```

I.2 Function to find the Next Node to Jump based on the Used Routing Strategy

```matlab
%Ruben Ortega Blanco
%Function that return the next node to jump, based on the employ routing strategy
%Post-Graduation Program in Electronics and Automation Engineering Systems (PGEA)
%Electric Engineering Department
%University of Brasilia
%Brazil

function [ next_node,dist_to_next_node ] = Next_node_Jump( origin_node,dest_node,
    distrib_nodes,Phi)
%Reference vector from origin to destiny
dist_to_next_node=realmax;
next_node=-1;
    for i=1:length(distrib_nodes)      %i is the testing node
        if i~=origin_node                %Next node to jump diff from the origin
```

77

```
            %Temporaly vector to check angle
            temp_vect=distrib_nodes(:,i)-distrib_nodes(:,origin_node);
            %Cosine of the angle between the two vectors
            CosTheta=dot(distrib_nodes(:,dest_node)-distrib_nodes(:,origin_node),
                temp_vect)/(norm(distrib_nodes(:,dest_node)-distrib_nodes(:,
                origin_node))*norm(temp_vect));
            %Angle between the two vectors
            Theta=acos(CosTheta);
            %Comparing that the deviation be inside the angle
            if ((-Phi/2)<=Theta)&&(Theta<=(Phi/2))
                distance=norm(temp_vect);              %Calculating the distance
                if (distance<dist_to_next_node)        %Finding the shortest one
                    dist_to_next_node=distance;        %Distance to next node
                    next_node=i;                       %Next node
                end
            end
        end
    end
end
```

I.3   End-to-End BER Matlab Simulations and Model varying Central Transmitting Frequency

```
%Ruben Ortega Blanco
%Simulation and Model varying Central Transmitting Frequency of:
    %End-to-End BER
    %Hops number
%Post-Graduation Program in Electronics and Automation Engineering Systems (PGEA)
%Electric Engineering Department
%University of Brasilia
%Brazil

clear
clc

%Parameters
R=1;                %Radius (km)
N=10;               %Number of Nodes
Phi=pi/3;           %Max aperture angle (rad)
A0=10^(0.1*25);     %Normalization factor
k=1.5;              %Spreading factor
P_ts=20;            %Transmission Power (W)
T=1;                %Average rate of paq. trans. for a node (pck/sec)
L=768;              %Paq. Size (bits)
Rb=2400;            %Data transm. rate (bits/sec)
Pa=1035;            %density(kg/m^3)
c=1507;             %Sound Speed(m/s)
r=1;                %Output reference radius(m)
v=20;               %Wind Speed (knots)
```

```matlab
DF=5*(10^3);         %Noise Frequency Bandwith (Hz)

m=100;               %Iterations

%Transmitting Frequency values
beg=0;               %beginning value
step=1;              %steps
finish=50;           %last value
p=0;

%Matrix to store values
for f=beg:step:finish
    p=p+1;
end
A_sim=zeros(p);                  %Store Path loss simulation
A_m=zeros(p);                    %Store Path loss model
SNIR_model_matrix_W=zeros(p);    %Store SNIR model
SNIR_sim_W=zeros(p);             %Store SNIR simulation
BER_sim_BPSK_W=zeros(p);         %Store End-to-End BER simulation for BPSK
BER_model_BPSK_W=zeros(p);       %Store End-to-End BER model for BPSK
BER_sim_OOK_RZ_W=zeros(p);       %Store End-to-End BER simulation for OOK-RZ
BER_model_OOK_RZ_W=zeros(p);     %Store End-to-End BER model for OOK-RZ
BER_sim_OOK_NRZ_W=zeros(p);      %Store End-to-End BER simulation for OOK-NRZ
BER_model_OOK_NRZ_W=zeros(p);    %Store End-to-End BER model for OOK-NRZ
BER_sim_NC_FSK_W=zeros(p);       %Store End-to-End BER simulation for NC-FSK
BER_model_NC_FSK_W=zeros(p);     %Store End-to-End BER model for NC-FSK
BER_sim_C_FSK_W=zeros(p);        %Store End-to-End BER simulation for C-FSK
BER_model_C_FSK_W=zeros(p);      %Store End-to-End BER model for C-FSK
HOP_sim=zeros(p);                %Store number of hops simulation
HOP_model=zeros(p);              %Store number of hops model
X=zeros(3,N);                    %Store the uniforms and random points
Inter=zeros(N-1,1);              %Store the Interferences from the N nodes
p=0;

Imp=Pa*c;                        %Impedance
Area=4*pi*(r)^2;                 %Output Reference Area
Ps=N/((4/3)*pi*(R^3));           %Nodes Spatial Density
Z=(3/4)*R;                       %Dist. to central node model
E_Phi=(2/Phi)*(sin(Phi/2));      %Average deviation. Model
%Average Distance of the hop. Model
W=(3/4)*R*exp(-(1/2)*((2/3)*pi*Ps*(1-cos(Phi/2)))*R^3)*whittakerM(1/6, 2/3, ((2/3)*
    pi*Ps*(1-cos(Phi/2)))*R^3)/((1-exp(-((2/3)*pi*Ps*(1-cos(Phi/2)))*R^3))*(((2/3)*
    pi*Ps*(1-cos(Phi/2)))*R^3)^(1/6));
%AVERAGE HOP NUMBER. MODEL
hop_number_model=Z/(W*E_Phi);

%ITERATIONS VARYING FREQUENCY
for f=beg:step:finish
    p=p+1;

    %Absortion Coeficient for frequency values bigger than 0.1kHz
```

```matlab
a = 10^(0.1*(0.11*((f^2)/(1+f^2))+44*((f^2)/(4100+f^2))+(2.75*10^(-4))*f
    ^2+0.003));

%NOISE
Ntur=30-30*log10(f);                          %Turbulency
Ntr=10*log10((3*10^8)/(1+(10^4)*(f^4)));  %Trafic
Nsea=40+10*log10((v^2)/(1+(f^(5/3))));    %Sea movement
Nth=-15+20*log10(f);                          %Thermal
%Total Noise in Pascal/Hz
Nt=(10^(0.1*Ntr)+10^(0.1*Ntur)+10^(0.1*Nsea)+10^(0.1*Nth))*(10^(-6));
%Total Noise in Watts
Nt_W=((Nt*DF)^2)*Area/Imp;


%Store values of each iteration of simulation
A_tot_matrix_sim=zeros(m,1);
A_tot_matrix_med=zeros(m,1);
SNIR_tot_matrix_sim_W=zeros(m,1);
BER_tot_matrix_sim_BPSK_W=zeros(m,1);
BER_tot_matrix_sim_OOK_RZ_W=zeros(m,1);
BER_tot_matrix_sim_OOK_NRZ_W=zeros(m,1);
BER_tot_matrix_sim_NC_FSK_W=zeros(m,1);
BER_tot_matrix_sim_C_FSK_W=zeros(m,1);
hop_number_matrix_sim=zeros(m,1);


%%%%%%%%%%%%%SIMULATION%%%%%%%%%%%%%%%%%%%%%%%
for n=1:m
    i=1;
    %Filling nodes inside the sphere
    while i<N
        x=2*R*rand(3,1)-R;   %Storing random posit of node (i+1)
        if norm(x)<=R        %Delimiting x vec. to sphere of rad R
            i=i+1;
            X(:,i)=x;
        end
    end
    %Store values for each node inside the sphere
    A_each_matrix=zeros(1,N);
    SNIR_each_matrix_W=zeros(1,N);
    BER_tot_matrix_BPSK_W=zeros(1,N);
    BER_tot_matrix_OOK_RZ_W=zeros(1,N);
    BER_tot_matrix_OOK_NRZ_W=zeros(1,N);
    BER_tot_matrix_NC_FSK_W=zeros(1,N);
    BER_tot_matrix_C_FSK_W=zeros(1,N);
    hop_number_matrix=zeros(1,N);
    %Calculating for each node
    for j=1:N
        trans_posit=j;                        %Selecting the transm posit
        node_trans=X(:,trans_posit);   %Selecting the transm node

        %NEXT NODE TO JUMP
        node=0;
        receiver_node=1;
```

```
hop_number=0;

%Store values for each hop on the route
SNIR_one_matrix_W=zeros(1,N);
BER_one_matrix_BPSK_W=zeros(1,N);
BER_one_matrix_OOK_RZ_W=zeros(1,N);
BER_one_matrix_OOK_NRZ_W=zeros(1,N);
BER_one_matrix_NC_FSK_W=zeros(1,N);
BER_one_matrix_C_FSK_W=zeros(1,N);
A_one_matrix=zeros(1,N);

%Calculating for each hop on the route
if norm(node_trans)~=0    %Dest node different than the transm
    while node~=1
        %Function that return the next node to jump and dist
        [node,dist]=Next_node_Jump(trans_posit,1,X,Phi);

        %Matrix to store the interferences from the N nodes
        Inter=zeros(N-1,1);
        %Calculating Interference for the hop
        for i=1:N
            %Distance from the dest node to nodes i
            l=norm(X(:,i)-X(:,node));
            if l~=0 && i~=j
                %Storing the nodes interference
                Inter(i,1)=P_ts/(A0*(l^k)*(a^l));
            end
        end
        I_tot=(1-exp((-T*L)/Rb))*sum(Inter); %Tot. Interference

        %Changing to the next node
        trans_posit = node;
        %Increasing the hop number
        hop_number=hop_number+1;

        %ACOUSTIC PATH LOSS
        A=A0*(dist^k)*(a^dist);
        A_one_matrix(:,hop_number)=A;

        %RECEIVED SIGNAL
        P_rs=P_ts/A;

        %SNIR
        SNIR_W=P_rs/(Nt_W+I_tot);
        SNIR_one_matrix_W(:,hop_number)=SNIR_W;

        %ONE-HOP BER
        %QPSK Modulation
        BER_one_BPSK_W=qfunc((2*SNIR_W)^0.5);
        BER_one_matrix_BPSK_W(:,hop_number)=BER_one_BPSK_W;
        %OOK RZ Modulation
        BER_one_OOK_RZ_W=(1/2)*erfc((1/2)*((SNIR_W)^0.5));
```

```matlab
            BER_one_matrix_OOK_RZ_W(:,hop_number)=BER_one_OOK_RZ_W;
            %OOK NRZ Modulation
            BER_one_OOK_NRZ_W=(1/2)*erfc((1/(2*(2^0.5)))*((SNIR_W)^0.5));
            BER_one_matrix_OOK_NRZ_W(:,hop_number)=BER_one_OOK_NRZ_W;
            %FSK Not-coherent Modulation
            BER_one_NC_FSK_W=(1/2)*exp(-SNIR_W/2);
            BER_one_matrix_NC_FSK_W(:,hop_number)=BER_one_NC_FSK_W;
            %FSK coherent Modulation
            BER_one_C_FSK_W=qfunc(SNIR_W^(0.5));
            BER_one_matrix_C_FSK_W(:,hop_number)=BER_one_C_FSK_W;
        end
    end
    %Initialating values
    BER_end_BPSK_W=1;
    BER_end_OOK_RZ_W=1;
    BER_end_OOK_NRZ_W=1;
    BER_end_NC_FSK_W=1;
    BER_end_C_FSK_W=1;
    %Calculating the End-to-End BER
    for i=1:hop_number
        BER_end_BPSK_W=BER_end_BPSK_W*(1-BER_one_matrix_BPSK_W(:,i));
        BER_end_OOK_RZ_W=BER_end_OOK_RZ_W*(1-BER_one_matrix_OOK_RZ_W(:,i));
        BER_end_OOK_NRZ_W=BER_end_OOK_NRZ_W*(1-BER_one_matrix_OOK_NRZ_W(:,i
            ));
        BER_end_NC_FSK_W=BER_end_NC_FSK_W*(1-BER_one_matrix_NC_FSK_W(:,i));
        BER_end_C_FSK_W=BER_end_C_FSK_W*(1-BER_one_matrix_C_FSK_W(:,i));
    end
    SNIR_each_matrix_W(j)=SNIR_one_matrix_W(:,1);
    BER_tot_matrix_BPSK_W(j)=1-BER_end_BPSK_W;
    BER_tot_matrix_OOK_RZ_W(j)=1-BER_end_OOK_RZ_W;
    BER_tot_matrix_OOK_NRZ_W(j)=1-BER_end_OOK_NRZ_W;
    BER_tot_matrix_NC_FSK_W(j)=1-BER_end_NC_FSK_W;
    BER_tot_matrix_C_FSK_W(j)=1-BER_end_C_FSK_W;
    hop_number_matrix(j)=hop_number;
    if hop_number~=0
        A_each_matrix(j)=(sum(A_one_matrix))/hop_number;
    end
    end
    end
    %Calculating values for each iteration
    A_tot_matrix_sim(n)=(sum(A_each_matrix))/(N-1);
    SNIR_tot_matrix_sim_W(n)=(sum(SNIR_each_matrix_W))/(N-1);
    BER_tot_matrix_sim_BPSK_W(n)=(sum(BER_tot_matrix_BPSK_W))/(N-1);
    BER_tot_matrix_sim_OOK_RZ_W(n)=(sum(BER_tot_matrix_OOK_RZ_W))/(N-1);
    BER_tot_matrix_sim_OOK_NRZ_W(n)=(sum(BER_tot_matrix_OOK_NRZ_W))/(N-1);
    BER_tot_matrix_sim_NC_FSK_W(n)=(sum(BER_tot_matrix_NC_FSK_W))/(N-1);
    BER_tot_matrix_sim_C_FSK_W(n)=(sum(BER_tot_matrix_C_FSK_W))/(N-1);
    hop_number_matrix_sim(n)=sum(hop_number_matrix)/(N-1);
end


%%%%%%%%%%%%%%%MODEL%%%%%%%%%%%%%%%%
%INTERFERENCE
```

```matlab
Ecal=6*log(a)^(-2+k)*P_ts*(2^(-1-(1/2)*k)*log(a)^(-1-k)*R^(-1-k)*(k-3)*(-2+k)*(
    log(a)*R)^((1/2)*k)*exp(-log(a)*R)*whittakerM(-(1/2)*k, -(1/2)*k+1/2, 2*log(
    a)*R)/(-k+3)+2^(-1-(1/2)*k)*log(a)^(-1-k)*R^(-1-k)*(2*log(a)*R-k+2)*(k-3)*(
    log(a)*R)^((1/2)*k)*exp(-log(a)*R)*whittakerM(-(1/2)*k+1, -(1/2)*k+1/2, 2*
    log(a)*R)/(-k+3))/(R^2*A0)-(9/2)*log(a)^(k-3)*P_ts*(-2^(-1-(1/2)*k)*log(a)
    ^(-1-k)*R^(-1-k)*(k^2-5*k+6)*(k-4)*(log(a)*R)^((1/2)*k)*exp(-log(a)*R)*
    whittakerM(-(1/2)*k, -(1/2)*k+1/2, 2*log(a)*R)/(4-k)+2^(-1-(1/2)*k)*log(a)
    ^(-1-k)*R^(-1-k)*(4*R^2*log(a)^2-2*log(a)*R*k+k^2+6*log(a)*R-5*k+6)*(k-4)*(
    log(a)*R)^((1/2)*k)*exp(-log(a)*R)*whittakerM(-(1/2)*k+1, -(1/2)*k+1/2, 2*
    log(a)*R)/(4-k))/(R^3*A0)+(3/8)*log(a)^(k-5)*P_ts*(-2^(-1-(1/2)*k)*log(a)
    ^(-1-k)*R^(-1-k)*(k^4-14*k^3+71*k^2-154*k+120)*(-6+k)*(log(a)*R)^((1/2)*k)*
    exp(-log(a)*R)*whittakerM(-(1/2)*k, -(1/2)*k+1/2, 2*log(a)*R)/(6-k)
    +2^(-1-(1/2)*k)*log(a)^(-1-k)*R^(-1-k)*(16*log(a)^4*R^4-8*log(a)^3*R^3*k+4*
    log(a)^2*R^2*k^2-2*log(a)*R*k^3+k^4+40*log(a)^3*R^3-36*R^2*k*log(a)^2+24*log
    (a)*R*k^2-14*k^3+80*R^2*log(a)^2-94*log(a)*R*k+71*k^2+120*log(a)*R-154*k
    +120)*(-6+k)*(log(a)*R)^((1/2)*k)*exp(-log(a)*R)*whittakerM(-(1/2)*k+1,
    -(1/2)*k+1/2, 2*log(a)*R)/(6-k))/(R^5*A0);
I_tot_model=(1-exp((-T*L)/Rb))*(N-2)*Ecal;

%ACOUSTIC PATH LOSS
A_model=A0*(W^k)*(a^W);

%RECEVED SIGNAL
P_rs_model=P_ts/A_model;

%ONE-HOP SNIR
SNIR_model_W=P_rs_model/(Nt_W+I_tot_model);

%ONE-HOP BER
BER_one_model_BPSK_W=qfunc((2*SNIR_model_W)^0.5);
BER_one_model_OOK_RZ_W=(1/2)*erfc((1/2)*((SNIR_model_W)^0.5));
BER_one_model_OOK_NRZ_W=(1/2)*erfc((1/(2*(2^0.5)))*((SNIR_model_W)^0.5));
BER_one_model_NC_FSK_W=(1/2)*exp(-SNIR_model_W/2);
BER_one_model_C_FSK_W=qfunc(SNIR_model_W^(0.5));

%END-TO-END BER
BER_end_model_BPSK_W=1-(1-BER_one_model_BPSK_W)^hop_number_model;
BER_end_model_OOK_RZ_W=1-(1-BER_one_model_OOK_RZ_W)^hop_number_model;
BER_end_model_OOK_NRZ_W=1-(1-BER_one_model_OOK_NRZ_W)^hop_number_model;
BER_end_model_NC_FSK_W=1-(1-BER_one_model_NC_FSK_W)^hop_number_model;
BER_end_model_C_FSK_W=1-(1-BER_one_model_C_FSK_W)^hop_number_model;

%%%%%%%RESULTS%%%%%%%%%%%%%%%%
%PATH LOSS
%Simulation
A_simulation_av=(sum(A_tot_matrix_sim))/n;
A_sim(p)=A_simulation_av;
%Model
A_m(p)=A_model;

%SNIR
%Simulation
```

```matlab
        SNIR_sim_W(p)=(sum(SNIR_tot_matrix_sim_W))/n;
        %Model
        SNIR_model_matrix_W(p)=SNIR_model_W;

        %END-TO-END BER
        %Simulation
        BER_simulation_av_BPSK_W=(sum(BER_tot_matrix_sim_BPSK_W))/n;
        BER_sim_BPSK_W(p)=BER_simulation_av_BPSK_W;
        BER_simulation_av_OOK_RZ_W=(sum(BER_tot_matrix_sim_OOK_RZ_W))/n;
        BER_sim_OOK_RZ_W(p)=BER_simulation_av_OOK_RZ_W;
        BER_simulation_av_OOK_NRZ_W=(sum(BER_tot_matrix_sim_OOK_NRZ_W))/n;
        BER_sim_OOK_NRZ_W(p)=BER_simulation_av_OOK_NRZ_W;
        BER_simulation_av_NC_FSK_W=(sum(BER_tot_matrix_sim_NC_FSK_W))/n;
        BER_sim_NC_FSK_W(p)=BER_simulation_av_NC_FSK_W;
        BER_simulation_av_C_FSK_W=(sum(BER_tot_matrix_sim_C_FSK_W))/n;
        BER_sim_C_FSK_W(p)=BER_simulation_av_C_FSK_W;
        %Model
        BER_model_BPSK_W(p)=BER_end_model_BPSK_W;
        BER_model_OOK_RZ_W(p)=BER_end_model_OOK_RZ_W;
        BER_model_OOK_NRZ_W(p)=BER_end_model_OOK_NRZ_W;
        BER_model_NC_FSK_W(p)=BER_end_model_NC_FSK_W;
        BER_model_C_FSK_W(p)=BER_end_model_C_FSK_W;

        %HOP NUMBER
        %Simulation
        HOP_simulation_av=(sum(hop_number_matrix_sim))/n;
        HOP_sim(p)=HOP_simulation_av;
        %Model
        HOP_model(p)=hop_number_model;
end

% plot(beg:step:finish,BER_sim_BPSK_W,'-k',beg:step:finish,BER_model_BPSK_W,'-g');
% plot(beg:step:finish,BER_sim_OOK_RZ_W,'-k',beg:step:finish,BER_model_OOK_RZ_W,'-g
    ');
% plot(beg:step:finish,BER_sim_OOK_NRZ_W,'-k',beg:step:finish,BER_model_OOK_NRZ_W
    ,'-g');
% plot(beg:step:finish,BER_sim_NC_FSK_W,'-k',beg:step:finish,BER_model_NC_FSK_W,'-g
    ');
% plot(beg:step:finish,BER_sim_C_FSK_W,'-k',beg:step:finish,BER_model_C_FSK_W,'-g')
    ;
% plot(beg:step:finish,BER_model_BPSK_W,'-r',beg:step:finish,BER_model_OOK_RZ_W,'-b
    ',beg:step:finish,BER_model_OOK_NRZ_W,'-k',beg:step:finish,BER_model_NC_FSK_W,'-
    g',beg:step:finish,BER_model_C_FSK_W,'-y');
% plot(beg:step:finish,HOP_sim,'-k',beg:step:finish,HOP_model,'-g');
```

I.4 Three Dimensional Matlab Models varying the Central Transmitting Frequency and the Number of Nodes

```matlab
%Ruben Ortega Blanco
```

```matlab
%Model varying Central Transmitting Frequency and Number of Nodes of:
    %One-Hop BER
    %End-to-End BER
    %Hops number
%Post-Graduation Program in Electronics and Automation Engineering Systems (PGEA)
%Electric Engineering Department
%University of Brasilia
%Brazil

clear
clc

%Initialazing
R=1;                %Radius (km)
Phi=pi/18;          %Max aperture angle (rad)
A0=10^(0.1*25);     %Normalization factor
k=1.5;              %Spreading factor
P_ts=20;            %Transmission Power (W)
T=1;                %Average rate of paq. trans. for a node (pck/sec)
L=768;              %Paq. Size (bits)
Rb=2400;            %Data transm. rate (bits/sec)
Pa=1035;            %density (kg/m^3)
c=1507;             %Sound Speed(m/s)
r=1;                %Output reference radius(m)
v=20;               %Wind Speed (knots)
DF=5*(10^3);        %Noise Frequency Bandwith(Hz)


%Transmitting Frequency values
beg_freq=1;         %beginning value
step_freq=1;        %steps
finish_freq=50;     %last value
p_freq=0;
for f=beg_freq:step_freq:finish_freq
    p_freq=p_freq+1;
end

%Number of Nodes values
beg_nodes=3;            %beginning value
step_nodes=2;           %steps
finish_nodes=100;       %last value
p_nodes=0;
for N=beg_nodes:step_nodes:finish_nodes
    p_nodes=p_nodes+1;
end

%Matrix to store values
BER_one_W_plot=zeros(p_nodes,p_freq);   %Store One-Hop BER
BER_end=zeros(p_nodes,p_freq);          %Store End-to-End BER
hops=zeros(p_nodes,p_freq);             %Store Number of Hops

p_freq=0;
```

```matlab
Imp=Pa*c;                              %Impedance
Area=4*pi*(r)^2;                       %Output Reference Area


Z=(3/4)*R;                             %Distance to central node
E_Phi=(2/Phi)*(sin(Phi/2));            %Average deviation


for f=beg_freq:step_freq:finish_freq
    p_freq=p_freq+1;

    %Absortion Coeficient for frequency values bigger than 0.1kHz
    a = 10^(0.1*((0.11*((f.^2)./(1+f.^2)))+44*((f.^2)./(4100+f.^2))+((2.75*10^-4)*f
        .^2)+0.003)));


    %Noise
    Ntur=30-30*log10(f);                         %Turbulency
    Ntr=10*log10((3*10^8)./(1+(10^4)*f.^4));     %Trafic
    Nsea=40+10*log10((v.^2)./(1+f.^(5/3)));      %Sea movement
    Nth=-15+20*log10(f);                         %Thermal
    %Total Noise in Pascal/Hz
    Nt=(10.^(0.1*(Ntr))+10.^(0.1*(Ntur))+10.^(0.1*(Nsea))+10.^(0.1*(Nth)))*10^(-6);
    %Total Noise in Watts
    Nt_W=((Nt*DF)^2)*Area/Imp;


    %Interference
    Ecal=6*log(a)^(-2+k)*P_ts*(2^(-1-(1/2)*k)*log(a)^(-1-k)*R^(-1-k)*(k-3)*(-2+k)*(
        log(a)*R)^((1/2)*k)*exp(-log(a)*R)*whittakerM(-(1/2)*k, -(1/2)*k+1/2, 2*log(
        a)*R)/(-k+3)+2^(-1-(1/2)*k)*log(a)^(-1-k)*R^(-1-k)*(2*log(a)*R-k+2)*(k-3)*(
        log(a)*R)^((1/2)*k)*exp(-log(a)*R)*whittakerM(-(1/2)*k+1, -(1/2)*k+1/2, 2*
        log(a)*R)/(-k+3))/(R^2*A0)-(9/2)*log(a)^(k-3)*P_ts*(-2^(-1-(1/2)*k)*log(a)
        ^(-1-k)*R^(-1-k)*(k^2-5*k+6)*(k-4)*(log(a)*R)^((1/2)*k)*exp(-log(a)*R)*
        whittakerM(-(1/2)*k, -(1/2)*k+1/2, 2*log(a)*R)/(4-k)+2^(-1-(1/2)*k)*log(a)
        ^(-1-k)*R^(-1-k)*(4*R^2*log(a)^2-2*log(a)*R*k+k^2+6*log(a)*R-5*k+6)*(k-4)*(
        log(a)*R)^((1/2)*k)*exp(-log(a)*R)*whittakerM(-(1/2)*k+1, -(1/2)*k+1/2, 2*
        log(a)*R)/(4-k))/(R^3*A0)+(3/8)*log(a)^(k-5)*P_ts*(-2^(-1-(1/2)*k)*log(a)
        ^(-1-k)*R^(-1-k)*(k^4-14*k^3+71*k^2-154*k+120)*(-6+k)*(log(a)*R)^((1/2)*k)*
        exp(-log(a)*R)*whittakerM(-(1/2)*k, -(1/2)*k+1/2, 2*log(a)*R)/(6-k)
        +2^(-1-(1/2)*k)*log(a)^(-1-k)*R^(-1-k)*(16*log(a)^4*R^4-8*log(a)^3*R^3*k+4*
        log(a)^2*R^2*k^2-2*log(a)*R*k^3+k^4+40*log(a)^3*R^3-36*R^2*k*log(a)^2+24*log
        (a)*R*k^2-14*k^3+80*R^2*log(a)^2-94*log(a)*R*k+71*k^2+120*log(a)*R-154*k
        +120)*(-6+k)*(log(a)*R)^((1/2)*k)*exp(-log(a)*R)*whittakerM(-(1/2)*k+1,
        -(1/2)*k+1/2, 2*log(a)*R)/(6-k))/(R^5*A0);


    p_nodes=0;
    for N=beg_nodes:step_nodes:finish_nodes
        p_nodes=p_nodes+1;

        Ps=N/((4/3)*pi*(R.^3));       %Nodes Spatial Density
        %Average Distance of the hop
        W=(3/4)*R*exp(-(1/2)*((2/3)*pi*Ps*(1-cos(Phi/2)))*R^3)*whittakerM(1/6, 2/3,
            ((2/3)*pi*Ps*(1-cos(Phi/2)))*R^3)/((1-exp(-((2/3)*pi*Ps*(1-cos(Phi/2)))
            *R^3))*(((2/3)*pi*Ps*(1-cos(Phi/2)))*R^3)^(1/6));
        %AVERAGE HOP NUMBER
```

```
            hop_number=Z/(W*E_Phi);
            hops(p_nodes,p_freq)=hop_number;

            P_int_mod=(1-exp((-T*L)/Rb))*(N-2)*Ecal;      %Interference

            A_path_mod=A0*(W^k)*(a^W);                     %Acoustic Path Loss

            P_rec_mod=P_ts/A_path_mod;                     %Received Signal

            SNIR_one_W=P_rec_mod/(Nt_W+P_int_mod);         %One-Hop SNIR

            BER_one_W=qfunc((2*SNIR_one_W)^0.5);           %One-Hop BER

            BER_one_W_plot(p_nodes,p_freq)=BER_one_W;
            %End-to-End BER
            BER_end(p_nodes,p_freq)=1-(1-BER_one_W)^hop_number;
        end
end
% surf(beg_freq:step_freq:finish_freq,beg_nodes:step_nodes:finish_nodes,
    BER_one_W_plot);
% surf(beg_freq:step_freq:finish_freq,beg_nodes:step_nodes:finish_nodes,BER_end);
% surf(beg_freq:step_freq:finish_freq,beg_nodes:step_nodes:finish_nodes,hops);
```

I.5   Optimal Central Transmitting Frequency Model varying the Number of Nodes

```
%Ruben Ortega Blanco
%Optimal Transmitting Frequency varying the Number of Nodes for:
    %One-Hop BER with Interference
    %One-Hop BER without Interference
    %End-to-End BER with Interference
    %End-to-End BER without Interference
%Post-Graduation Program in Electronics and Automation Engineering Systems (PGEA)
%Electric Engineering Department
%University of Brasilia
%Brazil

clear
clc

%Initialazing
R=1;             %Radius (km)
Phi=pi/18;       %Max aperture angle (rad)
A0=10^(0.1*25);  %Normalization factor
k=1.5;           %Spreading factor
P_ts=20;         %Transmission Power (W)
T=1;             %Average rate of paq. trans. for a node (pck/sec)
L=768;           %Paq. Size (bits)
Rb=2400;         %Data transm. rate (bits/sec)
```

```
Pa=1035;                %density (kg/m^3)
c=1507;                 %Sound  Speed (m/s)
r=1;                    %Output  reference  radius (m)
v=20;                   %Wind  Speed  (knots)
DF=5*(10^3);            %Noise  Frequency  Bandwith (Hz)


%Number  of  Nodes  values
beg=3;                  %beginning  value
step=1;                 %steps
finish=100;             %last  value
p=0;
for  N=beg:step:finish
    p=p+1;
end
%Matrix  to  store  values
f_opt_BER_SNIR_mat=zeros(p);        %End-to-End BER  with  Interference
f_opt_BER_one_SNIR_mat=zeros(p);    %One-Hop-BER  with  Interference
f_opt_BER_SNR_mat=zeros(p);         %End-to-End BER  without  Interference
f_opt_BER_one_SNR_mat=zeros(p);     %One-Hop BER  without  Interference
p=0;


for  N=beg:step:finish
    p=p+1;

    FUNC_BER_SNIR=@(f)  BER_SNIR_Func(f,R,N,A0,k,P_ts,T,L,Rb,Pa,c,r,v,DF,Phi);
    FUNC_BER_one_SNIR=@(f)  BER_one_SNIR_Func(f,R,N,A0,k,P_ts,T,L,Rb,Pa,c,r,v,DF,Phi
        );
    FUNC_BER_SNR=@(f)  BER_SNR_Func(f,R,N,A0,k,P_ts,Pa,c,r,v,DF,Phi);
    FUNC_BER_one_SNR=@(f)  BER_one_SNR_Func(f,R,N,A0,k,P_ts,Pa,c,r,v,DF,Phi);

    f_opt_BER_SNIR=fminbnd(FUNC_BER_SNIR,0,100);
    f_opt_BER_one_SNIR=fminbnd(FUNC_BER_one_SNIR,0,100);
    f_opt_BER_SNR=fminbnd(FUNC_BER_SNR,0,200);
    f_opt_BER_one_SNR=fminbnd(FUNC_BER_one_SNR,0,200);



    f_opt_BER_SNIR_mat(p)=f_opt_BER_SNIR;
    f_opt_BER_one_SNIR_mat(p)=f_opt_BER_one_SNIR;
    f_opt_BER_SNR_mat(p)=f_opt_BER_SNR;
    f_opt_BER_one_SNR_mat(p)=f_opt_BER_one_SNR;
end
% plot(beg:step:finish,f_opt_BER_SNIR_mat,'k',beg:step:finish,f_opt_BER_SNR_mat,'b
    ');
% plot(beg:step:finish,f_opt_BER_SNIR_mat,'k',beg:step:finish,
    f_opt_BER_one_SNIR_mat,'b');
% plot(beg:step:finish,f_opt_BER_SNR_mat,'k',beg:step:finish,f_opt_BER_one_SNR_mat
    ,'b');
```

I.6 Function that returns the One-Hop BER considering Interference

```matlab
%Ruben Ortega Blanco
%Function that return the One-Hop BER with interference
%Post-Graduation Program in Electronics and Automation Engineering Systems (PGEA)
%Electric Engineering Department
%University of Brasilia
%Brazil

function [ BER_one_SNIR ] = BER_one_SNIR_Func( f,R,N,A0,k,P_ts,T,L,Rb,Pa,c,r,v,DF,
    Phi )
    Imp=Pa*c;                   %Impedance
    Area=4*pi*(r)^2;            %Area

    %Absortion Coeficient for frequency values bigger than 0.1kHz
    a = 10^(0.1*(0.11*((f^2)/(1+f^2))+44*((f^2)/(4100+f^2))+(2.75*10^(-4))*f
        ^2+0.003));
    %NOISE
    Ntur=30-30*log10(f);                            %Turbulency
    Ntr=10*log10((3*10^8)/(1+(10^4)*(f^4)));        %Trafic
    Nsea=40+10*log10((v^2)/(1+(f^(5/3))));          %Sea movement
    Nth=-15+20*log10(f);                            %Thermal
    %Noise in Pascal/Hertz
    Nt=(10^(0.1*Ntr)+10^(0.1*Ntur)+10^(0.1*Nsea)+10^(0.1*Nth))*(10^(-6));
    %Noise in Watts
    Nt_W=((Nt*DF)^2)*Area/Imp;


    Ps=N/((4/3)*pi*(R^3));  %Nodes Spatial Density
    %AVERAGE DISTANCE OF THE HOP
    W=(3/4)*R*exp(-(1/2)*((2/3)*pi*Ps*(1-cos(Phi/2)))*R^3)*whittakerM(1/6, 2/3,
        ((2/3)*pi*Ps*(1-cos(Phi/2)))*R^3)/((1-exp(-((2/3)*pi*Ps*(1-cos(Phi/2)))*R^3)
        )*(((2/3)*pi*Ps*(1-cos(Phi/2)))*R^3)^(1/6));


    %INTERFERENCE
    Ecal=6*log(a)^(-2+k)*P_ts*(2^(-1-(1/2)*k)*log(a)^(-1-k)*R^(-1-k)*(k-3)*(-2+k)*(
        log(a)*R)^((1/2)*k)*exp(-log(a)*R)*whittakerM(-(1/2)*k, -(1/2)*k+1/2, 2*log(
        a)*R)/(-k+3)+2^(-1-(1/2)*k)*log(a)^(-1-k)*R^(-1-k)*(2*log(a)*R-k+2)*(k-3)*(
        log(a)*R)^((1/2)*k)*exp(-log(a)*R)*whittakerM(-(1/2)*k+1, -(1/2)*k+1/2, 2*
        log(a)*R)/(-k+3))/(R^2*A0)-(9/2)*log(a)^(k-3)*P_ts*(-2^(-1-(1/2)*k)*log(a)
        ^(-1-k)*R^(-1-k)*(k^2-5*k+6)*(k-4)*(log(a)*R)^((1/2)*k)*exp(-log(a)*R)*
        whittakerM(-(1/2)*k, -(1/2)*k+1/2, 2*log(a)*R)/(4-k)+2^(-1-(1/2)*k)*log(a)
        ^(-1-k)*R^(-1-k)*(4*R^2*log(a)^2-2*log(a)*R*k+k^2+6*log(a)*R-5*k+6)*(k-4)*(
        log(a)*R)^((1/2)*k)*exp(-log(a)*R)*whittakerM(-(1/2)*k+1, -(1/2)*k+1/2, 2*
        log(a)*R)/(4-k))/(R^3*A0)+(3/8)*log(a)^(k-5)*P_ts*(-2^(-1-(1/2)*k)*log(a)
        ^(-1-k)*R^(-1-k)*(k^4-14*k^3+71*k^2-154*k+120)*(-6+k)*(log(a)*R)^((1/2)*k)*
        exp(-log(a)*R)*whittakerM(-(1/2)*k, -(1/2)*k+1/2, 2*log(a)*R)/(6-k)
        +2^(-1-(1/2)*k)*log(a)^(-1-k)*R^(-1-k)*(16*log(a)^4*R^4-8*log(a)^3*R^3*k+4*
        log(a)^2*R^2*k^2-2*log(a)*R*k^3+k^4+40*log(a)^3*R^3-36*R^2*k*log(a)^2+24*log
        (a)*R*k^2-14*k^3+80*R^2*log(a)^2-94*log(a)*R*k+71*k^2+120*log(a)*R-154*k
        +120)*(-6+k)*(log(a)*R)^((1/2)*k)*exp(-log(a)*R)*whittakerM(-(1/2)*k+1,
```

```
                 −(1/2)*k+1/2,  2*log(a)*R)/(6−k))/(R^5*A0);
    %Power
    I_tot_model=(1−exp((−T*L)/Rb))*(N−2)*Ecal;
    %ACOUSTIC PATH LOSS (With VA Z)
    A_model=A0*(W^k)*(a^W);
    %RECEVED SIGNAL
    %Power
    P_rs_model=P_ts/A_model;
    %SNIR
    SNIR=P_rs_model/(Nt_W+I_tot_model);


    %One−Hop BER for SNIR
    BER_one_SNIR=qfunc((2*SNIR)^0.5);
end
```

I.7 Function that returns the One-Hop BER not considering Interference

```
%Ruben Ortega Blanco
%Function that return the Bit Error Rate (BER) without interference
%Post−Graduation Program in Electronics and Automation Engineering Systems (PGEA)
%Electric Engineering Department
%University of Brasilia
%Brazil


function [ BER_one_SNR ] = BER_one_SNR_Func( f,R,N,A0,k,P_ts,Pa,c,r,v,DF,Phi )
    Imp=Pa*c;              %Impedance
    Area=4*pi*(r)^2;       %Area

    %Absortion Coeficient for frequency values bigger than 0.1kHz
    a = 10^(0.1*(0.11*((f^2)/(1+f^2))+44*((f^2)/(4100+f^2))+(2.75*10^(−4))*f
        ^2+0.003));
    %NOISE
    Ntur=30−30*log10(f);                          %Turbulency
    Ntr=10*log10((3*10^8)/(1+(10^4)*(f^4)));      %Trafic
    Nsea=40+10*log10((v^2)/(1+(f^(5/3))));        %Sea movement
    Nth=−15+20*log10(f);                          %Thermal
    %Noise in Pascal/Hertz
    Nt=(10^(0.1*Ntr)+10^(0.1*Ntur)+10^(0.1*Nsea)+10^(0.1*Nth))*(10^(−6));
    %Noise in Watts
    Nt_W=((Nt*DF)^2)*Area/Imp;


    Ps=N/((4/3)*pi*(R^3));        %Nodes Spatial Density
    %AVERAGE DISTANCE OF THE HOP
    W=(3/4)*R*exp(−(1/2)*((2/3)*pi*Ps*(1−cos(Phi/2)))*R^3)*whittakerM(1/6, 2/3,
        ((2/3)*pi*Ps*(1−cos(Phi/2)))*R^3)/((1−exp(−((2/3)*pi*Ps*(1−cos(Phi/2)))*R^3)
        )*(((2/3)*pi*Ps*(1−cos(Phi/2)))*R^3)^(1/6));


    %ACOUSTIC PATH LOSS (With VA Z)
```

```matlab
    A_model=A0*(W^k)*(a^W);
    %RECEVED SIGNAL
    %Power
    P_rs_model=P_ts/A_model;
    %SNIR
    SNR=P_rs_model/(Nt_W);


    %One-Hop BER for SNIR
    BER_one_SNR=qfunc((2*SNR)^0.5);
end
```

I.8 Function that returns the End-to-End BER considering Interference

```matlab
%Ruben Ortega Blanco
%Function that return the End-to-End BER with interference
%Post-Graduation Program in Electronics and Automation Engineering Systems (PGEA)
%Electric Engineering Department
%University of Brasilia
%Brazil


function [ BER_SNIR ] = BER_SNIR_Func( f,R,N,A0,k,P_ts,T,L,Rb,Pa,c,r,v,DF,Phi )
    Imp=Pa*c;                %Impedance
    Area=4*pi*(r)^2;         %Area

    %Absortion Coeficient for frequency values bigger than 0.1kHz
    a = 10^(0.1*(0.11*((f^2)/(1+f^2))+44*((f^2)/(4100+f^2))+(2.75*10^(-4))*f
        ^2+0.003));
    %NOISE
    Ntur=30-30*log10(f);                          %Turbulency
    Ntr=10*log10((3*10^8)/(1+(10^4)*(f^4)));      %Trafic
    Nsea=40+10*log10((v^2)/(1+(f^(5/3))));        %Sea movement
    Nth=-15+20*log10(f);                          %Thermal
    %Noise in Pascal/Hertz
    Nt=(10^(0.1*Ntr)+10^(0.1*Ntur)+10^(0.1*Nsea)+10^(0.1*Nth))*(10^(-6));
    %Noise in Watts
    Nt_W=((Nt*DF)^2)*Area/Imp;


    Ps=N/((4/3)*pi*(R^3));   %Nodes Spatial Density
    %AVERAGE DISTANCE OF THE REFERENCE LINE
    Z=(3/4)*R;
    %AVERAGE DISTANCE OF THE HOP
    W=(3/4)*R*exp(-(1/2)*((2/3)*pi*Ps*(1-cos(Phi/2)))*R^3)*whittakerM(1/6, 2/3,
        ((2/3)*pi*Ps*(1-cos(Phi/2)))*R^3)/((1-exp(-((2/3)*pi*Ps*(1-cos(Phi/2)))*R^3)
        )*(((2/3)*pi*Ps*(1-cos(Phi/2)))*R^3)^(1/6));
    %AVERAGE DEVIATION
    E_Phi=(2/Phi)*(sin(Phi/2));
    %AVERAGE HOP NUMBER
    hop_number=Z/(W*E_Phi);
```

```matlab
%INTERFERENCE
Ecal=6*log(a)^(-2+k)*P_ts*(2^(-1-(1/2)*k)*log(a)^(-1-k)*R^(-1-k)*(k-3)*(-2+k)*(
    log(a)*R)^((1/2)*k)*exp(-log(a)*R)*whittakerM(-(1/2)*k, -(1/2)*k+1/2, 2*log(
    a)*R)/(-k+3)+2^(-1-(1/2)*k)*log(a)^(-1-k)*R^(-1-k)*(2*log(a)*R-k+2)*(k-3)*(
    log(a)*R)^((1/2)*k)*exp(-log(a)*R)*whittakerM(-(1/2)*k+1, -(1/2)*k+1/2, 2*
    log(a)*R)/(-k+3))/(R^2*A0)-(9/2)*log(a)^(k-3)*P_ts*(-2^(-1-(1/2)*k)*log(a)
    ^(-1-k)*R^(-1-k)*(k^2-5*k+6)*(k-4)*(log(a)*R)^((1/2)*k)*exp(-log(a)*R)*
    whittakerM(-(1/2)*k, -(1/2)*k+1/2, 2*log(a)*R)/(4-k)+2^(-1-(1/2)*k)*log(a)
    ^(-1-k)*R^(-1-k)*(4*R^2*log(a)^2-2*log(a)*R*k+k^2+6*log(a)*R-5*k+6)*(k-4)*(
    log(a)*R)^((1/2)*k)*exp(-log(a)*R)*whittakerM(-(1/2)*k+1, -(1/2)*k+1/2, 2*
    log(a)*R)/(4-k))/(R^3*A0)+(3/8)*log(a)^(k-5)*P_ts*(-2^(-1-(1/2)*k)*log(a)
    ^(-1-k)*R^(-1-k)*(k^4-14*k^3+71*k^2-154*k+120)*(-6+k)*(log(a)*R)^((1/2)*k)*
    exp(-log(a)*R)*whittakerM(-(1/2)*k, -(1/2)*k+1/2, 2*log(a)*R)/(6-k)
    +2^(-1-(1/2)*k)*log(a)^(-1-k)*R^(-1-k)*(16*log(a)^4*R^4-8*log(a)^3*R^3*k+4*
    log(a)^2*R^2*k^2-2*log(a)*R*k^3+k^4+40*log(a)^3*R^3-36*R^2*k*log(a)^2+24*log
    (a)*R*k^2-14*k^3+80*R^2*log(a)^2-94*log(a)*R*k+71*k^2+120*log(a)*R-154*k
    +120)*(-6+k)*(log(a)*R)^((1/2)*k)*exp(-log(a)*R)*whittakerM(-(1/2)*k+1,
    -(1/2)*k+1/2, 2*log(a)*R)/(6-k))/(R^5*A0);
%Power
I_tot_model=(1-exp((-T*L)/Rb))*(N-2)*Ecal;
%ACOUSTIC PATH LOSS (With VA Z)
A_model=A0*(W^k)*(a^W);
%RECEVED SIGNAL
%Power
P_rs_model=P_ts/A_model;
%SNIR
SNIR=P_rs_model/(Nt_W+I_tot_model);

%One-Hop BER for SNIR
BER_one_SNIR=qfunc((2*SNIR)^0.5);

%End-to-End BER for SNIR
BER_SNIR=1-(1-BER_one_SNIR)^hop_number;
end
```

I.9 Function that returns the End-to-End BER not considering Interference

```matlab
%Ruben Ortega Blanco
%Function that return the Bit Error Rate (BER) without interference
%Post-Graduation Program in Electronics and Automation Engineering Systems (PGEA)
%Electric Engineering Department
%University of Brasilia
%Brazil

function [ BER_SNR ] = BER_SNR_Func( f,R,N,A0,k,P_ts,Pa,c,r,v,DF,Phi )
    Imp=Pa*c;            %Impedance
    Area=4*pi*(r)^2;     %Area
```

```matlab
    %Absortion Coeficient for frequency values bigger than 0.1kHz
    a = 10^(0.1*(0.11*((f^2)/(1+f^2))+44*((f^2)/(4100+f^2))+(2.75*10^(-4))*f
        ^2+0.003));
    %NOISE
    Ntur=30-30*log10(f);                        %Turbulency
    Ntr=10*log10((3*10^8)/(1+(10^4)*(f^4)));    %Trafic
    Nsea=40+10*log10((v^2)/(1+(f^(5/3))));      %Sea movement
    Nth=-15+20*log10(f);                        %Thermal
    %Noise in Pascal/Hertz
    Nt=(10^(0.1*Ntr)+10^(0.1*Ntur)+10^(0.1*Nsea)+10^(0.1*Nth))*(10^(-6));
    %Noise in Watts
    Nt_W=((Nt*DF)^2)*Area/Imp;


    Ps=N/((4/3)*pi*(R^3));  %Nodes Spatial Density
    %AVERAGE DISTANCE OF THE REFERENCE LINE
    Z=(3/4)*R;
    %AVERAGE DISTANCE OF THE HOP
    W=(3/4)*R*exp(-(1/2)*((2/3)*pi*Ps*(1-cos(Phi/2)))*R^3)*whittakerM(1/6, 2/3,
        ((2/3)*pi*Ps*(1-cos(Phi/2)))*R^3)/((1-exp(-((2/3)*pi*Ps*(1-cos(Phi/2)))*R^3)
        )*(((2/3)*pi*Ps*(1-cos(Phi/2)))*R^3)^(1/6));
    %AVERAGE DEVIATION
    E_Phi=(2/Phi)*(sin(Phi/2));
    %AVERAGE HOP NUMBER
    hop_number=Z/(W*E_Phi);


    %ACOUSTIC PATH LOSS (With VA Z)
    A_model=A0*(W^k)*(a^W);
    %RECEVED SIGNAL
    %Power
    P_rs_model=P_ts/A_model;
    %SNIR
    SNR=P_rs_model/(Nt_W);


    %One-Hop BER for SNIR
    BER_one_SNR=qfunc((2*SNR)^0.5);


    %End-to-End BER for SNIR
    BER_SNR=1-(1-BER_one_SNR)^hop_number;
end
```